VILSMEIER-HAACK SYNTHESIS OF NEW STEROIDAL PYRAZOLES

Ayaz Mahmood Dar[a]* and Shamsuzzaman[a]

Keywords: Thiosemicarbazone, pyrazole, Vilsmeier-Haack, acetamide, $POCl_3$.

A novel expeditious and convenient synthesis of hitherto unknown 5α-cholestano [6,7-c]-5'-methyl-1'-carbothioic acid amide pyrazoles based on the reaction of 5α-cholestan-6-one thiosemicarbazones with modified Vilsmeier-Haack reagent (H_3C-CO-NH_2/$POCl_3$) is described. The compounds presented here are novel scaffolds and have not been described before. Structural assignment of these newly synthesized compounds was performed by IR, ^{1}HNMR, ^{13}CNMR, MS and analytical data. A general mechanistic scheme for these reactions is also suggested based on the current and previous data.

* Corresponding Authors
Fax:
E-Mail: ayazchem09@gmail.com
[a] Department of Chemistry Aligarh Muslim University, Aligarh 202 002, India

Introduction

Pyrazole moiety, being called as pharmacophore, plays an important role in many biologically active compounds and therefore represents an interesting template for combinatorial as well as medicinal chemistry.[1-5] In addition pyrazoles have played a vital role in developing the theory in heterocyclic chemistry and are also used extensively as useful synthons in organic synthesis.[6] These derivatives have wide spread biological activities such as anticancer, analgesic, anti-inflammatory, antimicrobial, antiviral, anticonvulsant, antihistaminic, and anti-HIV.[6-17] The recent success of pyrazole COX-2 inhibitor has further highlighted the importance of these heterocycles in medicinal chemistry.[6] Some of the biologically active steroids fused with heterocycles are shown in Figure 1.a vital role in developing the theory in heterocyclic chemistry and are also used extensively as useful synthons in organic synthesis.[6] These derivatives have wide spread biological activities such as anticancer, analgesic, anti-inflammatory, antimicrobial, highlighted the importance of these heterocycles as antiviral, anticonvulsant, antihistaminic, and anti-HIV.[6-17] The recent success of pyrazole COX-2 inhibitor has further highlighted the importance of these heterocycles in medicinal chemistry.[6] Some of the biologically active steroids fused with heterocycles are shown in Figure 1.

Since the discovery of the Vilsmeier-Haack reagent (halomethyleniminium salt) in 1927, formed from the interaction of a dialkyl formamide (e.g. DMF) with phosphorus oxychloride ($POCl_3$) has attracted the attention of synthetic organic chemists.[18] It is one of the most commonly used reagents for the introduction of an aldehydic (CHO) group into electron rich aromatic systems.[19] However, the scope of the Vilsmeier reagent is not confined to the aromatic formylation reaction alone. A wide variety of alkene derivatives,[20] carbonyl compounds,[21] activated methyl and methylene groups[22] exhibit reactivity towards the Vilsmeier reagent. In addition to the carbon nucleophiles, some oxygen and nitrogen nucleophiles[23,24] are also reactive towards Vilsmeier reagent. Numerous transformations of the iminium salts into products other than aldehydes have been achieved[25,26] and these transformations enhance the scope and versatility of the Vilsmeier–Haack reaction. In continuation of our previous work[27] and following interest on the Vilsmeier-Haack reaction, we hereby report an effort to introduce the methyl group instead of an aldehydic group into the steroidal system by modifying the iminium cation, formed by the expeditious reaction of acetamide and $POCl_3$.

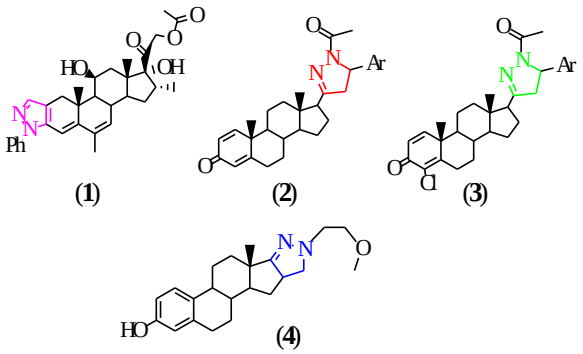

Figure 1. Some biologically active steroidal appended pyrazoles

Experimental

Materials and instruments

All the reagents and solvents were obtained from best known commercial sources and were freshly distilled. Melting points were determined on a Kofler apparatus and are uncorrected. The IR spectra were recorded on KBr pellets with Pye Unicam SP3-100 Spectrophotometer and values are given in cm^{-1}. ^{1}H and ^{13}C NMR spectra were run in $CDCl_3$ on a JEOL Eclipse (400 MHz) instrument with TMS as internal standard and values are given in ppm (δ). Mass spectra were recorded on a JEOL SX 102/DA-6000 mass spectrometer. Thin layer chromatography (TLC) plates

were coated with silica gel G and exposed to iodine vapours to check the progress of reaction. Anhydrous sodium sulphate was used as a drying agent.

General procedure for the synthesis of steroidal pyrazoles (4-6)

To the solution of steroidal thiosemicarbazones[21] (**1-3**) (1 mmol) in CH_3CN (10 mL), was added acetamide (1 mmol) under ice-cold condition. $POCl_3$ (1 mmol) was then added with stirring at such a rate that the temperature of the reaction mixture did not exceed 10 °C. After complete addition, the reaction-mixture was allowed to attain room temperature and stirred for about 1-3 h. After ensuring the completion of reaction (TLC), the contents were poured into crushed ice and into and left overnight in a refrigerator. The precipitate thus obtained was filtered, washed with water, dried and purified by recrystallization from methanol to afford 5α-cholestano[6,7-c]-5'-methyl-1'-carbothioic acid amide pyrazole derivatives (**4-6**).

3β-Acetoxy-5α-cholestano[6,7-c]-5'-methyl-1'-carbothioic acid amide pyrazole (4)

Yield 65 %; mp: 147-149 °C; Anal. Calcd. for $C_{32}H_{51}N_3O_2S$: C, 70.89, H, 9.19, N, 7.55; found; C, 70.97, H, 9.42, N, 7.76; IR (KBr) ν cm^{-1}: 3390 (NH_2), 1714 ($OCOCH_3$), 1655 (C=N), 1632 (C=C), 1376 (C-N), 1269 (C=S), 1210 (C-O); ^{1}H NMR ($CDCl_3$, 400 MHz): δ 8.2 (s, 2H, NH_2, exchangeable with D_2O), 4.7 (m, 1H, $C_3\alpha$-H, W ½ = 15 Hz), 2.3 (s, 3H, CH_3), 2.03 (s, 3H, $OCOCH_3$), 1.18 (s, 3H, C_{10}-CH_3), 0.70 (s, 3H, C_{13}-CH_3), 0.97 & 0.83 (other methyl protons); ^{13}C NMR ($CDCl_3$, 100 MHz): δ 181.2 (C=S), 171.0 (OAc), 148.3 (C_6), 134 (C_5'), 119.3 (C_7), 75.1 (C_3), 40.5 (C_5), 39.52, 37.98, 36.70, 35.76, 30.73, 30.08, 28.11, 28.07, 24.04, 23.86, 22.89, 22.63, 21.57, 19.09, 18.70, 13.21, 12.08; ESI MS: m/z 541[$M^{+\cdot}$].

3β-Chloro-5α-cholestano[6,7-c]5'-methyl-1'-carbothioic acid amide pyrazole (5)

Yield 65 %; mp: 156-158 °C; Anal. Calcd. for $C_{30}H_{48}N_3ClS$: C, 69.49, H, 9.11, N, 8.02; found; C, 69.63, H, 9.28, N, 8.12; IR (KBr) ν cm^{-1}: 3410 (NH_2), 1650 (C=N), 1625 (C=C), 1378 (C-N), 1275 (C=S), 756 (C-Cl); ^{1}H NMR ($CDCl_3$, 400 MHz): δ 7.8 (s, 2H, NH_2, exchangeable with D_2O), 3.9 (m, 1H, $C_3\alpha$-H, W ½ = 17 Hz), 2.4 (s, 3H, CH_3), 1.19 (s, 3H, C_{10}-CH_3), 0.75 (s, 3H, C_{13}-CH_3), 0.97 & 0.80 (other methyl protons); ^{13}C NMR ($CDCl_3$, 100 MHz): δ 184.2 (C=S), 144.5 (C_6), 132 (C_5'), 119.2 (C_7), 59.6 (C_3), 42.2 (C_5), 42.92, 39.32, 38.13, 36.64, 35.72, 30.68, 30.14, 30.08, 28.42, 28.12, 24.18, 23.56, 22.62, 22.43, 21.47, 18.68, 13.23; ESI MS: m/z 515/517 [$M^{+\cdot}$].

5α-Cholestano[6,7-c]5'-methyl-1'-carbothioic acid amide pyrazole (6)

Yield 60 %; mp: 119-121 °C; Anal. Calcd for $C_{30}H_{49}N_3S$: C, 74.40, H, 10.07, N, 8.60; found; C, 74.53, H, 10.14, N, 8.69; IR (KBr) ν cm^{-1}: 3393 (NH_2,), 1652 (C=N) 1620 (C=C), 1375 (C-N), 1275 (C=S); ^{1}H NMR ($CDCl_3$, 400 MHz): δ 7.6 (s, 2H, NH_2, exchangeable with D_2O), 2.4 (s, 3H, CH_3), 1.19 (s, 3H, C_{10}-CH_3), 0.75 (s, 3H, C_{13}-CH_3), 0.96 and 0.83 (other methyl protons); ^{13}C NMR ($CDCl_3$, 100 MHz): δ 179.2 (C=S), 150.1 (C_6), 137 (C_5'), 118 (C_7), 41.8 (C_5), 42.76, 39.45, 38.24, 36.53, 35.87, 30.52, 30.34, 30.12, 28.57, 28.07, 24.38, 23.82, 22.46, 22.36, 21.82, 18.48, 17.62, 13.27, 12.16; MS: m/z 483[$M^{+\cdot}$].

Results and Discussion

Chemistry

Development of highly functional molecules from simple building blocks has always been the aim of synthetic chemists. With this aim, we here report a new route for the synthesis of novel steroidal pyrazoles (**4-6**) from steroidal thiosemicarbazones (**1-3**) by using the Vilsmeier-Haack protocol, during which the steroidal thiosemicarbazones (**1-3**) reacts with iminium cation (formed by the reaction of acetamide and $POCl_3$ under cold conditions), afforded steroidal pyrazoles (**4-6**) (Scheme 1). The yield of steroidal pyrazoles (**4-6**) was in the range of 60-65 %. A probable mechanism for the formation of compounds (**4-6**) is shown in Scheme 2.

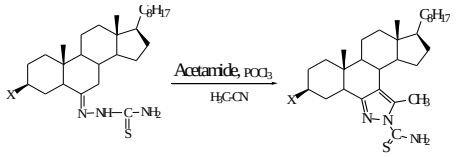

X
OAc (**1**)
Cl (**2**)
H (**3**)

X
OAc (**4**)
Cl (**5**)
H (**6**)

Scheme 1. Showing the formation of steroidal pyrazoles **4-6**

The selected diagnostic bands of IR spectra of synthesized products provide useful information for determining structures of the steroidal pyrazole derivatives. All the compounds (**4-6**) show a band in the range of 3390-3410 cm^{-1} assigned to (NH) while the bands in the range of 1655-1650, 1632-1620, 1378-1375, 1269-1275 cm^{-1} were be ascribed to (C=N), (C=C), (C-N) and (C=S) respectively. The formation of steroidal pyrazoles (**4-6**) was further confirmed with the NMR studies where the assignments of signals are based on the chemical shift and intensity pattern. In ^{1}HNMR spectra the compounds (**4-6**) exhibited singlet for three protons at δ 2.3-2.4 (CH_3) and two proton singlet (exchangeable with D_2O) at δ 8.2-7.6 (NH_2). Other peaks were observed at δ 1.18, 0.70, 0.97 and 0.83 indicating the presence of angular and side chain methyl groups. ^{13}CNMR signals are in good agreement with proposed structures of synthesized compounds. All the compounds exhibited signals at δ 184-179, 150-144, 137-132,119-118 due to C=S, C=N, C-N and C=C respectively. The distinctive signals were observed in the mass spectra of compounds (**4-6**) which followed the similar fragmentation pattern. The molecular ion peaks ($M^{+\cdot}$) for compounds (**4-6**) were observed at m/z 541, 515/517 and 483 respectively.

 DOI: 10.17628/ecb.2014.3.1104-1106

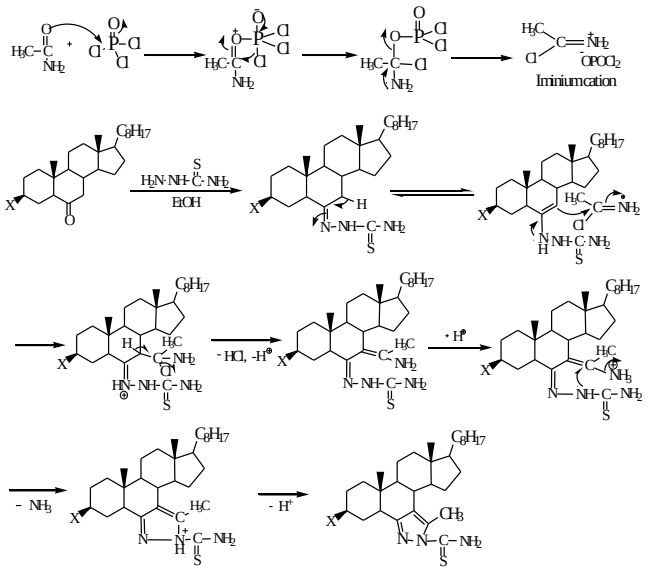

Scheme 2. Showing the reaction mechanism for the formation of steroidal pyrazoles

The mechanism for the formation of steroidal pyrazoles (4-6) involves the formation of an iminium cation by the reaction of acetamide and phosphorus oxychloride. The steroidal thiosemicarbazones undergo keto-enol tautomerization before reacting with iminium cation. Facilitated by the migration of the lone pair of electron from nitrogen, the attack of the double bond to the iminium cation occur which in turn expels hydrogen chloride and ammonia, leading to the formation of steroidal pyrazoles

Conclusion

In conclusion, we have developed an efficient synthetic approach for the synthesis of a novel class of steroidal pyrazoles via modified Vilsmeier reagent (acetamide/$POCl_3$). This is a simple, mild and straightforward reaction, which is completed in a short span of time. The novelty of the entire process lies in the Vilsmeier cyclization of cholestane-6-one thiosemicarbazones into steroidal pyrazoles, which, to the best of our knowledge, is unprecedented. Further studies to broaden the scope towards the synthesis of the novel steroidal derivatives are under investigation in our laboratory.

References

[1] Temperini, C., Scozzafava, A., Supuran, C. T., *Bioorg. Med. Chem. Lett.*, **2006**, *16*, 5152-5156.

[2] Fevig, J. M., Cacciola, J., Buriak, J. J., Rossi, K. A., Knabb, R. M., Luettgen, J. M., Wong, P. C., Bia, S. A., Wexler, R. R., Lam, P. Y., *Bioorg. Med. Chem. Lett.*, **2006**, *16*, 3755-3760.

[3] Kahn, M. G. C., Konde, E., Dossou, F., Labaree, D. C., Hochberg, R. B., *Bioorg. Med. Chem. Lett.*, **2006**, *16*, 3454-3458.

[4] Penning, T. D., Khilevich, A., Chenn, B. B., Russell, M. A., Boys, M. L., Wang, Y., Duffin, T., *Bioorg Med Chem Lett.*, **2006**, *16*, 3156-3161.

[5] Pevarello, P., Fancelli, D., Vulpetti, A., Amici, R., Villa, M., Pittalà, V., Vianello, P., Cameron, A., Ciomei, M., Mercurio, C., Bischoff, J. R., Roletto, F., Varasi, M., Brasca, M. G., *Bioorg. Med.Chem. Lett.*, **2006**, *16*, 1084-1090.

[6] Chirag, K. P., Rami, C. S., Panigrahi, B., Patel, C. N., *J. Chem. Pharm. Res.*, **2010**, *2*, 73-78.

[7] Tewari, A. K., Mishra, A., *Bioorg. Med. Chem.*, **2001**, *9*, 715-718.

[8] Wiley, R. H., Wiley, P., *Pyrazolones, Pyrazolidones and Derivatives*; John Wiley and Sons: New York, **1964.**

[9] Pimerova, E. V., Voronina, E. V., *Pharm. Chem. J.*, **2001**, *35*, 18-20.

[10] Janus, S. L., Magdif, A. Z., Erik, B. P., Claus, N., *Monatsh. Chem.* **1999**, *130*, 1167-1174.

[11] Park, H. J., Lee, K., Park, S., Ahn, B., Lee, J. C., Cho, H. Y., Lee, K. I., *Bioorg. Med. Chem. Lett.*, **2005**, *15*, 3307-3312.

[12] Bouabdallah, I., M'barek, L. A., Zyad, A., Ramadan, A., Zidane, I., Melhaoui, A., *Nat. Prod. Res.*, **2006**, *20*, 1024-1030.

[13] Michon, V., Penhoat, C. H. D., Tombret, F., Gillardin, J. M., Lepagez, F., Berthon, L., *Eur. J. Med. Chem.*, **1995**, *30*, 147-155.

[14] Yildirim, I., Ozdemir, N., Akcamur, Y., Dincer, M., Andac, O., *Acta Cryst. E*, **2005**, *61*, 256-258.

[15] Bailey, D. M., Hansen, P. E., Hlavac, A. G., Baizman, E. R., Pearl, J., Defelice, A. F., Feigenson, M. E., *J. Med. Chem.*, **1985**, *28*, 256-260.

[16] Chu, C. K., Cutler, J., *J. Heterocycl. Chem.*, **1986**, *23*, 289-319.

[17] Kees, K. L., Fitzgerald, J. J. J., Steiner, K. E., Mattes, J. F., Mihan, B., Tosi, T., Mondoro, D., McCaleb, M. L., *J. Med. Chem.*, **1996**, *39*, 3920-3928.

[18] Vilsmeier, A., Haack, A., *Chem. Ber.*, **1927**, *60*, 119-122.

[19] Pedras, M. S. C., Jha, M. J., *Org. Chem.*, **2005**, *70*, 1828-1834.

[20] Reddy, M. P., Rao, G. S. K., *J. Org. Chem.*, **1981**, *46*, 5371-5373.

[21] Katritzky, A. R., Marson, C. M., *J. Am. Chem. Soc.*, **1983**, *105*, 3279-3283.

[22] Mittelbach, M. Junek, H., *J. Heterocycl. Chem.*, **1982**, *19*, 1021-1024.

[23] Nohara, A., Umetani, T., Sanno, Y., *Tetrahedron*, **1974**, *30*, 3553-3561.

[24] Brehme, R., Nikolajewski, H. E., *Tetrahedron Lett.*, **1982**, *23*, 1131-1134.

[25] Meth-Cohn, O., Westwood, K. T., *J. Chem. Soc., Perkin Trans. 1*, **1983**, 2089-2092.

[26] Meth-Cohn, O., Narine, B., Tarnowski, B., *Tetrahedron Lett.*, **1979**, *20*, 3111-3114.

[27] (a) Naseem, S., Gatoo, M. A., Dar, A, M., Qasim, K., *Eur. Chem. Bull.*, **2014**, *3(10)*, 992-1000; (b) Shamsuzzaman, Dar, A, M., Gatoo, M. A., *Eur. Chem. Bull.*, **2014**, *3(8)*, 770-775.

Received: 28.10.2014.
Accepted: 12.01.2015.

GREEN CHEMICAL SYNTHESIS OF DIVERSE IMINOSACCHARIDES OF SUBSTITUTED PYRAZOLE USING IONIC LIQUID

Arpit Kumar Pathak,[a] Chetna Ameta,[a] Manish Kumar Rawal,[b] Rakshit Ameta[c] and Pinki B. Punjabi*[a]

Keywords: [bbim][BF_4], iminosaccharides, ionic liquid, microwave irradiation, green chemistry

An efficient and mild synthesis of some diverse iminosaccharides of pyrazole has been carried out. Compounds **(8a-b)** have been synthesized by the treatment of isoniazide with chalcones **(6a-b)** using [bbim][BF_4] ionic liquid as a solvent under microwave irradiation. Compounds **(8a-b)** on reaction with various aldoses afforded corresponding iminosaccharides compounds containing pyrazole moiety **(9a-l)** in presence of ionic liquid under microwaves. The products have been isolated, purified and characterized by different spectral methods i.e. IR, ^{1}H NMR, ^{13}C NMR and Mass spectra. The potent antimicrobial effects (MIC) of the synthesized compounds were investigated.

* Corresponding Authors
E-Mail: pb_punjabi@yahoo.com
[a] Department of Chemistry, University College of Science, Udaipur (Rajasthan), India
[b] Department of Chemistry, Vidya Bhawan Rural Institute, Udaipur (Raj.), India
[c] Department of Chemistry, Pacific College of Basic and Applied sciences, Udaipur (Raj.), India.

Introduction

To improve chemical process and to reduce environmental pollution has become an urgent task for chemical researchers these days. Microwave-assisted synthesis using ionic liquid as a solvent and catalyst shows distinct advantages over the traditional process, such as energy conservation, short reaction time and elimination of volatile organic solvent. Ionic liquids, the molten salts with melting points at or below ambient temperature, have attracted intense focus due to their remarkable chemical and physical properties such as high thermal stability,[1,2] negligible vapor pressure[3] and high ionic conductivity.[4] They have been used as an alternative to volatile organic solvents for organic synthesis in homogeneous as well as biphasic processes.[5]

Pyrazoles and its derivatives have been found to possess biological activities such as antimicrobial,[6] antihistamatic,[7] anticancer,[8] anticonvulsant[9] and antiinflammatory[10] activity. Schiff base (also known as imine and azomethine) is a nitrogen analogue of an aldehyde or ketone in which the carbonyl group (C=O) has been replaced by an imine or azomethine group. They are used as a pigments, dyes, catalyst, intermediate in organic synthesis and polymer stabilizer.[11] Schiff bases also show a broad range of biological activities, including anti-inflammatory, antiviral, antimalarial, antipyretic and antimicrobial properties.[12]

Recently, carbohydrates and their derivatives have emerged as an important tool for stereoselective synthesis and as a chiral pool for the design of chiral ligands. They are used as chiral building blocks, precursors for drug synthesis and chiral catalysts in asymmetric catalysis.[13] Carbohydrates also possess antibacterial, antiviral, antineoplastic, antiprotozoal and antifungal activities.[14,15] In carbohydrate chemistry, a large number of imines have been reported, both by reaction of sugar aldehydes with amines and by reaction of aminosugars with aldehydes.[16-18] Rawal *et al*.[19] reported the synthesis of quinozoline and its iminosugars derivatives by using sodium zeolite catalyst under microwave irradiation.

Looking at the role of pyrazole, Schiff base and carbohydrate in medicinal chemistry and the impact of ionic liquid and microwave irradiation in green chemistry, it was planned to synthesis some diverse iminosaccharide of pyrazole using ionic liquid under microwave irradiation.

Experimental

All the reactions were carried out in a domestic microwave oven (Kenstar, Model No. OM-26 EGO). TLC was carried out on silica plates precoated with silica (0.2 mm), and visualization was accomplished by iodine vapours. NMR spectra were taken on a Bruker Avance II 400 NMR Spectrometer using TMS as internal standard and chemical shift were expressed in δ ppm. The FT-IR spectra were recorded on Bruker FT-IR spectrometer. Melting points were determined in open capillaries and are uncorrected. Solvents and reagents were obtained from commercial sources and were used without further purification.

Synthesis of ionic liquid 1,3-dibutylimidazolium tetrafluoroborate [bbim][BF_4] (3)

1,3-Dibutylimidazolium bromide (0.1 mol), **(2)** was dissolved in dry acetone and sodium tetrafluoroborate (0.1 mol) was added to it. The reaction mixture was refluxed with stirring for 48 hours. After reflux, the solvent was evaporated under reduced pressure and dichloromethane

was added. Then it was again stirred for 2-3 hours. Filtration of the solution by silica filter 8-10 times afforded a viscous yellow liquid as a final product. Progress of the reaction was monitored by silver nitrate test.

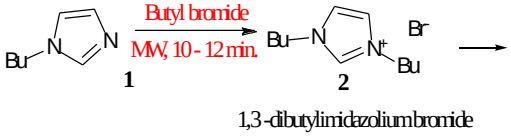

1,3-dibutylimidazolium bromide

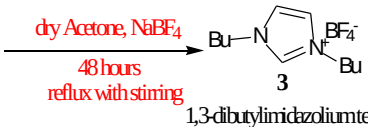

1,3-dibutylimidazolium tetrafluoroborate

IR (KBr cm^{-1}): 1645 (C=C str.), 3049 (C-H str. in olefin), 1070 (C-N str.), 2960 (C-H str. in CH_3-CH_2) and 1600 (C=N str.); ^{1}H NMR: δ ppm: 0.5 (t, 6H, CH_3), 1.20-1.30 (m, 4H, CH_2), 1.95 (m, 4H, CH_2), 2.5 (t, 2H, CH_2), 3.40 (t, 2H, CH_2), 4.6-4.7 (d, 2H, CH) and 10.41 (s, 1H, CH); ^{13}C NMR: δ ppm: 12.5, 20.0, 30.1, 57.6, 132, 121.2 and 124.

Synthesis of substituted 1-(4-aminophenyl)-3-phenylprop-2-en-1-one (6a-b)

p-Aminoactophenone (0.01 mol), **(4)** was dissolved in ethanol and benzaldehyde/p-chlorobenzaldehyde (0.01 mol), **(5a/5b)** and 10% NaOH was added to it. The reaction mixture was irradiated under microwave irradiation for 6 to 8 min at 300 W. After completion of reaction, the viscous mass formed was poured into ice cold water with vigorous stirring and left for complete precipitation. The crude product was dried and purified by recrystallization from ethanol.

1-(4-Aminophenyl)-3-phenylprop-2-en-1-one (6a)

Yield 70 %, M.P. 160-165 ˚C; $C_{15}H_{13}NO$; IR (KBr) cm^{-1}: 1630 (C=C str.), 3450 (N-H str.), 1680 (α,β-unsaturated C=O str.), 1600, 1550 and 1450 (C-C str. in aromatic ring), 3000 (=C-H str.); ^{1}H NMR (ppm): 6.55-7.40 (Ar-H, 5H, m), 7.90 (CH, d, 1H), 7.60 (CH, d, 1H) and 4.00 (NH, 2H); ^{13}C-NMR (ppm): 115.4 (2C), 122.0, 125.5 (2C), 126.7, 127.2, 129.4 (2C), 130.0 (2C), 134.5, 142.5, 151.5 and 184.5 (unsaturated C=O); Mass (m/z): 223 $[M]^{\cdot+}$

1-(4-Aminophenyl)-3-(4-chlorophenyl)prop-2-en-1-one (6b)

Yield 70 %, M.P. 140-142˚C; $C_{15}H_{12}ClNO$; IR (KBr) cm^{-1}: 1630 (C=C str.), 3400 (N-H str.), 1685 (α,β-unsaturated C=O str.), 1600, 1550 and 1450 (C-C str. in aromatic ring), 3040 (=C-H str.) and 840 (p-substituent in aromatic ring); ^{1}H NMR (ppm): 6.50-7.55 (Ar-H, 8H, m), 8.05 (CH, d, 1H), 7.60 (CH, d, 1H) and 4.10 (NH, 2H); ^{13}C-NMR (ppm): 115.0 (2C), 123.5, 125.5 (2C), 126.7, 127.6 (2C), 129.5 (2C), 131.4, 133.0 (Ar-Cl), 142.5, 151.5 and 180.5 (unsaturated C=O); Mass (m/z): 257 $[M]^{\cdot+}$,259 [M+2]

Synthesis of substituted [5-(4-aminophenyl)-3-phenyl-4,5-dihydro-1*H*-pyrazol-1-yl](pyridin-4-yl)methanone (8a-b)

Compound **(6a/6b)** (0.01 mol), isoniazide (0.01 mol), **(7)** and few drops of acetic acid were dissolved in ionic liquid. (10 mL) **(3)**.The reaction mixture was irradiated under microwave irradiation for 10-12 min. The reaction mixture was poured into ice cold water and stirred for few minutes to afford final product. The solid product was filtered and it was purified by recrystallization from ethanol.

[5-(4-Aminophenyl)-3-phenyl-4,5-dihydro-1*H*-pyrazol-1-yl](pyridin-4-yl)methanone (8a)

Yield 75 %, M.P. 120-122 ˚C; $C_{21}H_{18}N_4O$; IR (KBr) cm^{-1}: 3450 (N-H str.), 1650 (C=O str. amide), 1600, 1500 and 1450 (C-C str. in aromatic ring); ^{1}H NMR (ppm): 6.0-9.06 (Ar-H, 13H, m), 2.00 (CH_2, d, 2H) and 4.00 (CH, t, 1H, weak); ^{13}C-NMR (ppm): 38.5, 42.5, 114.5 (2C), 122.5 (2C), 126.5 (2C), 128.5 (2C), 130.0, 129.6 (2C), 131.0, 132.5, 142.5, 146.5, 150.5 (2C), 154.5 and 160.0 (C=O).

[5-(4-Aminophenyl)-3-(4-chlorophenyl)-4,5-dihydro-1*H*-pyrazol-1-yl](pyridin-4-yl)methanone (8b)

Yield 65 %, M.P. 110-112 ˚C; $C_{21}H_{17}ClN_4O$; IR (KBr) cm^{-1}: 3400 (N-H str.), 1690 (C=O str. amide), 1600, 1550, 1450 (C-C str. in aromatic ring) and 840 (p-substituent in aromatic ring); ^{1}H NMR (ppm): 6.0-9.06 (Ar-H, 12H, m), 2.5 (CH_2, d, 2H) and 4.0 (CH, t, 1H, weak); ^{13}C-NMR (ppm): 38.0, 44.5, 115.5 (2C), 123.5 (2C), 127.5 (2C), 129.0, 129.6 (2C), 130.0 (2C), 132.5, 136.6 (C-Cl), 142.5, 146.5, 150.5 (2C), 154.5 and 167.0 (C=O); Mass (m/z): 376 $[M]^{\cdot+}$,378 [M+2]

Synthesis of iminosaccharides (9a-l)

Compound **(7)** (0.01 mol) and sugar was dissolved in ionic liquid (10 mL), **(3)**. Few drops of acetic acid were added to it. The reaction mixture was irradiated under microwave irradiation for 12 min at 720 W. On completion of reaction, the resultant mass was poured into ice cold water with vigorous stirring. The solid product was filtered, washed and dried. The product was recrystallized by ethanol.

IR (KBr) cm^{-1}: 1590 (cyclic C=N str.), 1070 (C-N str.), 1680 (C=O str.), 1620, 1550, 1450 (C-C str. in aromatic ring), 1640 (open C=N str.) and 3400 (OH str.); ^{1}H NMR (ppm): 7.5 (d, 1H, CH=N), 6.0-9.06 (Ar-H, 12H, m), 2.5 (CH_2, doublet, 2H), 4.0 (CH, triplet, 1H), 4.44 – 3.67 (sugar proton) and 5.04 (OH, 1H, s). ^{13}C-NMR (ppm): 38.5, 41.5, 114.5 (2C), 122.8 (2C), 127.5 (2C), 128.5 (2C), 129.6 (2C), 130.5, 131.0, 132.5, 141.5, 146.9, 150.8 (2C), 154.6, 160.0 (C=O), 163.7 (C=N), 70.5, 73.0, 72.5, 74.0 and 65.0. Mass (m/z): 504 **(9a)**, 474 **(9b)**, 474 **(9c)**, 504 **(9d)**, 444 **(9e)**, 474 **(9f)**, 538 **(9g)**, 508 **(9h)**, 508 **(9i)**, 538 **(9j)**, 478 **(9k)** and 508 **(9l)**.

Results and Discussion

Reaction between p-aminoacetophenone with benzaldehyde/p-chlorobenzaldehyde afforded chalcones **(6a** and **6b)**. The structures of the chalcones were established on the basis of their spectral data. Appearance of IR bands at 1644 cm^{-1} for C=C, 1685 cm^{-1} for α,β-unsaturated carbonyl group and 3050 cm^{-1} for =C-H bond confirms the synthesis of chalcone. Appearance of a doublet for =C-H at δ 7.9 ppm further confirms the structure of product. The products **6a** or **6b** were confirmed by a signal at 184.5 for unsaturated carbonyl group in ^{13}C NMR. These compounds showed molecular ion (m/z) peaks at 233 and 257 and 259 (M+2).

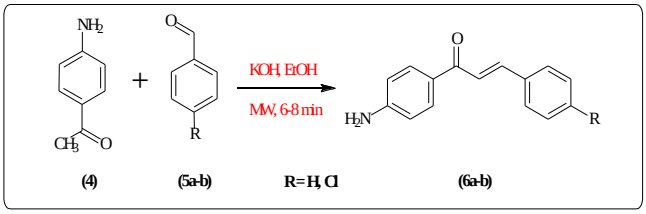

Scheme 2a. Synthesis of chalcone **6a-b**

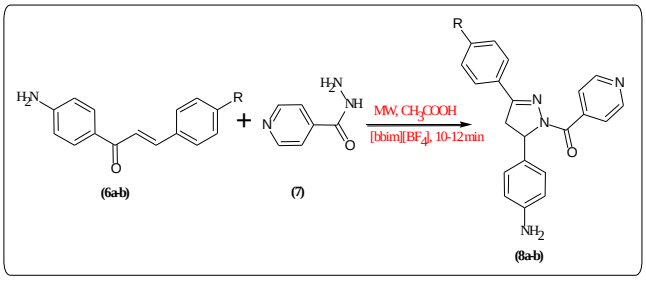

Scheme 2b. Synthesis of pyrazole derivative **8a-b**

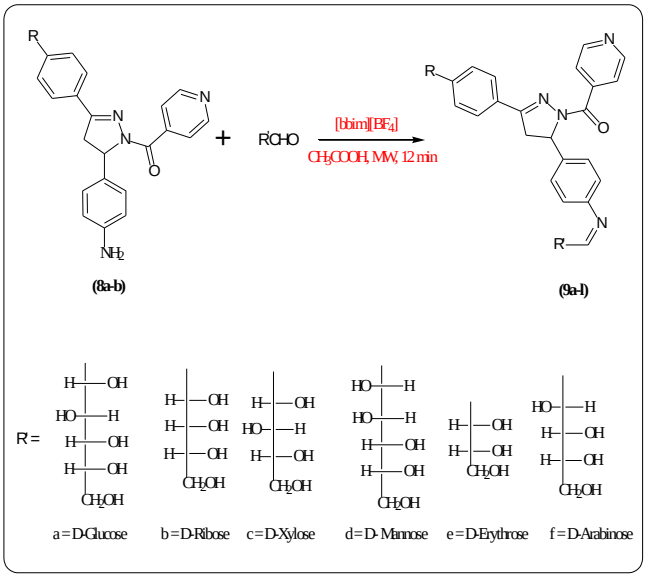

Scheme 2c. Synthesis of iminosaccharide derivative **9a-l**

The structures of compound **(8a-b)** were confirmed by the appearance of IR band at 2220 and 1650 cm^{-1} for C=N and C-N stretching frequency, respectively and disappearance of a band due to α,β-unsaturated C=O stretching frequency at 1685 cm^{-1}. In proton NMR a doublet for CH_2 and a triplet for C-H at δ 2.5 and δ 4.0 ppm, respectively also support the formation of product. In ^{13}C NMR, signals for cyclic C=N at 155.5 ppm and cyclic C-N at 46.0 ppm also support the formation of product **(8a-b)**. According to mass spectral data compounds **(8a-b)** showed molecular ion peaks at 342 and 376 and 378 (M+2) respectively, supporting the formation of product.

Reaction of substituted pyrazole derivatives **(8a-b)** with various aldoses sugars in ethanol using acetic acid as a catalyst afforded iminosaccharide (Schiff bases) with azomethine linkage **(9a-l)**. 10-12 hours of reflux was required for this process. When the same reaction was carried out in microwaves the reaction time was reduced from hours to minutes and the yield of products was also increased. But in this process, ethanol is still used, which is a pollutant and difficult to use. When imino sugars were synthesized using ionic liquid as a solvent under microwave irradiation, reaction time was reduced and the yield of product was also increased.

The structures of the final products were established on the basis of their spectral data. Disappearance of two bands at 3400 and 3250 cm^{-1} due to $–NH_2$ stretching (symmetric and asymmetric) and appearance of bands in the region of 3400-3450 cm^{-1} for OH stretching and 1630-1640 cm^{-1} corresponding to C=N stretching confirmed the assigned structure of iminosaccharides. In ^1H NMR spectrum, the absence of signal at δ 5.80-5.86 due to proton of NH_2 and presence of a doublet for imino protons (CH=N) at δ 8.52 and a singlet for OH proton at δ 5.04 favoured the formation of final product **(9a-l)**. Signal of proton of sugar chain were congregated with the solvent absorption in a broad signal at δ 4.45-3.64. The final products were also confirmed by ^{13}C NMR, where appearance of signal at 163.5 ppm for imine and 65-72.0 ppm for C-OH supported the proposed structures. Further, mass spectrum also in favour of the structure of iminosaccharides by the molecular ion peak (m/z) at 504, 474, 444, 538 and 508. Physical data of all synthesized compound have been given in Table 1.

Table 1. Physical data of synthesized compounds

Com-pounds	Molecular formula	Molecular weight	Yield, %	Melting point, ˚C
6a	$C_{15}H_{13}NO$	233	70	160-165
6b	$C_{15}H_{12}ClNO$	257	70	140-142
8a	$C_{21}H_{18}N_4O$	342	75	120-122
8b	$C_{21}H_{17}N_4OCl$	376	65	110-112
9a	$C_{27}H_{28}N_4O_6$	504	80	100-102
9b	$C_{26}H_{26}N_4O_5$	474	75	150-152
9c	$C_{26}H_{26}N_4O_5$	474	82	140-142
9d	$C_{27}H_{28}N_4O_6$	504	70	165-168
9e	$C_{25}H_{24}N_4O_4$	444	82	200-210
9f	$C_{26}H_{26}N_4O_5$	474	75	185-188
9g	$C_{27}H_{27}N_4O_6Cl$	538	80	170-172
9h	$C_{26}H_{25}N_4O_5Cl$	508	75	180-182
9i	$C_{26}H_{25}N_4O_5Cl$	508	79	130-132
9j	$C_{27}H_{27}N_4O_6Cl$	538	85	260-262
9k	$C_{25}H_{23}N_4O_4Cl$	478	80	120-122
9l	$C_{26}H_{25}N_4O_5Cl$	508	80	190-192

 DOI: 10.17628/ecb.2014.3.1107-1111

Table 2. Microbial activity of synthesized compound (minimum inhibition concentration) (mg mL^{-1})

Com-pounds	R/R'	Bacteria (MIC) (mg mL^{-1})				Fungi (MIC) (mg mL^{-1})		
		E. coli	*P. aeuroginosa*	*S. aureus*	*S. pyogenus*	*C. albicans*	*A. niger*	*A. clavatus*
8[a]	R=H	250	200	250	200	500	1000	1000
8b	R=Cl	125	200	250	125	500	500	1000
9a	D-Glucose	200	125	200	250	250	1000	500
9b	D-Ribose	100	200	125	200	1000	>1000	1000
9c	D-Xylose	100	250	250	200	>1000	1000	500
9d	D- Mannose	100	200	250	125	1000	1000	500
9e	D-Erythrose	100	200	200	250	500	500	500
9f	D-Arabinose	125	125	200	125	1000	>1000	1000
9g	D-Glucose	100	250	100	200	250	500	1000
9h	D-Ribose	100	125	200	125	500	1000	1000
9i	D-Xylose	62.5	250	200	250	1000	1000	1000
9j	D- Mannose	200	125	200	100	1000	500	500
9k	D-Erythrose	100	125	250	100	250	500	1000
9l	D-Arabinose	125	100	125	125	500	1000	1000
Standards								
1	Ampicillin	100	----	250	100	-	-	-
2	Greseofulvin	-	-	-	-	500	100	100

Biological activities

Representative synthesized compounds were screened *in vitro* for their antimicrobial activities against Gram-negative bacteria *E. coli* and *P. aeruginosa* and Gram-positive bacteria *S. aureus* and *S. pyogenus*. The synthesized compounds were also screened against three strains of fungi (*A. niger*, *C. albicans* and *A. clavatus*). Antibacterial activity was evaluated by agar cup plate method and antifungal assay was carried out by disc diffusion method using Ampicillin (antibacterial) and Greseofulvin (antifungal) as standard drugs respectively.

The synthesized iminosugars have excellent antibacterial, but relatively poor antifungal activity. Compound **(9i)** shows excellent antimicrobial activity against *E.coli* bacteria strain and also good activity against other bacteria strain. Compounds **(9a)**, **(9g)** and **(9k)** show good fungicidal activities against *C. albicans.* Compounds **(9j)**, **(9d)** and **(9e)** show moderate activity against all the three fungi strain. Almost all the titled compounds exhibited weak, moderate or high antimicrobial activity and moderate to weak antifungal activity (Table 2)

Acknowledgement

We are thankful to Prof. Suresh C. Ameta for giving valuable suggestions during the progress of the work and Head, Department of Chemistry, M.L. Sukhadia University, Udaipur for providing laboratory facilities. Our thanks are also due to the Director, SAIF Chandigarh, India for providing spectral data and Micro Care Laboratory Surat (Guj.) for providing antimicrobial activity (MICs).

References

[1]Rogers, R. D., Seddon, K. R., *Science*, **2003**, *302*, 792.

[2]Sheldon, R., *Green Chem.*, **2005**, *7*, 267.

[3]Earle, M. J., Esperanc, J. M. S. S., Gilea, M. A., Lopes, J. N. C., Rebelo, L. P. N., Magee, J. W., Seddon, K. R., Widegren, J. A., *Nature*, **2006**, *439*, 831.

[4]Sakaebe, H., Matsumoto, H., *Electrochem. Commun.*, **2003,** *5*, 594.

[5]Plechkova, N. V., Seddon, K. R., *Chem. Soc. Rev.*, **2008**, *37*, 123.

[6]Pimerova, E. V., Voronina, E. V., *Pharm. Chem. J.*, **2001**, *35*, 18.

[7]Michon, V., Du Penhoat, C. H., Tombret, F., Gillardin, J. M., Lepagez, F., Berthon, L., *Eur. J. Med. Chem.*, **1995,** *30*, 147.

[8]Park, H. J., Lee, K., Park, S., Ahn, B., Lee, J. C., Cho, H. Y., Lee, K. I., *Bioorg. Med. Chem. Lett.*, **2005,** *15*, 3307.

[9]Bouabdallah, I., Barret, L. A., Zyad, A., Ramadan, A., Zidane, I., Melhaoui, A., *Nat. Prod. Res.*, **2006,** *20*, 1024.

[10]Tewari, A. K., Mishra, A., *Bioorg. Med. Chem.*, **2001**, *9*, 715.

[11]Dhar, D. N., Taploo, C. L., *J. Sci. Ind. Res.*, **1982**, *41*, 501.

[12]da Silva, C. M., da Silva, D. L., Modolo, L. V., Alves, R. B., de Resende, M. A., Martins, C. V. B., de Fatima, A., *J. Adv. Res.*, **2011**, *2*, 1.

[13]Dieguez, M. Ramies, O. Ruiz, A. Diaz, Y. Castillon, S., Claver, C., *Coord. Chem. Rev.*, **2004,** *248*, 2165.

[14]Nogueira, C. M., Parmanhan, B. R., Farias, P. P., Correa, A. G., *Rev. Virtual Quim.*, **2009**, *1(2)*, 149.

[15]Wong, C. H., Ed., Carbohydrate-based Drug Discovery, *Wiley VCH, Weinheim, Germany*, **2003.**

[16]Costamagna, J., Barroso, N. P., Matsuhiro, B., Villagran, M., *Inorg. Chim. Acta.*, **1998**, *273*, 191.

[17]Costamagna, J., Lillo, L. E., Matsuhiro, B., Noseda, M. D., Villagran, M., *Carbohydr. Res.*, **2003**, *338*, 1535.

[18]Perez, E. M. S., Ávalos, M., Babiano, R., *Carbohydr. Res.*, **2010,** *345*, 23.

[19]Rawal, M. K., Tiwari, U., Parashar, B., Ameta, R., Punjabi, P. B., *Indian J. Chem.*, **2011**, *50B*, 734.

Received: 12.11.2014.
Accepted: 14.01.2015.

CARBON DIOXIDE GEOSEQUESTRATION: OPTIMUM GAS INJECTION TEMPERATURE REQUIRED FOR CAP ROCK GEOMECHANICAL INTEGRITY

Adango Miadonye[a] and Mumuni Amadu[b]

Keywords: Carbon dioxide, tensile failure, shear failure, steady state, geosequestration, diffusivity, thermophysical.

In the efforts to mitigate the unprecedented anthropogenic carbon dioxide presence in the atmosphere, the decision to store this greenhouse gas in geologic repositories has received global appreciation with assured technical and financial viability. The implication is that the injection temperature of flue gas in the potential geologic sites will be typically those encountered in combustion power plants. This, obviously has a geomechanical consequence considering the fact that heat transferred from the aquifer to the low permeability cap rock will cause excessive pore pressure build up due to poor pore pressure diffusion characteristics of these rocks. While these low permeability rocks are required to provide stratigraphic trapping mechanisms such excessive pore pressure build up can result in compromising the geomechanical integrity. This article has used heat transfer theories and geomechanical concepts to obtain steady state temperature distribution in cap rocks for temperatures ranging from 50 to 800^{0}C. In so doing, cap rock critical temperatures for tensile and shear failures have been established for a potential on-site gas injection into saline aquifers.

* Corresponding Authors
E-Mail: adango_miadonye@cbu.ca
[a] Department of Chemistry, Cape Breton University, P.O. Box 5300, Sydney, NS, Canada.
[b] Department of Process Engineering and Applied Science, Dalhousie University, Halifax, NS, Canada.

Introduction

In the deeper zones of the sedimentary basin that have for geologic years been cut off from oxygen supply there exist formations containing ultra-high saline waters. The saline formations are natural, salt-water-bearing intervals of porous and permeable rocks that occur beneath the level of potable groundwater. On the basis of mean global geothermal and/or geostatic gradient it is estimated that such a geologic repository must be located at least 2500 ft below mean sea level.[1,2] This mean depth ensures a supercritical state where the gas occupies less volume than in the non-super critical state. One geologic condition for such a deep sequestration is the existence of thickness of rocks or cap rocks above the potential injection zones to act as a geologic seal.

Combustion power plants are the most single stable and intensive carbon dioxide emitters. The CO_2 concentration depends on whether the fuel is gas or coal, on the particular power station technology notably pulverised coal plants (PF), natural gas combined cycle plants and integrated combined gas cycle plants and the age of the plant. In all combustion technologies flue gas production with different concentrations of carbon dioxide is measured per megawatt hour of electrical energy generation. Natural gas combined cycle has the lowest carbon emission while the pulverized coal technology generates the greatest carbon concentration in the flue gas.[3] To mitigate global warming by carbon emission, carbon dioxide capture and geological storage is widely seen as a cost effective way to reduce industrial CO_2 emissions into the atmosphere. While the capture of anthropogenic carbon dioxide from combustion power plants and its geological sequestration have been universally accepted as a technically and economically feasible mitigating step in reducing global warming the need to embark on cost effective and environmentally friendly carbon sequestration is essential. This is because carbon capture and its ultimate geological storage is an additional cost to the power provider unlike the case where carbon sequestration through carbon dioxide enhanced oil recovery is a value added oriented project in the petroleum industry.

In the carbon dioxide capture and storage chain the most single expensive step is that connected to capture. The global availability of the saline aquifers makes it possible for future sequestration projects to be located at injection sites and this has the obvious advantage that flue gas captured from coal combustion processes can be injected directly into saline aquifers. This option reduces transportation cost. The high temperatures of the injection gas will result in geomechanical problems in the cap rock of the saline aquifer that is supposed to offer long term hydrodynamic trapping. It is also necessary to determine the extent to which direct flue gas from the combustion plant will have to be cooled to subcritical temperatures required for avoiding two phase flow in the well bore that can lead to poor injectivity in the injection interval due to gravity segregation.

To be able to determine the optimum temperature of injection under all cases of carbon dioxide sequestration in a chosen aquifer there is the need to scientifically address the cap rock geomechanical problem using established principles of failure criteria in geomechanics. The aim of this paper is to theoretically determine the conditions under which a cap rock will fail under tensile loading due to the thermal pressurization of its pore-fluid. This theoretical condition that will utilise rock strength properties and thermophysical property data in the formulation will be used in conjunction with heat transfer theories in order to determine optimum temperature conditions of injection for a particular chosen deep saline aquifer.

Theoretical Development

For heat transfer processes governed by pure diffusion a characteristic diffusive time lag parameter[4] can be defined for the system as the time required for steady state heat transfer conditions where temperature is a function only of space coordinate in the system. Normally the smaller the coefficient of heat diffusion the bigger the diffusive time lag. In the case of carbon dioxide injection into saline aquifers, two mechanisms of heat transfer can be distinguished. They are heat transfer by convective processes involving mass transfer and heat transfer by diffusion that depends on the effective diffusion coefficient of the system. For a typical carbon sequestration projects seeking to reduce global warming the anticipated high injection rates, coupled with the conventional requirement for higher injection rates required for limiting capillary forces effect in the two face flow system will result in a convective dominated heat transfer. The steady state heat transfer in such a system will be achieved well within the time frame of fluid injection and possibly earlier than will be expected for diffusive dominated heat transfer. Since the source of heat transfer to the cap rock is the heat of the injected fluid in the aquifer the temperature profile field of the aquifer is the governing factor for that of the cap rock. Consequently, the steady state temperature of the cap rock that is required for obtaining knowledge about final pore pressures and stress conditions of the cap rock will be established by the steady state temperature field of the aquifer. This requirement justifies the steady state temperature computations in this paper using existing steady state solutions for the combined aquifer and cap rock heat transfer problem.

Tensile Failure Criterion

The following are the assumptions considered pertinent for the derivation of tensile and shear failure under undrain loading:

1. The only source of stresses (vertical and horizontal principal stresses) in the shale column is that derived from the overburden material. In this regard stresses due to tectonic forces are neglected.

2. for simplicity a normally pressure shale lithology or column is assumed

3. Mean global values of hydrostatic and geostatic pressure gradients are considered to be 0.46 and 1 psi per foot respectively

4. The aquifer is very extensive and not confined so that injected gas rising to the top of the formation will migrate under the cap rock without exerting significant pressure at the base of the cap rock to constitute a source of stress in the shale column.

5. The injection of supercritical carbon dioxide into a saline aquifer constitutes a two phase flow called drainage. The hydrodynamics of such a system depends on dimensionless parameter called gravity number which is the ratio of buoyancy forces to viscous forces. A high value of this parameter means that buoyancy forced dominant and this will cause injected gas to rise to the top of the aquifer earlier before injection stops. On the contrary a low value means viscous dominant hydrodynamics which will cause injected gas to predominantly move in a radial direction. We assume a high injection rate characteristic of carbon geosequestration in response to high carbon dioxide generation from a medium power plant. Under such conditions stresses on the base of the cap rock which could be transmitted to the cap rock will be negligible.

For fluid injection under non-isothermal conditions total horizontal stress consists of the effect of fluid pressure and thermal stress effect given as:

$$\sigma_{hT}=\frac{1-2\nu}{1-\nu}\Delta\sigma_v+\frac{\nu}{1-\nu}\Delta\sigma_z+\frac{\beta E}{1-\nu}\Delta T+\sigma_{oh} \qquad (1)$$

where σ_T, σ_{oh}, σ_v, ν are total horizontal stress, initial horizontal stress, vertical stress and Poisson's ratio, respectively.

It has been reported[5,6] that the change in vertical stress is exactly equal to the increase in pore fluid pressure due to thermal loading. This is given as:

$$\Delta P_p=\frac{\left[\alpha_S(1-\varphi)+\varphi\alpha_f\right]}{c_w\varphi}\Delta T \qquad (2)$$

The horizontal stress increase due to thermal loading of pore fluid is given by using the Poisson's effect as:

$$\Delta P_p=\frac{1-2\nu}{1-\nu}\frac{\left[\alpha_S(1-\varphi)+\varphi\alpha_f\right]}{c_w\varphi}\Delta T \qquad (3)$$

α_S, α_f, χ_w, φ, ΔP_p, ΔT are thermal expansivity of rock solid grains, thermal expansivity of fluid, pore-water compressibility, porosity of sediment, pore pressure change and temperature change respectively.

Initial horizontal stress is given by:

$$\sigma_{oh}=\frac{1-2\nu}{1-\nu}G_{st}D \qquad (4)$$

where G_{st} and D are mean value of geostatic gradient (1 psi/foot) and depth respectively.

Substitution into Eqn. 2 gives total horizontal stress as:

$$\sigma_{hT}=\frac{1-2\nu}{1-\nu}\frac{\left[\alpha_s(1-\phi)+\phi\alpha_f\right]}{c_w\phi}\frac{\beta E}{1-\nu}\Delta T+\frac{1-2\nu}{1-\nu}D \qquad (5)$$

 DOI: 10.17628/ecb.2014.3.1112-1118

For tensile failure the following stress conditions[7] must be met:

$$P_p \succ T_p + \sigma_h \quad (6a)$$
$$P_p \succ T_n + \sigma_v \quad (6b)$$

where P_p, T_h, T_v, σ_h, σ_v are pore pressure, tensile strength in the horizontal direction, tensile strength in the vertical direction, horizontal stress and vertical stress respectively. Eqn. (6a) defines tensile failure in the horizontal direction while (6b) defines tensile failure in the vertical direction. The sum of the stress components on the right hand sides of Eqn. (6a) and (6b) gives total stresses, horizontal and veridical stresses respectively. For failure in the horizontal direction the failure stress and pore pressure condition must therefore be met. This gives:

$$\sigma_{hT} = \frac{1-2\nu}{1-\nu}\frac{\left[\alpha_s(1-\phi)+\phi\alpha_f\right]}{c_w\phi}\Delta T + \frac{\beta E}{1-\nu}\Delta T + \frac{1-2\nu}{1-\nu}D \quad (7)$$

For a normal pressure basis and for tectonically relaxed basin[8] pore pressure after temperature change is given by:

$$P_p = 0.46DG_{st} + \left[\frac{\alpha_s(1-\phi)+\phi\alpha_f}{c_w\phi}\right]\Delta T \quad (8)$$

Substitution of this into Eqn. (6) for the failure condition gives Eqn. (9)

$$0.46D + \left[\frac{\alpha_s(1-\phi)+\phi\alpha_f}{\phi c_w}\right]\Delta T \succ \frac{1-2\nu}{1-\nu}\frac{\alpha_s\left[(1-\phi)+\phi\alpha_f\right]}{c_w\phi}\Delta T + \frac{\beta E}{1-\nu}\Delta T + \frac{1-2\nu}{1-\nu}G_{st}D + T_p \quad (9)$$

Vertical stress is given by:

$$\sigma_v = G_{st}D \quad (10)$$

where G_{st}= geostatic gradient psi/foot

The following quantity will hence forth be defined:

$$\mu = \frac{\left[\alpha_s(1-\phi)+\phi\alpha_f\right]}{c_w\phi} \quad (11)$$

Substitution of Eqn. (11) into failure condition gives:

$$0.46D + [\mu]\Delta T \succ \frac{1-2\nu}{1-\nu}\mu + \frac{\beta E}{1-\nu}\Delta T + \frac{1-2\nu}{1-\nu}D + T_p \quad (12)$$

Assuming pore pressure is just equal to total stress then the failure condition gives:

$$0.46D + [\mu]\Delta T = \frac{1-2\nu}{1-\nu}\mu + \frac{\beta E}{1-\nu}\Delta T + \frac{1-2\nu}{1-\nu}D + T_p \quad (13)$$

Grouping the temperature change terms gives:

$$\Delta T\left[\mu - \frac{1-2\nu}{1-\nu}\mu - \frac{\beta E}{1-\nu}\right] = \frac{1-2\nu}{1-\nu}G_{st}D + T_p - 0.46D \quad (14)$$

Using a value of Poisson's ratio of 0.2 for lean shale[9] and rearranging this equation for temperature change gives:

$$\Delta T = \frac{0.7G_{st}D + T_p - 0.46D}{\left[0.30\mu - \frac{\nu}{1-\nu}\beta E\right]} \quad (15)$$

Typical value for the thermal expansivity of shale materials[9] (in $1/^0$C) is:

$$\beta = \alpha_s = 0.8*10^{-4}; \qquad \alpha_f = 10^{-4}$$

and the compressibility of brine[10] is (in psi^{-1}) :

$$c = 03.6*10^{-6}$$

Using a porosity of 0.3 for typical North Sea shales and formation water compressibility values gives the value of μ defined in Eqn. (11) as:

$$\mu = \frac{\left[0.8*10^{-4}(1-0.3)+0.3*10^{-4}\right]}{3.6*10^{-6}*0.3} = \frac{0.56*10^{-4}+0.3*10^{-4}}{1.08*10^{-6}} = \frac{86*10^{-6}}{1.08*10^{-6}} = 79.6\ psi\ ^oC^{-1} \quad (16)$$

Using a value of Poisson's ratio of 0.2 gives:

$$\frac{1-2\nu}{1-\nu} = \frac{1-2*0.2}{1-0.2} = 0.70 \quad (17)$$

Substituting values into the temperature change Eqn. (15) and using the tensile strength value of shale 8.6 MPa (1247 psi)[11] gives:

 DOI: 10.17628/ecb.2014.3.1112-1118

$$\Delta T = \frac{[0.7]D + 1247 - 0.46D}{\left[79.6*0.30 - \frac{1}{1-0.2}0.8*10^{-4}*2.9*10^{4}\right]} = \frac{0.24D + 1247}{23.88 - 2.9} = 59.43 + 0.011D \quad (18)$$

Eqn. (18) of this work gives the threshold temperature change required to cause horizontal tensile failure conditions at a given depth during thermal pressurization of cap rock pore fluid in response to heat conduction from the injected fluid in the aquifer into the overlying cap rock. Given the local value of mean geostatic stress gradient the change in temperature can be calculated using typical values of cap rock tensile stress strength, thermal expansivity of pore fluid and rock material and Young modulus of rock grains. The equation shows that the critical temperature change is a linear function of depth.

Temperature change due to Depth in Cap Rock Interval

By using the mean local geothermal gradient the temperature at a given depth is calculated as:

$$T_D = T_{suf} + G_{th}D \quad (19)$$

where T_D, T_{suf}, $G_{th}D$ are temperature at a given depth, surface temperature and mean local geothermal gradient respectively.

Assuming this was the depth temperature before temperature increase, thus, adding this to the critical temperature change gives:

$$T_{Der} = T_{sf} + G_{th}D + 59.43 + 0.011D \quad (20)$$

This temperature, expressed by Eqn. (20), gives the critical temperature at a given depth in the cap rock; where T_{Der}= critical temperature at a given depth.

Since Eqn. (20) addresses failure in low permeability cap rocks where undrain conditions persist under thermal loading the critical temperature and the threshold temperature change can be developed for different shales with different tensile strength characteristics.

Eqn. (18) through (20) will be used in conjunction with steady state temperature calculations in order to determine the technical feasibility of injecting direct flue gas with different outlet temperatures from an on-site combustion power plant into a saline aquifer capped by low permeability shale with a tensile strength value similar to that used for obtaining Eqn. (18).

Critical Temperature for Shear Failure

For a given temperature change the resulting pore pressure at a given depth after temperature change is given by:

$$\sigma_h' = 0.75G_{st}D + \frac{1}{1-\nu}\alpha_s E\Delta T - 0.46H - \frac{\left[\alpha_s(1-\phi) + \phi\alpha_f\right]}{\phi c_w}\Delta T \quad (21)$$

where: α_s, α_f, ϕ are thermal expansivity of solid, thermal expansivity of fluid and porosity respectively.

Vertical and horizontal effective stresses are given by:

$$P_{H_2O} = P_i + \frac{\left[\alpha_s(1-\phi) + \phi\alpha_f\right]\Delta T}{c_w\phi} \quad (22)$$

$$\sigma_z' = G_{st}D - 0.46H - \frac{\left[\alpha_s(1-\phi) + \phi\alpha_f\right]}{c_w\phi}\Delta T \quad (23)$$

The condition[8] for shear failure is given by Eqn. (2) as:

$$\frac{\sigma_v' - \sigma_h'}{2} = C\cos\varphi + \frac{\sigma_v' - \sigma_h'}{2}\sin\varphi \quad (24)$$

where C, φ are cohesion and friction angle, respectively.

Solving for the difference in the two stresses in (24) gives:

$$\left(\sigma_v' - \sigma_h'\right) = \frac{2C\cos\varphi}{(1-\sin\varphi)} \quad (25)$$

The difference between Eqn. (24) and (25) gives:

$$\left(\sigma_v' - \sigma_h'\right) = 0.25G_{st}D - \frac{1}{1-\nu}\alpha_s\Delta G \quad (26)$$

G= shear modulus, (psi).

Substituting the values in Eqn. (26) into (25) and solving for the temperature change required for shear failure at a given depth of the earth gives:

$$\Delta T = \left[0.25G_{st}D - \frac{2C\cos\varphi}{1-\sin\varphi}\right]\left[\frac{1}{1-\nu}\alpha_s G\right]^{-1} \quad (27)$$

Eqn. (27) gives the temperature change required for shear failure. To link this to depth requires using Eqn. (19) as:

$$T_{cD} = T_0 + G_{th}D + \left[0.25G_{st}D - \frac{2C\cos\varphi}{1-\sin\varphi}\right]\left[\frac{1}{1-\nu}\alpha_s G\right]^{-1} \quad (28)$$

 DOI: 10.17628/ecb.2014.3.1112-1118

To use Eqn. (27) requires inputs of shale strength properties in terms of cohesion C and friction angle phi. Using extensive data base, Lal[12] developed a correlation for compressional wave velocity in shales as:

$$\sin\varphi = \frac{V_p - 1}{V_p + 1} \quad (29)$$

$$C = \frac{5(V_p - 1)}{\sqrt{V_p}} \quad (30)$$

where V_p=compressional wave velocity in shale (km s^{-1}).

Compressional wave velocity in shale is given as[13] V_p = 2124 m s^{-1} = 2.124 km s^{-1}.

Substitution of compressional wave velocity in Eqn. (29) and (30) gives values of cohesion and friction angle as:

$$\sin\varphi = \frac{2.124 - 1}{2.124 + 1} = 0.35$$

This gives friction angle as: 20.5°

$$C = \frac{5(2.124 - 1)}{\sqrt{2.124}} = 3*8\ MPa$$

Substitution of values including the shear modulus of Shale[14] gives temperature change from Eqn. (27) as:

$$\Delta T = \left[0.25D - \frac{2*0.94*2465.6}{1 - 0.35}\right][2.9]^{-1} = [0.25D - 3012][2.9^{-1}] = 0.086D - 103 \quad (31)$$

Eqn. (31) gives the final equation for calculating the temperature change required to cause shear failure in the shale column. Linking this to depth gives:

$$T_{cD} = T_{sf} + G_{th}D + 0.086D - 103 \quad (32)$$

Discussion

To gain an insight into the technical suitability of direct flue gas injection, this investigation has considered the problem of cap rock thermal pressurization in relationship to tensile failure criterion encountered in geomechanics. This analytical consideration of the thermomechanical problem has led to the derivation of equations for predicting tensile and shears failures where stresses in the cap rock are due solely to thermal pressurization of the resident formation fluid.

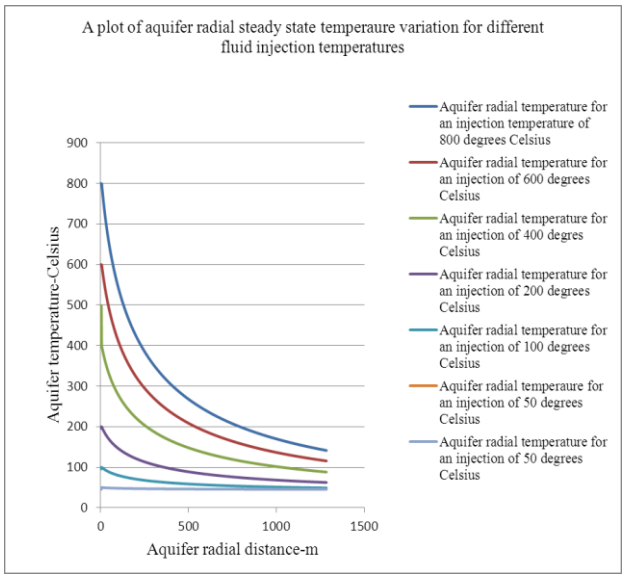

Figure 1. A plot of steady state aquifer radial temperature variation for different fluid injection temperatures.

To test the equations, a model aquifer at a depth typical of supercritical conditions of carbon dioxide storage has been used. For time frames typical of carbon geosequestration projects, steady state temperature fields and stresses are those of thermomechanical concern for the cap rocks. Accordingly, the steady state temperature field of the aquifer was used to deduce that of the cap rock. By using the derived equation that links critical temperature to depth in the cap rock it has been possible to determine the safe temperature required for maintaining the geomechanical integrity of the cap rock to avoid failure in tension and shear. In this work, it has been assumed that the potential aquifer is an open one with quite an appreciable radial extent and permeability such that the injected gas through the entire interval will flow laterally with negligible pressure against the cap rock. In this way stress changes in the cap rock are due only to thermal pressurization of pore fluid which could cause *in-situ* stress perturbation.

Figure 1 shows the temperature field of the aquifer for different temperatures of fluid injection. Based on the depth to the model aquifer a mean local geothermal gradient of 30 degrees per kilometre the initial ambient temperature of this system is calculated to be 41^0C using the depth to the midpoint of the interval. The average initial temperature of the upper cap rock was similarly calculated to be 34^0C. The figure shows that for injection temperatures far above the initial ambient temperature the steady state temperatures are far above the systems initial temperature except for injection at 50 and 100^0C. The steady state temperature obtained depends on the carbon dioxide injection temperature. The higher the injection temperature, the larger the exponential drop in the temperature to attain steady state temperature.

Figure 2, which is the most important geomechanically, indicates a plot of the steady state temperature of the cap rock versus depth in the cap rock for a radial temperature of 2.15 meters from the injection well. This location has been selected to determine the effect of heat on the near well bore environment because they are areas that are typically subjected to higher temperatures.

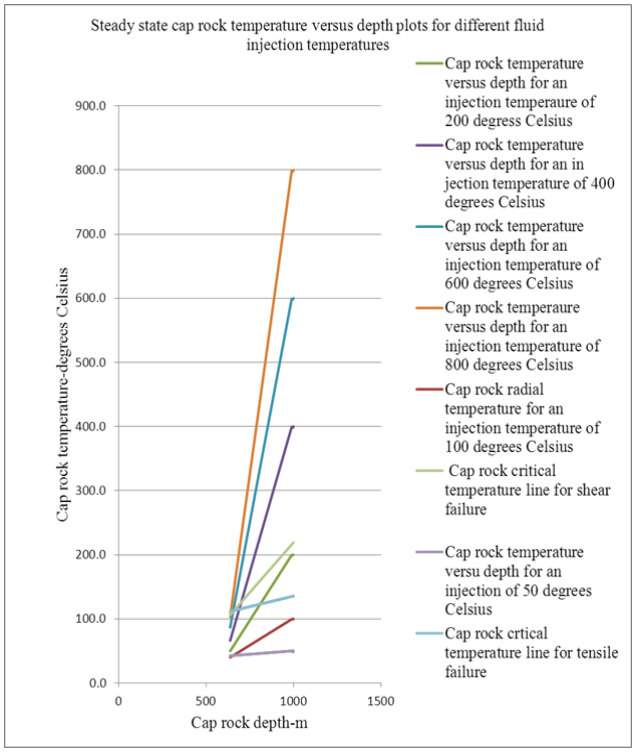

Figure 2. A plot of steady state temperature versus depth for the cap rock at a radial distance of 2.15 metres from sand face.

The figure shows that during steady state heat transfer a linear relationship exists between temperature and depth in the cap rock interval. The figure also shows a plot of the critical temperature lines for tensile and shear scenarios based on Eqn. (20) and (18). The critical temperatures are seen to be increasing with depth in the cap rock and this is quite consistent with the derivation of the thermal failure criterion because the earth stresses involved are horizontal stresses which increase with depth. The most important observation or finding is that all the injection temperatures except those at 50 and 100^0C will result in cap rock tensile failure. This is due to the fact that the plots for all these temperatures lie above the critical temperature lines for both tensile and shear failures determined by this study except those for 50 and 100^0C lines.

The study also shows that as far as this aquifer is concerned an injection temperature of 200^0C will be suitable as far as the upper parts of the cap rock is concerned but failure will occur close to the aquifer interval. One thing consistent about Figure 2 as far as failure in geomechanics is concerned is that it predicts lower failure temperatures for tensile than for shear and that is why the shear failure line lies above the tensile failure. This fact has been established in geomechanics relating where rocks are found to be weaker in tension than in shear[8]. The potential candidates for geological repositories for carbon dioxide sequestration include depleted oil and gas reservoirs. Among these reservoirs there are those that were developed using thermal recovery methods that are found to exist at depth typical of supercritical carbon dioxide existence. Most of these were developed using steam or hot water with temperatures above 200^0C. Judging from the findings in this study these types of depleted oil reservoirs must be thoroughly investigated for their intact geomechanical integrity before being considered as potential geologic repositories worthy of being included in the inventories of geological carbon sinks.

Conclusion

The following inferences are obtained from this work:

1. By virtue of their global availability and promising global carbon storage capacities saline aquifers are top ranked as geological repositories for long term carbon dioxide storage.

2. Under normal circumstances the well head temperature of injected carbon dioxide depends on the source with on-site temperatures being invariably those of ambient ones except in cases where they are maintained at subcritical with regard to temperature to avoid liquefaction in the well bore.

3. The excess heat of direct flue gas could cause thermomechanical problems in saline aquifer cap rock formations which could compromise the anticipated long term hydrodynamic trapping capabilities of these formations.

4. The work presented analytical equations based on thermomechanical related tensile and shear failure criteria which provide a guide to obtaining information about the temperature and pore pressure changes required for tensile and shear failure to occur due to thermal pressurization of pore-fluid in response to high temperature direct flue gas injection.

5. The optimum temperature to inject CO_2 is that at or close to the aquifer temperature and this is the ideal temperature required to maintain cap rock geomechanical integrity.

6. It also serves as a guide to determining the optimum temperature required for injection for all purposes of cap rock integrity due to thermal pressurization problems. In this regard where gas is to be injected from an onsite power plants the temperature does not need to be cooled to that of the aquifer. To reduce cost related to heat exchanger meant for heat extraction from flue gas the temperature can be cooled to near that of the aquifer but commensurate with the geomechanical integrity requirement of the cap rock which in this study is 150^0C, 100^0C, and 109^0C above the aquifer temperature.

ACKNOWLEDGMENT

The authors wish to acknowledge the technical and financial supports provided by Cape Breton University Office of Research and Graduate Studies and Dalhousie University.

Greek Letters

σ_T = total horizontal stress-psi

σ_{oh} = initial horizontal stress-psi

σ_v= vertical stress-psi

ϕ= porosity-fraction

φ= friction angle-degrees

α_S= thermal expansivity of solid- $^oK^{-1}$

α_f= thermal expansivity of fluid- $^oK^{-1}$

σ'_h= horizontal effective stress-psi

σ'_v= vertical effective stress-psi

ν= Poison ratio

References

[1]Rice, R. G., Do, D. D., *Applied Mathematics and Modeling for Chemical Engineers*, John Willey and Sons Inc., **1995.**

[2]Benson, S. M., Cole D., *Elements*, **2008**, *4*, 325–331.

[3]Nguyen, D. N., Allinson, W. G., *The Economic of CO_2 Capture and Geological Storage*, (SPE Paper No. 77810) SPE International, **2002**.

[4]Frisch, H. L., *J. Phys. Chem*., **1957**, *6*, 93–95.

[5]Palciauskas, V. V., Domenico, P. A., "*Water Resourc. Res.*, **1982**, 18, 281-290.

[6]Amadu, M., Miadonye, A., *Eur. Chem. Bull.*, **2014**, *3*, 1047-1054.

[7]Cogsgroove, J. W., *Geol. Soc., Spec. Publ.*, **1995**, *92*, 187-196.

[8] Aadnoy, B. S., *Modern Well Contro.*, 2nd Ed., CRC Press, **2010.**

[9]https://www.spec2000.net/10-closurestress.

[10]Eseme, E., Urai, J. L., Krooss, B. M., Littke, R., *Oil Shale*, **2007**, *24*, 159-174.

[11] Rijken, P., Cook, M., *Tectonophysics*, **2007**, 117-133.

[12]Lal, M., Shale Stability: *Drilling Fluid Interaction and Shale Strength*, (SPE Paper No. 54356) SPE Latin American and Caribbean, **1999.**

[13]http://answers.yahoo.com/question/index?qid=20060926005806AA9feUJ

[14]Diane L. J., Mechanical and Acoustical Properties of Sandstones and Shales, Ph.D. Thesis, Stanford University, **1991**.

Received: 29.12.2014.
Accepted: 17.01.2015.

ALCOHOLYSIS OF *N*-ACETOXY-*N*-ALKOXYCARBAMATES. SYNTHESIS OF *NH-N,N*-DIALKOXYAMINES FROM *N, N*-DIALKOXYCARBAMATES

Shtamburg V. Georgievich,[a] Anishchenko A. Alexandrovich,[b] Shtamburg V. Vasilievich,[c] Tsygankov A. Valerievich[d] and Kostyanovsky R. Grigorievich[e]

Keywords: Nucleophilic substitution at nitrogen, N-acyloxy-N-alkoxycarbamates, alcoholysis, N,N-dialkoxycarbamates, hydrolysis, NH-N,N-dialkoxyamines.

The alcoholysis of N-acetoxy-N-alkoxycarbamates by methanol or ethanol at 20 – 40 °C yields N,N-dialkoxycarbamates and acetic acid. At the lower temperature the competitive formation of N,N'-bis(alkoxycarbonyl)-N,N'-bis(alkoxy)hydrazines can occur. The alkaline hydrolysis of *N,N*-dialkoxycarbamates yields *N*H-*N,N*-dialkoxyamines.

* Corresponding Authors
Tel.:/Fax: +38(068) 410-41-79
E-Mail: Koloxai@gmail.com
[a] Ukrainian State Chemico-Technologycal University, 49038 Ukraine, Dnepropetrovsk, Mostovaya st., 2/6.
[b] Ukrainian State Chemico-Technologycal University, 49010 Ukraine, Dnepropetrovsk, Armeyskaya st. 22
[c] Ukrainian State Chemico-Technologycal University 61050 Ukraine, Kharkov, Moskovsky pr., 31/56.
[d] State Flight Academy of National Aviation University, 25013 Ukraine, Kirovograd, 50 Let Octiabrya,22/127,
[e] N .N. Semenov Institute of Chemical Physics, Russian Academy of Sciences 119991, Russian Federation, Moscow, Kosygina st. 4.

INTRODUCTION

The nature of the products of the alcoholysis of *N*-acyloxy-*N*-alkoxyureas, *N*-acyloxy-*N*-alkoxycarbamates, *N*-acyloxy-*N*-alkoxybenzamides depends of the electronegativity of third substituent at nitrogen atom in the O-N-O geminal system. *N*-Acyloxy-*N*-alkoxyureas[1-3] and *N*-acyloxy-*N*-alkoxy-*N*-*tert*-alkylamines[1] yield respectively the *N,N*-dialkoxyureas and *N,N*-dialkoxy-*N*-*tert*-alkylamines by the alcoholysis. *N*-Acyloxy-*N*-alkoxycarbamates convert into *N,N*-dialkoxycarbamates only by the alcoholysis by primary alcohols.[1] The alcoholysis of *N*-acyloxy-*N*-alkoxycarbamates by *tert*-butanol does not take place, probably, due to sterical hindrances to S_N2 nucleophilic substitution at the nitrogen.[1] Isopropanolysis of ethyl *N*-acetoxy-*N*-methoxycarbamate results in the formation of reduction products such as *N,N'*-bis(ethoxycarbonyl)-*N,N*-bis(methoxy)hydrazine and ethyl *N*-ethoxycarbamate[1] (Scheme 1).

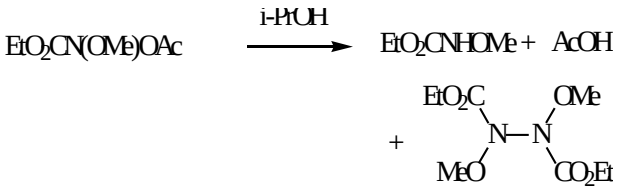

Scheme 1

The nature of products of *N*-acyloxy-*N*-alkoxobenzamides alcoholysis is strongly depended by of the nature of p-substituent in the phenyl group. Thus, methanolysis of *N*-acetoxy-*N*-ethoxybenzamide yields the mixture of methyl benzoate, benzoic and acetic acid,[1] however, as we have found, the methanolysis[4] of *N*-acetoxy-*N*-methoxy-4-nitrobenzamide (**1**) yields only *N,N'*-bis(methoxy)-*N,N'*-bis(4-nitrobenzoyl)hydrazine (**2**). Probably, last reaction occurs by a SET mechanism with consecutive formation the anion-radical **A**, then radical **B** (Scheme 2).

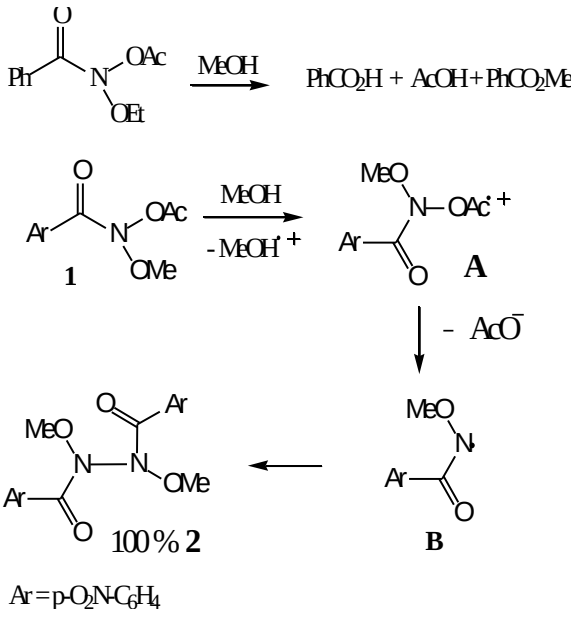

Scheme 2.

N-acyloxy-N-alkoxybenzamides,[5-9] N-acyloxy-N-alkoxycarbamates[1,10,11] and N-acyloxy-N-alkoxyureas [1,2,10,11] are called "anomeric amides" due to nO(Alk)→σ*N-OC(O)R anomeric effect domination. In RC(=O)O−N−O(Alk) group the amide nitrogen is sp^3 hybridized and has pyramidal configuration, (Alk)O−N

bond is shortened and N−OC(=O)R bond is elongated and destabilized.[2,4,5,7,10,11] Due to this N−OC(=O)R bond destabilization, the S_N2 nucleophilic substitution at amide nitrogen atom or homolysis of this bond become possible.[1,5,7]

However, in the case of *N*-acyloxy-*N*-alkoxycarbamates, the influence of their structure on the nature of products of alcoholysis remains unknown. We cannot predict under which conditions the alcoholysis of *N*-acyloxy-*N*-alkoxycarbamates by primary alcohols will selectively yield *N,N*-dialkoxycarbamates, which are regarded as the potential sources of *NH-N,N*-dialkoxyamines

EXPERIMENTAL

General

^{1}HNMR spectra were recorded on a "Varian VXP-300" spectrometer (300 MHz), "Mercury-400" (400 MHz) and "Bruker Avance DRX 500" (500 MHz). Me_4Si was used as an internal standard. Chemical shifts were measured in σ-scale (ppm) and coupling constants in Hz. ^{13}CNMR spectra were recorded on a "Varian VXP-300" spectrometer (75 MHz). IR spectra were recorded on "UR-20" spectrometer, in KBr or in the thin layer. Mass spectra were recorded on a "VG-70EQ 770" mass spectrometer in FAB mode (FAB) and on "Kratos MS 890" mass spectrometer, electron impact mode (EI) and chemical ionization mode (CI), gas-reagent was isobutane. MeOH and EtOH were dried by refuxing and distillation over metallic calcium.

Metanolysis of *N*-acetoxy-*N*-methoxy-4-nitrobenzamide (1)

A solution of (**1**)[4] (0.06137 mmol, 0.0156 g) in MeOH (3 ml) was kept at 20 °C for 72 h, then methanol was evaporated *in vacuo* (5 Torr) yielding 0.0120 g (100%) of *N,N'*-bis(methoxy)-*N,N'*-bis(4-nitrobenzoyl)hydrazine (**2**) as yellowish white crystals, m.p. 86 – 88 °C (with decomp.). ^{1}HNMR (400 MHz, $CDCl_3$): 3.948 (s, 6H, NOMe), 8.206 (d, 4H, $H_{C6H4}^{2,6}$, ^3J = 9.2 Hz), 8.305 (d, 4H, $H_{C6H4}^{3,5}$, ^3J = 9.2 Hz). ^{1}H NMR (400 MHz, $(CD_3)_2SO$): 3.948 (s, 6H, NOMe), 8.206 (d, 4H, $H_{C6H4}^{2,6}$, ^3J = 9.2 Hz), 8.329 (d, 4H, $H_{C6H4}^{3,5}$, ^3J = 9.2 Hz). MS (FAB, *m/z*, $I_{отн}$, (%)): 391 $[M+H]^+$ (10), 307(88), 289(45), 155(90), 137(96), 79 (100). MS (FAB, Na^+, *m/z*, $I_{отн}$, (%)): 413 $[M+Na]^+$ (10), 329 (100).

Methyl *N*-ethoxycarbamate (3)

A solution of ethoxyamine (29.06 mmol, 1.78 g) in MeCN (7 ml) was added to the solution of MeO_2CCl (37.77 mmol, 3.57 g) in MeCN (15 ml) at 10 °C, then K_2CO_3 (43.59 mmol, 6.0 g) and 18-crown-6 (0.10 g) were added. The reaction mixture was stirred and heated to 20 °C for 3 h, then it was stored at 20 °C for another 24 h. After that the precipitate was filtered off, washed with CH_2Cl_2, and the combined filtrate was evaporated *in vacuo*. The residue was distilled *in vacuo* yielding 2.49 g (72 %) methyl *N*-ethoxycarbamate, colourless liquid, b.p. 74-79 °C (5 Torr), n_D^{21} 1.4247 (cf. 1.4246[12]) identified by comparison its ^{1}HNMR spectra with that of an authentic sample.[12] ^{1}HNMR (300 MHz, $CDCl_3$): 1.18 (t, 3H, $NOCH_2\underline{Me}$, ^3J = 6.9 Hz), 3.69 (s, 3H, CO_2Me), 3.85 (q, 2H, $NO\underline{CH_2}Me$, ^3J = 6.9 Hz), 7.40 (br. s, 1H, NH). IR (ν, cm^{-1}, KBr): 3430 (NH), 1740 (C=O).

Other N-alkoxycarbamates were synthesized in a similar manner.

Methyl *N*-isopropyloxycarbamate (4), yield 78%, colourless liquid, b.p. 87-88 °C (10 Torr), n_D^{27} 1.4237. ^{1}H NMR (300 MHz, $CDCl_3$): 1.15 (d, 6H, $OCH\underline{Me_2}$, ^3J = 6.3 Hz), 3.68 (s, 3H, CO_2Me), 3.98 (sept, 1H, $O\underline{CH}Me_2$, ^3J = 6.3 Hz), 7.33 (br. s, 1H, NH). IR (ν, cm^{-1}, KBr): 3310 (NH), 1745 (C=O). Found (%): N 10.68. Calc. for $C_5H_{11}NO_3$ (%): N 10.52.

Methyl *N-n*-butyloxycarbamate (5), yield 76 %, colourless liquid, b.p. 105-107 °C (5 Torr), n_D^{22} 1.4312. ^{1}H NMR (300 MHz, $CDCl_3$): 0.94 (t, 3H, $OCH_2CH_2CH_2\underline{Me}$, ^3J = 7.2 Hz), 1.40 (sex, 2H, $OCH_2CH_2\underline{CH_2}Me$, ^3J = 7.2 Hz), 1.63 (quint, 2H, $OCH_2\underline{CH_2}CH_2Me$, ^3J = 7.2 Hz), 3.77 (s, 3H, CO_2Me), 3.87 (т, $O\underline{CH_2}CH_2CH_2Me$, ^3J = 7.2 Hz), 7.47 (br. s, 1H, NH). Found (%): N 9.31. Calc. for $C_6H_{13}NO_3$ (%): N 9.52.

Ethyl *N*-isopropyloxycarbamate (6), yield 67 %, colourless liquid, b.p. 68°C (2 Torr), n_D^{20} 1.4255. ^{1}HNMR (300 MHz, $CDCl_3$): 1.22 (d, 6H, $OCH\underline{Me_2}$, ^3J = 6.3 Hz), 1.27 (t, 3H, $CO_2CH_2\underline{Me}$, ^3J = 7.2 Hz), 4.05 (sept, 1H, $O\underline{CH}Me_2$, ^3J = 6.3 Hz), 4.19 (q, 2H, $CO_2\underline{CH_2}Me$, ^3J = 7.2 Hz). Found (%): N 9.43. Calc. for $C_6H_{13}NO_3$ (%): N 9.52.

General method for the synthesis of *N*-chloro-*N*-alkoxycarbamates

A solution of *t*-BuOCl (15 mmol) in CH_2Cl_2 (3 ml) was added to the solution of the alkyl *N*-alkoxycarbamate (5 mmol) in CH_2Cl_2 (6 ml) at -20 °C, the reaction solution was kept at 5 °C for 2 h, then it was evaporated *in vacuo* (10 Torr), the residue was kept at 3 Torr for 5 min. The yields were quantitative.

Methyl *N*-chloro-*N*-ethoxycarbamate (7), yellowish oil. ^{1}HNMR (300 MHz, $CDCl_3$): 1.31 (t, 3H, $NOCH_2\underline{Me}$, ^3J = 6.9 Hz), 3.92 (s, 3H, CO_2Me), 4.07 (q, 2H, $NO\underline{CH_2}Me$, ^3J = 6.9 Hz). IR (ν, cm^{-1}, thin layer): 1795 (C=O). Found(%): Cl 22.85. Calc. for $C_4H_8ClNO_3$ (%): Cl 23.09.

Methyl *N*-chloro-*N*-isopropyloxycarbamate (8), yellow oil. ^{1}HNMR (300 MHz, $CDCl_3$): 1.28 (d, 6H, $NOCH\underline{Me_2}$, ^3J = 6.3 Hz), 3.91 (s, 3H, CO_2Me), 4.31 (sept, 1H, $NOC\underline{H}Me_2$, ^3J = 6.3 Hz). IR (ν, cm^{-1}, thin layer): 1780 (C=O). Found (%): Cl 21.04. Calc. for $C_5H_{10}ClNO_3$ (%): Cl 21.15

Methyl *N*-chloro-*N-n*-butyloxycarbamate (9), yellowish oil, n_D^{25} 1.4383. ^{1}H NMR (300 MHz, $CDCl_3$): 0.95 (t, $OCH_2CH_2CH_2\underline{Me}$, ^3J = 7.3 Hz), 1.45 (sex, 2H, $OCH_2CH_2\underline{CH_2}Me$, ^3J = 7.3 Hz), 1.57 (quint, 2H, $OCH_2\underline{CH_2}CH_2Me$, ^3J = 7.3 Hz), 3.90 (s, 3H, CO_2Me), 3.97 (t, 2H, $O\underline{CH_2}CH_2CH_2Me$, ^3J =7.3 Hz). Found (%): Cl 19.16. Calc. for $C_6H_{12}ClNO_3$ (%): Cl 19.52.

Ethyl *N*-chloro-*N*-isopropyloxycarbamate (10), yellowish oil. ^{1}H NMR (300 MHz, $CDCl_3$): 1.28 (d, 6H, $NOCH\underline{Me_2}$, ^3J = 6.3 Hz), 1.36 (t, 3H, $CO_2CH_2\underline{Me}$, ^3J = 7.0

Hz), 4.31 (sept, 1H, NOCHMe$_2$, ^3J = 6.3 Hz), 4.33 (q, 2H, CO$_2$CH$_2$Me, ^3J = 7.0 Hz). Found (%): Cl 19.46. Calc. $C_6H_{12}ClNO_3$ (%): Cl 19.52.

General method for the synthesis of N-acetoxy-N-alkoxycarbamates

A mixture of the solution of *N*-chloro-*N*-alkoxycarbamate (8 mmol) in MeCN (20 ml) and AcONa (26 mmol) was stirred at 20 °C for 55 h, then CH_2Cl_2 (10 ml) was added, the precipitate was filtered off, washed with CH_2Cl_2, the combined filtrate was evaporated *in vacuo* (20 Torr). The residue was extracted by CH_2Cl_2 (20 ml), the extract was evaporated *in vacuo*, the residue was kept at 3 Torr and 20 °C for 30 min to yield the product.

Methyl *N*-acetoxy-*N*-ethoxycarbamates (11), yield 87 %, colourless liquid, n_D^{19} 1.4269. ^{1}HNMR (300 MHz, $CDCl_3$): 1.30 (t, 3H, NOCH$_2$Me, ^3J = 7.2 Hz), 2.19 (s, 3H, NOC(O)Me), 3.88 (s, 3H, CO$_2$Me), 4.13 (q, 2H, NOCH$_2$Me, ^3J = 7.2 Hz). IR (ν, cm^{-1}, thin layer): 1805 (C=O), 1780 (C=O). Found (%): C 40.41, H 6.31, N 7.78. Calc. for $C_6H_{11}NO_5$ (%): C 40.68, H 6.26, N 7.91.

Methyl *N*-acetoxy-*N*-isopropyloxycarbamate (12), yield 96 %, yellowish liquid. ^{1}HNMR (300 MHz, $CDCl_3$): 1.28 (d, 6H, OCHMe$_2$, ^3J = 6.3 Hz), 2.17 (s, 3H, NOC(O)Me), 3.87 (s, 3H, CO$_2$Me), 4.32 (sept, 1H, OCHMe$_2$, ^3J = 6.3 Hz). IR (ν, cm^{-1}, thin layer): 1805 (C=O), 1780 (C=O). MS (CI, *m/z*, I_{rel}, (%)): 192 $[M+H]^+$ (0.6), 191 M^+ (1.5), 148 (4.0), 132 (3.1), 59 (23.9), 45 (20.4), 43 (100). Found (%): C 43.81, H 6.82, N 7.18. Calc for $C_7H_{13}NO_5$ (%): C 43.98, H 6.85, N 7.33.

Methyl *N*-acetoxy-*N*-*n*-butyloxycarbamate (13), yield 81 %, yellowish liquid. ^{1}HNMR (300 MHz, $CDCl_3$): 0.95 (t, 3H, NO(CH$_2$)$_3$Me, ^3J = 7.5 Hz), 1.41 (sex, 2H, NOCH$_2$CH$_2$CH$_2$Me, ^3J = 7.5 Hz), 1.66 (quint, 2H, NOCH$_2$CH$_2$CH$_2$Me, ^3J = 7.5 Hz), 2.19 (s, 3H, NOC(O)Me), 3.88 (s, 3H, CO$_2$Me), 4.08 t (2H, NOCH$_2$CH$_2$CH$_2$Me, ^3J = 7.5 Hz). IR (ν, cm^{-1}, thin layer): 1805 (C=O), 1780 (C=O). Found (%): C 46.68, H 7.34, N 6.79. Calc. for $C_8H_{15}NO_5$ (%): C 46.83, H 7.38, N 6.83.

Ethyl *N*-acetoxy-*N*-isopropyloxycarbamate (14), yield 98 %, yellowish liquid, n_D^{22} 1.4211. ^{1}HNMR (300 MHz, $CDCl_3$): 1.28 (d, 6H, OCHMe$_2$, ^3J = 6.3 Hz), 1.33 (t, 3H, CO$_2$CH$_2$Me, ^3J = 7.2 Hz), 2.17 (s, 3H, NOC(O)Me), 4.30 (q, 2H, CO$_2$CH$_2$Me, ^3J = 7.2 Hz), 4.33 (sept, 1H, NOCHMe$_2$, ^3J = 6.3 Hz). MS (CI, *m/z*, I_{rel}, (%)): 206 $[M+H]^+$ (2.0), 204 (0.6), 132 (100). Found (%): C 46.61, H 7.35, N 6.59. Calc. for $C_8H_{15}NO_5$ (%): C 46.82, H 7.37, N 6.83.

Methyl *N*-ethoxy-*N*-methoxycarbamate (15). Methyl *N*-acetoxy-*N*-ethoxycarbamate **11** (2.442 mmol, 0.432 g) was dissolved in MeOH (5 ml) at -12°C, the solution was heated to 0°C for 3 h, then it was kept at 24 °C for 44 h. Then it was evaporated *in vacuo* (2 Torr) yielding 0.248 g (68%) methyl *N*-ethoxy-*N*-methoxycarbamate (**15**), which was contaminated with some *N,N'*-bis(ethoxy)-*N,N'*-bis(methoxycarbonyl)hydrazine[12] (**16)** according to ^{1}HNMR. After distillation *in vacuo* 0.080 g (22 %) pure (**15**) was obtained as colourless liquid. ^{1}HNMR (300 MHz, $CDCl_3$): 1.33 (t, 3H, NOCH$_2$Me, ^3J = 7.0 Hz), 3.84 (s, 3H, NOMe), 3.90 (s, 3H, CO$_2$Me), 4.11 (q, 2H, NOCH$_2$Me, ^3J = 7.0 Hz). Found (%): C 40.55, H 7.35. Calc. for $C_5H_{11}NO_4$ (%): C 40.27, H 7.43.

Ethanolysis of methyl *N*-acetoxy-*N*-ethoxycarbamate (11) at 4°C. Methyl *N*-acetoxy-*N*-ethoxycarbamate (**11**) (6.960 mmol, 1.232 g) was dissolved in EtOH (12 ml) at 4°C, this solution was kept at 4 - 5°C for 94 h, then it was evaporated *in vacuo*, yielding 1.1986 g of a yellowish liquid. According to ^{1}HNMR this residue is a mixture of unreacted (**11**) and *N,N'*-bis(ethoxy)-*N,N'*-bis(methoxycarbonyl)hydrazine[12] (**16)** in molar ratio 97:3. ^{1}H NMR of hydrazine (**16**) (300 MHz, $CDCl_3$): 1.31 (t, 6H, NOCH$_2$Me, ^3J = 7.2 Hz), 3.91 (3, 6H, CO$_2$Me), 4.05 (q, 4H, NOCH$_2$Me, ^3J = 7.2 Hz). On keeping of the solution of (**11**) in EtOH at 4 – 5 °C for 163 h, the ratio of compounds (**11**) and (**16**) became 63:37.

Ethanolysis of methyl *N*-acetoxy-*N*-ethoxycarbamate (11) at 18 °C. Methyl *N*-acetoxy-*N*-ethoxycarbamate (**11**) (6.766 mmol, 1.199 g) was dissolved in EtOH (12 ml) at 18°C, this solution was kept at 17 – 18 °C for 219 h, then it was evaporated *in vacuo* (8 Torr), the residue was kept at 2 Torr and 20 °C yielding 0.563 g (51 %) methyl *N,N*-diethoxycarbamate (**17**), colourless liquid, b.p. 46-47 **°**C(2 Torr), n_D^{25} 1.4139. ^{1}HNMR (300 MHz, $CDCl_3$): 1.30 (t, 6H, NOCH$_2$Me ^3J = 7.2 Hz), 3.87 (s, 3H, CO$_2$Me), 4.07 (q, 4H, NOCH$_2$Me, ^3J = 7.2 Hz). . ^{13}CNMR (75 MHz, $CDCl_3$): 13.40 (NOCH$_2$Me), 54.25 (NOCH$_2$Me); 69.86 (CO$_2$Me), 159.84 (C=O). MS (EI, *m/z*, I_{rel}.(%)): 164 $[M+H]^+$ (0.4), 163 M^+ (2.0), 118 (1.7), 105 (3.1), 104 (2.7), 59 (59.8), 43 (100). Found (%): C 44.08, H 8.14, N 8.51. Calc. for $C_6H_{13}NO_4$ (%): C 44.17, H, 8.03, N 8.58.

Methyl *N*-isopropyloxy-*N*-metoxycarbamate (18). Methyl *N*-acetoxy-*N*-isopropyloxycarbamate (**12**) (8.68 mmol, 1.66 g) was dissolved in MeOH (21 ml) and kept at -32 °C, for 4 h, the solution was then heated to 20 °C and was kept at 20 °C for 7 days. The solution was then evaporated *in vacuo* (20 Torr). MeOH-condensate was trapped. The residue was distillated *in vacuo* yielding 0.86 g (60.4 %) methyl *N*-isopropyloxy-*N*-metoxycarbamate (**18**), colourless liquid, b.p. 50-53 °C (3 Torr), n_D^{23} 1.4168. IR (ν, cm^{-1}, thin layer): 1770 (C=O). ^{1}HNMR (300 MHz, $CDCl_3$): 1.29 (д, 6H, OCHMe$_2$, ^3J = 6.3 Hz), 3.77 (s, 3H, NOMe), 3.86 (s, 3H, CO$_2$Me), 4.27 (sept, 1H, OCHMe$_2$, ^3J = 6.3 Hz). MS (EI, 70 Ev, *m/z*, $I_{отн}$ (%)): 163 M^+ (3.4), 105 (5.6), 91 (14.0), 60 (21.3), 59 (54.8), 58 (24.3), 46 (16.9), 45 (36.7), 44 (21.3), 43 (100). Found (%): C 44.23, H 8.17, N 8.42. Calc. for $C_6H_{13}NO_4$ (%): C 44.17, H 8.03, N 8.58.

In the MeOH-condensate 0.076 g (9.7 %) of dimethylcarbonate was found by GLC.

Methyl *N*-*n*-butyloxy-*N*-methoxycarbamate (19). Methyl *N*-acetoxy-*N*-*n*-butyloxycarbamate (**13**) (7.718 mmol, 1.584 g) was dissolved in MeOH (11 ml), the solution was kept at 18°C for 148 h, then MeOH was evaporated *in vacuo* (20 Torr) and the MeOH-condensate was collected in a cold trap. The residue was kept at 20 °C and 3 Torr for 1 h yielding 1.122 g (82.3%) of methyl *N*-*n*-butyloxy-*N*-methoxycarbamate (**19**)**,** colourless liquid, ^{1}HNMR (300 MHz, $CDCl_3$): 0.95 (t, 3H, NO(CH$_2$)$_3$Me, ^3J = 7.2 Hz), 1.45 (sex, 2H, NO(CH$_2$)$_2$CH$_2$Me, ^3J = 7.2 Hz), 1.66 (quint, 2H, NOCH$_2$CH$_2$CH$_2$Me, ^3J = 7.2 Hz), 3.90 (s, 6H,

NOMe and CO_2Me), 3.97 (t, 2H, $NOCH_2$, ^3J = 7.2 Hz). IR (ν, cm^{-1}, thin layer): 1780 (C=O). MS (EI, *m/z*, I_{rel} (%)): 177 M^+ (3.8), 150 (76.7), 149 (87.6), 146 (40.9), 118 (14.6), 115 (9.7), 105 (29.1), 91 (57.5), 90 (52.1), 60 (64.9), 59 (100), 58 (22.1), 57 (76.5). Found (%): C 47.29, H 8.39, N 7.64. Calc. for $C_7H_{15}NO_4$ (%): C 47.45, H 8.53, N 7.90.

In the MeOH-condensate 0.0028 g (0.4 %) of dimethylcarbonate was found by GLC.

Ethyl *N*-ethoxy-*N*-isopropyloxycarbamate (20). A solution of ethyl *N*-acetoxy-*N*-isopropyloxycarbamate (**14**) (0.817 mmol, 0.168 g) in EtOH (2 ml) was kept at 20 °C for 66 h, then at 40 °C for 57 h. Then it was evaporated *in vacuo* (13 Torr) and EtOH-condensate was caught in a cold trap. The residue was kept at 20 °C and 2 Torr for 20 min yielding 0.097 g (62.2%) of ethyl *N*-ethoxy-*N*-isopropyloxycarbamate (**20**), colourless liquid, ^{1}HNMR (300 MHz, $CDCl_3$): 1.276 (t, 3H, $NOCH_2\underline{Me}$, ^3J = 7.2 Hz), 1.278 (d, 6H, $NOCH\underline{Me_2}$, ^3J = 6.3 Hz), 1.34 (t, $CO_2CH_2\underline{Me}$, ^3J = 7.2 Hz), 4.04 (q, 2H, $NO\underline{CH_2}Me$, ^3J = 7.2 Hz), 4.26 (sept, 1H, $NO\underline{CH}Me_2$, ^3J = 6.3 Hz), 4.27 (q, 2H, $CO_2\underline{CH_2}Me$, ^3J = 7.2 Hz). MS (FAB, K^+, *m/z*, I_{rel} (%)): 230 $[M+K]^+$ (6), 215 (5), 192 $[M+H]^+$ (100), 176 (10). Found (%): N 7.05. Calc. for $C_8H_{17}NO_4$ (%): N 7.32.

In the EtOH-condensate 0.023 g (23.4 %) of diethylcarbonate was found by GLC.

***NH*-*N*-Methoxy-*N*-*n*-octyloxyamine (22)**. A sodium methylate solution, prepared by dissolving Na (13.82 mmol, 0.318 g) in MeOH (20 ml), was added to the solution of methyl *N*-methoxy-*N*-*n*-octyloxycarbamate (**21**)[1] (6.910 mmol, 1.612 g) in MeOH (20 ml) The reaction mixture was kept at 18-20 °C for 7 h, then a solution of acetic acid (17.275 mmol, 1.04 g) in MeOH (7 ml) was added. The precipitate was filtered off, washed with MeOH, the combined MeOH-filtrate evaporated *in vacuo* (20 Torr). The residue was extracted by hexane (23 ml), the extract was evaporated *in vacuo* (20 Torr). The residue was kept at 20°C and 2 Torr for 30 min yielding 1.148 g (94.8 %) *NH*-*N*-methoxy-*N*-*n*-octyloxyamine (**22**), colourless liquid, ^{1}HNMR (300 MHz, $CDCl_3$): 0.82 (t, 3H, $NO(CH_2)_7\underline{Me}$, ^3J = 6.9 Hz), 1.12-1.35 (m, 10H, $NOCH_2CH_2\underline{(CH_2)_5}Me$), 1.52 (quint, 2H, $NOCH_2\underline{CH_2}$, ^3J = 6.9 Hz), 3.62 (s, 3H, NOMe), 3.80 (t, 2H, $NOCH_2$, ^3J = 6.9 Hz), 7.80 (br. s, 1H, NH). Found (%): N 7.72. Calc. for $C_9H_{21}NO_2$ (%): N 7.99.

***NH*-*N*-*n*-Butyloxy-*N*-methoxyamine (23)**. The mixture of a solution of methyl *N*-*n*-butyloxy-*N*-methoxycarbamate (**19**) (2.240 mmol, 0.397 g) in Et_2O (4 ml) and a solution of NaOH (3.360 mmol, 0.134 g) in water (16 ml) was stirred at 20 °C for 1 h, then it was extracted by Et_2O (25 ml). The extract was dried over $MgSO_4$ and after that it was evaporated *in vacuo*. The residue was kept at 5 Torr and 20 °C for 1 h to yield 0.253 g (94.5 %) *NH*-*N*-*n*-butyloxy-*N*-methoxyamine **23**, colourless liquid, ^{1}HNMR (300 MHz, $CDCl_3$): 0.95 (t, 3H, $NO(CH_2)_3\underline{Me}$, ^3J = 7.2 Hz), 1.41 (sextett, 2H, $NOCH_2CH_2\underline{CH_2}Me$, ^3J = 7.2 Hz), 1.63 (quint, 2H, $NOCH_2\underline{CH_2}CH_2Me$, ^3J = 7.2 Hz), 3.78 (s, 3H, NOMe), 3.87 (t, 2H, $NOCH_2$, ^3J = 7.2 Hz), 7.36 (br. s, 1H, NH). MS (EI, *m/z*, I_{rel} (%)): 120 $[M+H]^+$ (1.2), 119 M^+ (6.1), 118 (1.9), 88 (2.1), 72 (14.7), 57 Bu^+ (81.2), 56 (53.4), 46 (21.7), 44 (31.2), 43 (100). Found (%): C 50.25, H 11.17, N 11.72. Calc. for $C_5H_{13}NO_2$ (%): C 50.40, H 11.00, N 11.75.

Hydrolysis of methyl *N*-isopropyloxy-*N*-metoxycarbamate (18). A mixture of a solution of methyl *N*-isopropyloxy-*N*-metoxycarbamate (**18**) (6.429 mmol, 1.049 g) in Et_2O (7 ml) and that of NaOH (12.858 mmol, 0.51 g) and 15-crown-5 (0.15 g) in water (26 ml) was stirred at 25 °C for 1 h, and then Et_2O (15 ml), acetic acid (11.66 mmol, 0.7 g) and water (2 ml) were added. The ether extract was separated, the aqueous phase was extracted with another 15 ml of Et_2O. Combined ether extract was dried over $MgSO_4$, and concentrated by removing of 3/4 of the ether (the bath temperature must be lower than 45 °C). The residue was condensed in two cold traps at different regime *in vacuo*:

(1) at 55 Torr and 35 °C to yield 0.176 g (26.0 %) *NH*-*N*-isopropyloxy-*N*-methoxyamine (**24**), colourless liquid. ^{1}H NMR (300 MHz, $CDCl_3$): 1.21 (d, 6H, $NOCH\underline{Me_2}$, ^3J = 6.3 Hz), 3.,66 (s, 3H, NOMe), 4.15 (септ, 1H, $NO\underline{CH}Me_2$, ^3J = 6.3 Hz), 7.87 (br. s, 1H, NH). Found (%): N 13.03. Calc. for $C_4H_{11}NO_2$ (%): N 13.32.

(2) at 3 Torr and 26 °C to yield 0.367 g (54.8 %) *N,N'*-bis(isopropyloxy)-*N,N'*-bis(methoxy)hydrazine (**25**), colourless liquid, ^{1}HNMR (300 MHz, $CDCl_3$): 1.224 (d, 12H, $NOCH\underline{Me_2}$, ^3J = 6.3 Hz), 3.68 (s, 6H, NOMe), 4.17 (sept, 2H, $NO\underline{CH}Me_2$, ^3J = 6.3 Hz). MS (EI, *m/z*, I_{rel} (%)): 209 $[M+H]^+$ (0.4), 208 M^+ (2.0), 207 (0.9), 177 (2.2), 105 (3.4), 104 (14.7), 60 (10.7), 59 (39.8), 58 (55.7), 46 (10.3), 45 (58.7), 44 (78.1), 43 (100). Found (%): N 13.34. Calc. for $C_8H_{20}N_2O_4$ (%): N 13.45.

***NH*-*N*,*N*-diethoxyamine (26)**. The mixture of a solution of methyl *N*,*N*-diethoxycarbamate (**17**) (2.542 mmol, 0.415 g) in Et_2O (2 ml) and that of NaOH (7.62 mmol, 0.31 g) and 15-crown-5 (0.06 g) in water (5 ml) was stirred at 20 °C for 2 h, then a solution of acetic acid (7.62 mmol, 0.457 g) in Et_2O (10 ml) was added. The ether layer was separated, the aqueous phase was extracted with Et_2O (6 ml). The combined ether extract was dried over $MgSO_4$. The extract was concentrated by evaporation (the bath temperature must be lower than 50 °C). The residue was recondensed in cold trap *in vacuo* (67 Torr) at 72 °C yielding 0.0141 g (5.2 %) *NH*-*N*,*N*-diethoxyamine (**26**), colourless liquid, ^{1}H NMR (300 MHz, $CDCl_3$): 1.23 (t, 6H, $NOCH_2\underline{Me}$, ^3J = 7.0 Hz), 3.93 (q, 4H, $NO\underline{CH_2}Me$, ^3J = 7.0 Hz), 7.95 (br. s, 1H, NH).

RESULTS AND DISCUSSION

The major objective of this work was to study the alcoholysis of *N*-acetoxy-*N*-alkoxycarbamates and to explore of the possibility of synthesis of *NH*-*N*,*N*-dialkoxyamines from methyl *NH*-*N*,*N*-dialkoxycarbamates. The last-named compounds may become useful synthones in organic synthesis but as of now only one method of their preparation is known.[13,14]

We have synthesized *N*-alkoxycarbamates (**3-6**) which were chlorinated to *N*-chloro-*N*-alkoxycarbamates (**7-10**) by *tert*-butyl hypochlorite in CH_2Cl_2 solution (Scheme 3). *N*-Chloro-*N*-alkoxycarbamates react with anhydrous AcONa in MeCN selectively yielding *N*-acetoxy-*N*-alkoxycarbamates (**11-14**).

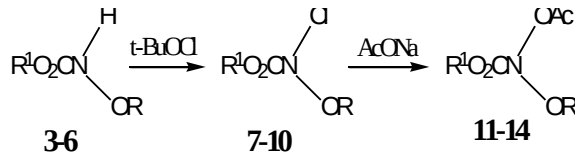

R^1 = Me, R = Et (**3, 7, 11**), i-Pr (**4, 8, 12**), n-Bu (**5, 9, 13**)

R^1 = Et, R = i-Pr (**6, 10, 14**)

Scheme 3.

We found that methyl *N*-acetoxy-*N*-ethoxycarbamate, (**11**) is converted mainly to methyl *N*-ethoxy-*N*-methoxycarbamate **(15)** by the methanolysis at 24 °C. A by-product of this methanolysis is *N,N'*-bis(ethoxy)-*N,N'*-bis(methoxycarbonyl)hydrazine[12] (Scheme 4).

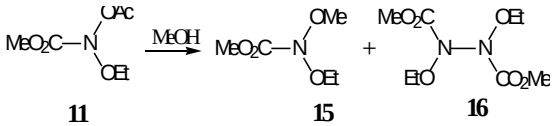

Scheme 4.

A study of ethanolysis of (**11**) showed that at 4 – 5 °C the nucleophilic substitution at nitrogen does not occur. On keeping of a solution of (**11**) in ethanol at 4 – 5 °C for 94 h, a mixture of unreacted (**11**) (main component, 97 mol. %) and *N,N'*-bis(ethoxy)-*N,N'*-bis(methoxycarbonyl)hydrazine (**16**) (3 mol. %) was obtained. On keeping the solution for 163 h, the ratio of unreacted (**11**) and the hydrazine (**16**) is 63:37 mol.%. The presence of methyl *N,N*-diethoxycarbamate (**17**) in reaction mixture was not detected. It may be supposed that at this temperature an S_N2 nucleophilic substitution at nitrogen atom of (**11**) is impossible. But (**11**) is slowly reduced by ethanol to the anion-radical **C** by a SET mechanism (Scheme 5). Then the anion-radical **C** loses an acetate ion and forms radical **D** which couples to yield *N,N'*-bis(ethoxy)hydrazine (**16**).

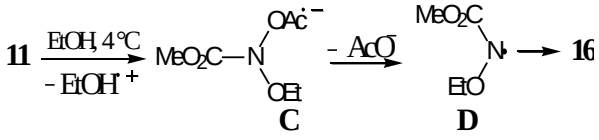

Scheme 5

But if ethanolysis of (**11**) is carried out at 17-18 °C, the S_N2 nucleophilic substitution at nitrogen occurs yielding methyl *N,N*-diethoxycarbamate **17** (Scheme 6).

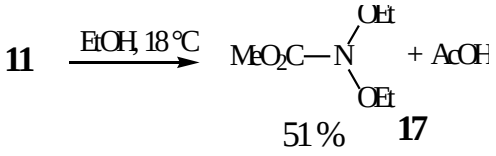

Scheme 6.

Methanolysis of N-acetoxy-N-alkoxycarbamate (**12,13**) at 20-23°C and of (**14**) at 40 °C yields alkyl *N,N*-dialkoxycarbamates (**18-20)** and AcOH as main products (Scheme 7, Table 1). Dialkylcarbonates are by-products of these cases of alcoholysis.

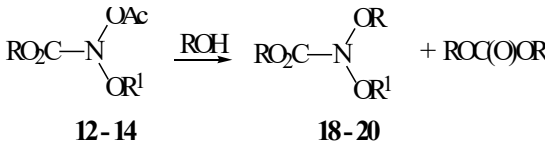

Scheme 7.

In the case of sterically hindered ethyl *N*-acetoxy-*N*-isopropoxycarbamate (**14**) the ethanolysis occurs more slowly than the methanolysies of *N*-acetoxy-*N*-alkoxycarbamates (**12**, **13)**.

On keeping of an ethanolic solution of (**14**) at 20 °C for 66 h, the molar ratio of unreacted (**14)** and product, *N*-ethoxy-*N*-isopropoxycarbamate (**20**) is 63:37. The complete alcoholysis take place only after keeping it at 40°C for additional 57 h yielding methyl *N*-ethoxy-*N*-isopropoxycarbamate (**20)** as main product (Table 1). The yield of by-product, diethylcarbonate is also quite high. Probably, the two competitive reactions take place simultaneously, the nucleophilic substitution at nitrogen by S_N2 mechanisn (route I) yielding *N,N*-dialkoxycarbamates (**18-20**) and a nucleophilic attack of the alcohol on carbonyl group (route II) yielding dialkylcarbonate (Scheme 8).

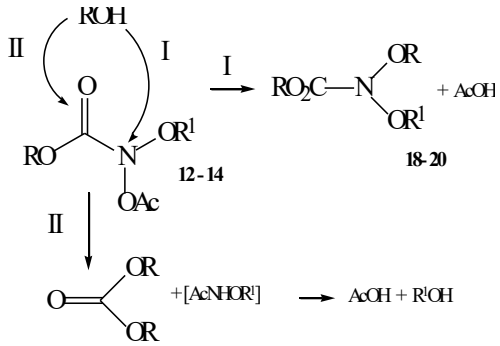

Scheme 8

On other hand, the alcoholysis products formation may also arises through generation of *N*-alkoxyntrenium cation, **E** (Scheme 9), which reacts with alcohol yielding *N,N*-dialkoxycarbamates (**18-20)**. The further fragmentation caution **E** to more stable acyl cation **F,** which finally yields the dialkylcarbonate.

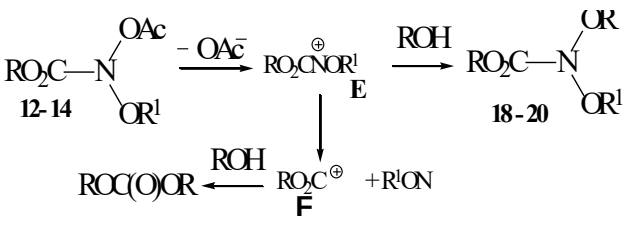

Scheme 9.

 DOI: 10.17628/ecb.2014.3.1119-1125

Table 1. Yields of products of alcoholysis of N-acetoxy-N-alkoxycarbamate **12-14**

No.	$RO_2CN(OR^1)OAc$		ROH	Temp., °C	Time, h	$RO_2CN(OR^1)OR$		ROC(O)OR
	R	R^1				R	Yield, %	Yield, %
12	Me	i-Pr	MeOH	20	164	Me (18)	60.4	9.7
13	Me	n-Bu	MeOH	21-23	120	Me (19)	82.3	0.4
14	Et	i-Pr	EtOH	(a) 20	66	Et (20)	62.2	23.4
				(b) 40	57			

In methyl *N,N*-dialkoxycarbamates, MeOC(O)-group can be easily eliminated by hydrolysis or alkoholysis in the presence of alkali to yield the particular *NH-N,N*-dialkoxyamines. But in every case the suitable reaction conditions must be carefully selected. Thus, methyl *N*-methoxy-*N*-*n*-octyloxycarbamate **(21)**[1] yields *NH-N*-methoxy-*N*-*n*-octyloxyamine (**22**) by treatment of MeONa solution in methanol then by action of acetic acid (Scheme 10).

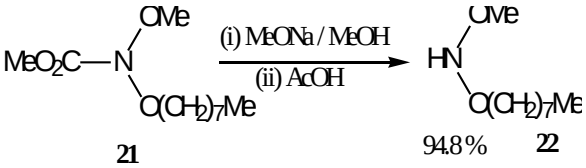

Scheme 10

The hydrolysis of methyl *N*-*n*-butyloxy-*N*-methoxycarbamate **(19)** by 1.5 eqivalent of NaOH in the water solution in the presence of ether (4:1) at 20° C for 1 h selectively yields *NH-N*-*n*-butyloxy-*N*-methoxyamine **23** (Scheme 11).

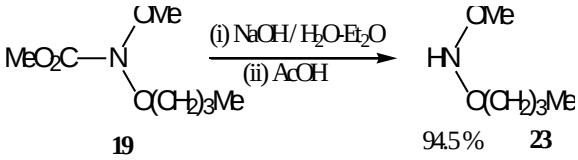

Scheme 11

The alkaline hydrolysis of methyl *N*-isopropyloxy-*N*-metoxycarbamate (**18**) occurs with the formation two main products, unstable *NH-N*-isopropyloxy-*N*-methoxyamine (**24**) and *N,N'*-bis(isopropyloxy)-*N,N'*-bis(methoxy)hydrazine (**25**) (Scheme 12).

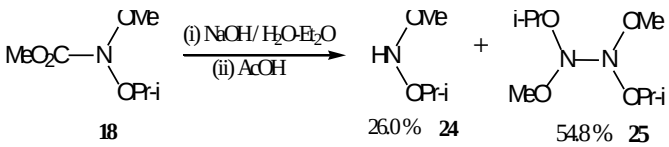

Scheme 12

Probably, in this case (Scheme 13) the initially generated anion **G** may be protonated to unstable (**24**) or may undergo aerial oxidation to a relatively stable dialkoxyaminyl radical **H** which dimerises[15] to (**25**).

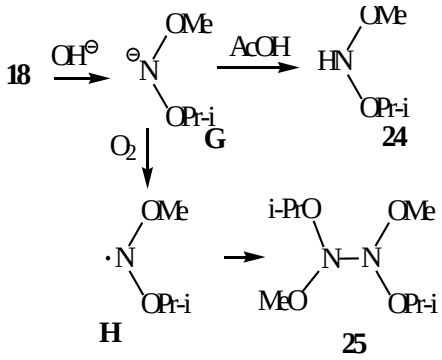

Scheme 13

NH-N,N-Diethoxyamine **(26)** was obtained in low yield by alkaline hydrolysis of methyl *N,N*-diethoxycarbamate (**17**) (Scheme 14). Probably the further rapid decomposition of (**17**) occurs in these reaction conditions.

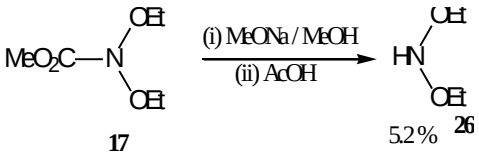

Scheme 14

The structure of *NH-N,N*-dialkoxyamines (**22-24** and **26)** and *N,N,N',N'*-tetraalkoxyhydrazine (**25)** was confirmed by their ^{1}HNMR spectra, the structure of compounds (**23)** and (**25**) were confirmed by mass spectra also. In ^{1}HNMR spectra of (**22-24**) and (**26**)**,** the characteristic signal of NH-proton as the broad singlet in field of 7.36 -7.95 ppm was observed.

Thus it was established that alcoholysis of N-acetoxy-N-alkoxycarbamates by methanol or ethanol at 20 – 40° C yields *N,N*-dialkoxycarbamates and acetic acid. At the lower temperature the competitive formation of *N,N*'-dialkoxycarbonyl-*N,N*'-dialkoxyhydrazines can occur. It was found that alkaline hydrolysis of *N,N*-dialkoxycarbamates yields *NH-N,N*-dialkoxyamines.

ACKNOWLEDGEMENTS

This work was supported by the Russian Foundation for Basic Research (grant no. 13-03-90460) and Ukrainian Foundation for Fundamental Research (grant no. F-53/105-2013).

REFERENCES

[1]Shtamburg, V. G., Klots, E. A., Pleshkova, A. P., Avramenko, V. I., Ivonin, S. P., Tsygankov, A. V., Kostyanovsky, R. G., *Russ. Chem. Bull*, **2003**, *52*, 2251 – 2260.

[2]Shtamburg, V. G., Shishkin, O. V., Zubatyuk, R. I., Kravchenko, S. V., Shtamburg, V. V., Distanov, V. B., Tsygankov, A. V., Kostyanovsky, R. G., *Mendeleev Commun.*, **2007**, *17*, 178 – 180**.**

[3]Shtamburg, V. G., Anichshenko, A. A., Shtamburg, V. V., Tsygankov, A. V., Mazepa, A. V., Kostyanovsky, R. G., *Eur. Chem. Bull*., **2014**, *3*, 869 – 872.

[4]Shtamburg, V. G., Tsygankov, A. V., Shishkin, O. V., Zubatyuk, R. I., Uspensky B. V., Shtamburg, V. V., Mazepa, A. V., Kostyanovsky, R. G., *Mendeleev Commun.*, **2012**, *22*, 164-166.

[5]Glover, S. A., *Tetrahedron*, **1998**, *54*, 7229-727.

[6]Gerdes, R. G., Glover, S. A., ten Have, J. F., Rowbottom, C. A., *Tetrahedron Lett.*, **1989**, *31*, 5377 – 5380.

[7]Glover, S. A. Chapter 18. "*N-Heteroaton-substituted hydroxamic esters*" in "*The Chemistry of Hydroxylamines, Oximes and Hydroxamic Acids*", Rappoport Z. and Liebman J. F. (Ed), John Wiley & Sons, Ltd, **2009**.

[8]Gillson, A-M. E., Glover, S. A., Tucker, D. J., Turner, P., *Org. Biomol. Chem.*, **2003**, *1*, 3430 – 3437.

[9]Cavanach, K. L., Glover, S. A., Price, H. L. Schumacher, R. R., *Aust. J. Chem.*, **2009**, *62*, 700 – 710.

[10]Shishkin, O. V., Zubatyuk, R. I., Shtamburg, V. G., Tsygankov, A. V., Klots, E. A., Mazepa, A. V., Kostyanovsky, R. G., *Mendeleev Commun.*, **2006**, *16*, 222 – 223.

[11]Shishkin, O. V., Shtamburg, V. G., Zubatyuk, R. I., Olefir, D. A., Tsygankov, A. V., Prosyanik, A. V., Mazepa, A.V., Kostyanovsky, R. G., *Chirality*, **2009**, *21*, 642 – 647.

[12]Crawford, R. J., Raaf, R., *J. Org. Chem.*, **1963**, *28*, 2419 – 2424**.**

[13]Rudchenko, V. F., Shevchenko, V. I., Ignatov, S. M., Kostyanovsky, R. G., *Bull. Acad. Sci. Div. Chem. Sci.*, **1983**, *32*, 2174.

[14]Rudchenko, V. F., Shevchenko, V. I., Kostyanovsky, R. G., *Bull. Acad. Sci. Div. Chem. Sci.*, **1987**, *36*, 1436 – 1440.

[15]Prokof'ev, A .I., Rudchenko, V .F., Ignatov, S. M., Chervin, I .I., Kostyanovsky, R.G., *Bull. Acad. Sci. Div. Chem. Sci.*, **1989**, *38*, 1666 – 1671.

Received: 28.11.2014.
Accepted: 18.01.2015.

REACTIONS OF ACENAPHTHENEQUINONE DERIVATIVES WITH SOME AROMATIC AND ALIPHATIC AMINES

Atef M. Amer,[a]* Sherif I. Askar,[b] and Tarek S. Muhdi[a]

Keywords: Diketones; dinitriles; hydrazones; spiro; thiazolidines.

Reaction of acenaphthenequinone and aceanthrenequinone (**1a,b**) with diaminomaleonitrile at reflux temperature gave acenatho[1,2-b]pyrazine-8,9-dicarbonitrile and aceanthryleno[1,2-b]pyrazine-10-11-dicarbonitrile (**2a,b**), respectively. The reaction of **2a,b** with hydrazine hydrate afforded the corresponding cyclic products, 8,11-diaminoacenatho[1,2-b]pyrazino[2,3-d]pyridazine and 10,13-diaminoaceanthryleno[1,2b]pyrazino[2,3-d]pyridazine (**3a,b**). The reaction of **1a,b** with *p*-bromoaniline in presence of $ZnCl_2$ afforded complexes bis(*p*-bromophenylimino)acenaphthene and -aceanthrene (**7a,b**). We have also described the synthesis of spiro[2H-aceanthrene-2,2'-thiazolidine]-1,4'-dione derivatives (**8a,b**). Reaction of **1b** with 1-amino-3-(N,N-dimethylamino)propane, benzylhydrazine and *p*-bromophenylhydrazine has been investigated for studying the utility of products as pharmacological agents. Chemical and spectroscopic evidences for the structures of the new compounds are presented.

* Corresponding Authors
E-Mail: amer_1eg@yahoo.com
[a] Department of Chemistry, Faculty of Science, Zagazig University, Egypt.
[b] Faculty of Science, Omar Al-Mukhtar University, El-Beida, Tobruk branch, Libya.

INTRODUCTION

Recent studies have shown that acenaphthenequinone and its derivatives exhibit various biological activities,[1-6] such as bactericidal, antihypoxic, fungicidal, and are useful as phospholipase A2 inhibitors.[7] Acenaphthenequinones hydrogensulfite had a narcotic effect on mice and it inhibited the growth of transplanted tumours.[3] In addition, the condensation product of acenaphthenequinone with 2,3-diaminopyrazine has been used to provoke ataxia by lowering central nervous system activity.[6] In the literature, there is an abundance of reports dealing with the chemistry of acenaphthenequinone, but very little is known about the reaction of benzoacenaphthenequinone (aceanthrene-quinone) and its derivatives. Moreover, aceanthrenequinone derivatives have been extensively utilized as intermediate for the synthesis of fused aceanthrenes of potential biological activity.[8,9] In view of these findings and our interest in the synthetic potential of fused nitrogen heterocyclic compounds,[10,11] we have studied the synthesis of some differently fused acenaphthene and aceanthrene derivatives for studying their utility as pharmacological agents.

EXPERIMENTAL

General

Melting points were measured on a Kofler hot stage microscope (Reichert, Vienna) and are uncorrected. ^1H and ^{13}C NMR spectra were recorded on a Bruker DPX 200 spectrometer at 200 MHZ (^1H) and 50 MHZ (^{13}C). Chemical shifts are given in δ units relative to internal TMS at 295 K. IR spectra were obtained on a Biorard FT-IR-45 instrument. All experiments were carried out with exclusion of moisture. For all newly synthesized compounds satisfactory elemental analyses were obtained.

Reaction of 1,2-diketones 1a,b with diaminomaleonitrile (General Method)

A mixture of **1a** or **1b** (1 mmol) and 1 mmol of diaminomaleonitrile in 50 mL acetic acid was heated under reflux for 3 h. The solvent was reduced under reduced pressure and the solid product obtained was filtered off and recrystallized from suitable solvent to give the corresponding condensed products **2a** or **2b** respectively.

Acenaphtho[1,2-b]pyrazine-8,9-dicarbonitrile, 2a.

Prepared from 0.25 g acenaphthenequinone (1 mmol); crystallization from DMF / H_2O gave red crystals; Yield (88 %); m.p.: 238 °C; IR (KBr): 3065, 2238, 1614, 1488, 1421 cm^{-1} ; ^{1}HNMR ($CDCl_3$): δ = 7.93-8.01 (t,$2H_{ar}$), 8.31-8.35 (d, $2H_{ar}$), 8.52-8.56 (d, $2H_{ar}$) ppm.

Aceanthryleno[1,2-b]pyrazine-10,11-dicarbonitrile,2b.

Prepared from 0.26 g aceanthrenequinone **1** (1 mmol); crystallization from benzene gave brown crystals; Yield (85 %); m.p.:322 °C; IR (KBr) :3065, 2234, 1625, 1577, 1521, 1431 cm^{-1} ; ^{1}HNMR ($CDCl_3$) : δ = 7.77-7.79 (t, $1H_{ar}$), 7.96-7.98 (m, $2H_{ar}$), 8.28-8.32 (d, $1H_{ar}$), 8.48-8.52(d, $1H_{ar}$), 8.66-8.69 (d, $1H_{ar}$), 8.97 (d, $1H_{ar}$), 9.34-9.38 (d, $1H_{ar}$) ppm.

Reaction of 1,2-dicarbonitriles 2a,b with hydrazine hydrate (General Method)

A mixture of **2a** or **2b** (1 mmol) and 1.5 mmol of hydrazine hydrate in 50 mL toluene was heated under reflux for 3h. The solvent was evaporated under reduced pressure

and the solid product obtained was filtered off and recrystallized from suitable solvent to give the corresponding condensed products **3a** or **3b** respectively.

8,11-Diaminoacenatho[1,2-b]pyrazino[2,3-d]pyridazine, 3a.

Prepared from acenatho[1,2-b]pyrazine-8,9-dicarbonitrile (1 mmol); crystallization from ethanol gave dark red crystals; Yield (72 %); m.p.: 289 ˚C; U.V.(DMSO): λ 316, 448 nm. IR (KBr): 3439, 3269, 3115, 1666, 1608, 1466, 1456 cm^{-1} ; ^{1}HNMR (DMSO): δ = 6.21 (br, $2NH_2$), 7.99-8.05 (t, $2H_{ar}$), 8.39-8.42 (d, $2H_{ar}$), 8.49-8.52 (d, $2H_{ar}$) ppm.

10,13-Diaminoaceanthryleno[1,2-b]pyrazino[2,3-d]pyrazidine, 3b.

Prepared from aceanthryleno[1,2-b]pyrazine-10,11-dicarbonitrile (1 mmol); crystallization from acetic acid gave dark brown crystals; Yield (75 %); m.p.: 349 ˚C; IR (KBr): 3442, 3367, 3118, 1661, 1624, 1577, 1541, 1489 cm^{-1}; ^{1}HNMR ($CDCl_3$): δ = 6.11 (br, $2NH_2$), 7.56-7.70 (m, $3H_{ar}$), 7.72-7.92 (d, $1H_{ar}$), 8.05-8.14 (m, $2H_{ar}$), 8.52 (s, $1H_{ar}$), 9.07-9.10 (d, $1H_{ar}$) ppm.

8,11-Diacetamidoacenatho[1,2-b]pyrazino[2,3-d]pyridazine, 4.

A mixture of 8,11-diaminoacenatho[1,2-b]pyrazino[2,3-d]pyrazine (1 mmol) and 20 ml acetic anhydride was refluxed for 3 h. After cooling, the precipitate was filtered to give **4**. Crystallization from acetic acid gave dark brown crystals: Yield (75 %); m.p.: 349 ˚C; IR (KBr): 3367, 3017, 1672, 1610, 1542, 1487 cm^{-1}; ^{1}HNMR (DMSO): δ = 2.37 (s, $2CH_3$), 8.05 (t, $2H_{ar}$), 8.45 (d, $2H_{ar}$), 8.60 (d, $2H_{ar}$), 10.50 (br, 2NH) ppm.

Bis(*p*-bromophenylimino)acenaphthene and aceanthrene, 5a,b.

(i) A mixture of **1a** or **1b** (5 mmol), 0.86 g anhydrous ZnCl2 (6 mmol) and 2.25 g of p-bromoaniline (12 mmol) in 30 mL acetic acid was heated under reflux for 1h. The suspension was cooled to 20 °C and the solid filtered off. The product was washed with acetic acid and diethyl ether and air dried, to give the complexes **5a** or **5b** respectively, as an orange solids (95 %). Compound **5a**, 1HNMR ($CDCl_3$): δ = 7.47-7.73 (m, $12H_{ar}$), 8.18 (d, $2H_{ar}$) ppm. Compound **5b**, 1HNMR ($CDCl_3$): δ = 6.96 (m, $4H_{ar}$), 7.37-7.85 (m, $8H_{ar}$), 8.01-8.33 (m, $4H_{ar}$), 8.74 (s, $1H_{ar}$), 9.23 (d, $1H_{ar}$) ppm.

(ii) Compound **5a** or **5b** (6.4 mmol) was added to a solution of 25 g K_2CO_3 in 25 mL water and the mixture was heated at reflux with vigorous stirring. After 2 h the mixture was cooled to 20 °C, the solid product filtered off and washed with water (5 x 30 mL). The product was extracted with boiling ethanol (200 mL), until the ethanol extracts were almost colorless. The combined ethanol extracts were evaporated to 120 mL and set aside at -20 °C. After one day the product was filtered and dried in vacuo, to give compounds **6a,b**.

Bis(*p*-bromophenylimino)acenaphthene, 6a.

Yield (62 %); m.p.: 311 °C; IR (KBr): 3092, 1658, 1637, 1579, 1485, 1459, cm^{-1}. ^{1}HNMR ($CDCl_3$): δ = 6.95 (m, $3H_{ar}$), 7.55-7.59 (m, $4H_{ar}$), 7.84 (m, $2H_{ar}$), 8.03-8.28 (m, $5H_{ar}$) ppm.

Bis(*p*-bromophenylimino)aceanthrene, 6b.

Yield (62 %); m.p.: 298 °C; IR (KBr): 3090, 1665, 1637, 1565, 1487, 1461 cm^{-1}. ^{1}HNMR ($CDCl_3$): δ = 6.92 (d, $2H_{ar}$), 7.01 (d, $2H_{ar}$), 7.56–8.31 (m, $10H_{ar}$), 8.75 (d, $1H_{ar}$), 9.12(d, $1H_{ar}$) ppm.

3'-Arylspiro[2H-aceanthrene-2,2'-thiazolidine]-1,4'-diones, 7a,b.

A mixture of 0.10 g **1b** (0.4 mmol) and 0.4 mmol of the aromatic amine namely, aniline, *p*-bromoaniline or *p*-chloroaniline was dissolved in 50 mL of benzene. The reaction mixture was heated under reflux for 5 h in presence of 1.0 mL acetic acid. The solvent was evaporated under reduced pressure and 0.05 g mercaptoacetic acid (0.5 mmol) was added to the residue dissolved in 50 mL of benzene. The reaction mixture was refluxed until no more water was collected in a Dean-Stark separator. The solvent was evaporated in vacuo and the yellowish solid obtained was filtered off and recrystallized from suitable solvent to give the corresponding condensed products **7a** and **7b** respectively.

3'-Phenylspiro[2H-aceanthrene-2,2'-thiazolidine]-1,4'-diones (**7a**) was crystallized from toluene to give yellowish crystals; Yield (62 %); m.p.: 298 ˚C; IR (KBr): 3090, 2933, 1699-1680, 1627, 1579, 1485, 1459 cm^{-1} . ^{1}HNMR ($CDCl_3$): δ = 3.85 (d, $1H_{ar}$), 4.38 (d, 1H), 7.15 (d, $2H_{ar}$), 7.33-7.74 (m, $7H_{ar}$), 7.94 (d, $1H_{ar}$), 8.15 (d, $1H_{ar}$), 8.65 (s, $1H_{ar}$), 9.08 (d, $1H_{ar}$) ppm.

3'-(p-Bromophenyl)spiro[2H-aceanthrene-2,2'-thiazolidine]-1,4'-diones (**7b**) was crystallized from toluene to give yellowish crystals; Yield (45 %); m.p.: >300 ˚C; IR (KBr): 3050, 2980, 1690-1680, 1618, 1580, 1485, cm^{-1} . ^{1}HNMR ($CDCl_3$): δ = 3.90 (d, 1H), 4.45 (d, 1H), 6.90 (d, $2H_{ar}$), 7.17 (d, $2H_{ar}$), 7.62-7.68 (m, $3H_{ar}$), 7.78 (t, $1H_{ar}$), 7.96 (d, $1H_{ar}$), 8.15 (d, $1H_{ar}$), 8.70 (s, $1H_{ar}$), 9.07 (d, $1H_{ar}$) ppm.

2-(3-Dimethyamino-propylimino)-2H-aceanthrylen-1-one, 9.

A mixture of 0.10 g **1b** (0.4 mmol) and 0.5 mmol of 1-amino-3-(N,N-dimethylamino)propane in 50 mL benzene was heated under reflux for 3 h until no more water was collected in a Dean-Stark separator. The solvent was evaporator under reduced pressure and the yellow solid obtained was filtered off and purified from methanol/$CHCl_3$ to give the corresponding condensed products **9**. Yield (35 %); m.p.: >250 ˚C; IR (KBr): 3046, 2932, 1710, 1665, 1625, 1585, 1532, 1489 cm^{-1} . ^{1}HNMR (CD_3COCD_3): δ = 1.83 (q, CH_2), 2.19 (s, $2CH_3$), 2.35 (t, CH_2), 4.41 (t, CH_2), 7.55-7.74 (m, $3H_{ar}$), 8.01(d, $1H_{ar}$), 8.28 (d, $1H_{ar}$), 8.52 (d, $1H_{ar}$), 8.77 (s, $1H_{ar}$), 9.78 (d, $1H_{ar}$) ppm. ^{13}C NMR (CD_3COCD_3): 35.50 (CH_2), 48.16 (CH_2), 54.36($2CH_3$), 66.80 (CH_2), 124.36,

133.46, 134.90, 135.44, 135.69, 136.40, 137.38, 137.93, 139.14, 140.37, 141.74, 142.36, 144.55, 145.83(aryl), 172.39 (C=N), 174.12 (C=O) ppm.

Reaction of aceanthrenequinone 1 with aroyl hydrazine derivatives

A mixture of 0.10 g aceanthrenequinone (0.4 mmol) and 0.4 mmol aroyl hydrazine derivatives namely, benzoyl hydrazine, p-methylbenzoyl hydrazine, p-bromobenzoyl hydrazine or m-chlorobenzoyl hydrazine was refluxed for 3 h in 30 mL of dry methanol and 1 mL acetic acid. After cooling, the precipitate was filtered to give **10a-d**.

Compound **10a** was crystallized from benzene to give orange crystals; Yield 2.28 g (65 %); m.p.: >250 °C; IR (KBr): 3239, 3046, 1710, 1695, 1625, 1612, 1585, 1522, 1489 cm^{-1}. Elemental analysis for $C_{23}H_{14}N_2O_2$ (350.38), Calcd. C, 78.84; H, 4.02; N, 7.99; found C, 78.70; H, 4.20; N, 7.80.

Compound **10b** was crystallized from methanol to give orange crystals; Yield 2.18 g (60 %); m.p.: >265 °C; IR (KBr): 3242, 3046, 2943, 1710, 1693, 1628, 1610, 1585, 1522, 1482 cm^{-1}. Elemental analysis for $C_{24}H_{16}N_2O_2$ (364.40), Calcd. C, 79.11; H, 4.42; N, 7.69: found C, 79.00; H, 4.50; N, 7.80 .

Compound **11c** was crystallized from toluene to give orange crystals; Yield 3.86 g (90 %); m.p.: 240 °C; IR (KBr): 3239, 3046, 1710, 1695, 1625, 1612, 1585, 1522, 1489 cm^{-1}. ^{1}HNMR ($CDCl_3$): δ = 7.65–7.71(m, 5Har + NH), 7.80 (m, $2H_{ar}$), 8.00 (d, $2H_{ar}$), 8.10 (d, $1H_{ar}$), 8.20 (d, $1H_{ar}$), 8.80 (s, $1H_{ar}$), 9.12(d, $1H_{ar}$) ppm. The mass spectrum showed molecular ion peak at m/e 430 [M^+ + 1], 245 [M^+ - C_6H_4Br], base peak at 217 [M^+ -COC_6H_4Br] [100 %], 189 [M^+ -$N_2COC_6H_4Br$], 157, 139, 104 and 75. Elemental analysis for $C_{23}H_{13}BrN_2O_2$ (429.27), Calcd. C, 64.25; H, 3.05; N, 6.53, found C, 64.40; H, 3.00; N, 6.40.

Compound **11d** on crystallization from benzene gave red yellow crystals; Yield 2.89 g (75 %); m.p.: 238 °C; IR (KBr): 3239, 3046, 1710, 1695, 1625, 1612, 1585, 1522, 1489 cm^{-1}. ^{1}HNMR ($CDCl_3$): δ = 7.52–8.11(m, $9H_{ar}$ + NH), 8.20 (d, $1H_{ar}$), 8.80 (s, $1H_{ar}$), 9.12 (d, $1H_{ar}$) ppm. The mass spectrum showed molecular ion peak at m/e 384 [M^+], 247 [M^+-C_6H_4-Cl], base peak at 217 [M^+-COC6H4Cl] [100 %], 189 [M^+-N_2COC6H4-Cl], 139, 101 and 75. Elemental analysis for $C_{23}H_{13}ClN_2O_2$ (384.82), Calcd. C, 71.79; H, 3.40; N, 7.28; found C, 71.90; H, 3.30; N, 7.50.

Reaction of 10b with malononitrile

A mixture of hydrazone **10b** (1mmol) and malononitrile (1 mmol) in 30 mL acetic acid was heated under reflux for 1 h. The solid formed during heating was filtered off and recrystallized from aqueous DMF to give the condensed product **11;** Yield (80 %); m.p.: 340 °C; IR (KBr): 3360, 3240, 3055, 2266, 2193, 1689, 1665, 1589, 1520 cm^{-1}. ^{1}HNMR ($CDCl_3$): δ = 7.63-7.72(m, $4H_{ar}$), 7.78-7.83 (t, $1H_{ar}$), 7.94-7.96 (d, $2H_{ar}$), 8.05-8.07 (d, 2H), 8.10-8.18 (d, 1Har), 8.77(s, $1H_{ar}$) , 9.04-9.06 (d, 2Har), 14.50(s, 1H, NH) ppm.^{13}CNMR ($CDCl_3$): δ = 108, 119.50, 123.76, 124.22, 127.02, 127.46, 127.81, 128.02, 128.50, 129.25, 129.47, 129.89, 130.45, 131.19, 132.27, 133.19, 134.90, 142.56, 160.20, 190.10 (aryl and C=O) ppm.

RESULTS AND DISCUSSION

The condensation of the 1,2-diketones with aliphatic diamine was carried out in the manner described by Chiodini[12] to give fused pyrazine derivatives in good yield. Based on these results, it was found that treatment of acenaphthenequinone and aceanthrenequinone (**1a,b)** with diaminomalenonitrile at reflux temperature gave acenaphtho[1,2-b]-pyrazine-8,9-dicarbonitrile and aceanthryleno[1,2-b]pyrazine-10,11-dicarbonitrile (**2a,b),** respectively. The reaction of **2a,b** with hydrazine hydrate afforded the corresponding cyclic product namely, 8,11-diamino-acenatho[1,2-b]pyrazino[2,3-d]pyridazine and 10, 13-diamino-aceanthryleno[1,2-b]pyrazino[2,3-d]pyridazine (**3a,b**). Treatment of **3a** with acetic anhydride under reflux temperature readily afforded 8,11-diacetamido-acenaphtho[1,2-b]pyrazino[2,3-d]pyridazine (**4)** (Scheme 1).

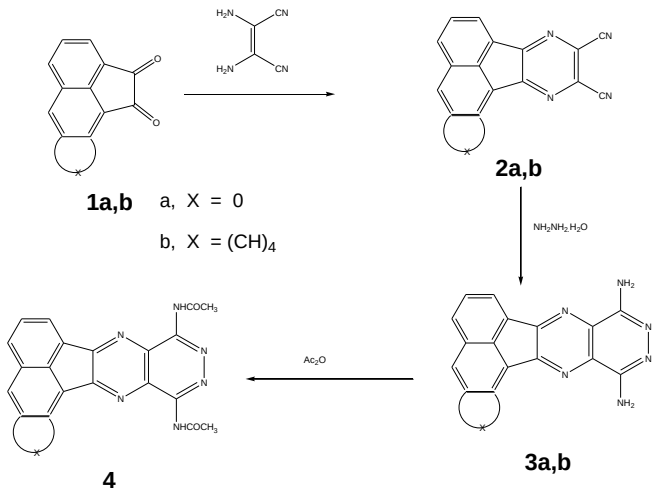

Scheme 1

We have been interested in the complexation properties of bis(arylimino)-acenaphthene and aceanthrene (**6a,b**) due to the presence of two exocyclicimine functionalities, which are not being part of a heteroaromatic ring system, is expected to lead to better O-donating and better π-accepting properties as compared with bipyridyl. Also, the rigid acenaphthene and aceanthere backbone prevents rotation around the imine carbon-carbon bond and as a consequence both imine-N atoms remain in a fixed *cis* orientation favouring chelating coordination to a metal center.

Compounds **6a,b** could not be obtained directly by the reaction of 1,2-diketones **1a,b** with *p*-bromoaniline under different conditions. In all cases reaction occurred to give monoimino compounds with mixtures of several compounds were formed, which were not further investigated. Compounds **5a,b** were synthesized form **1a,b** and *p*-bromoaniline in boiling acetic acid and zinc chloride. Compounds **6a,b** were synthesized from 5**a,b** by replacing the zinc chloride with aqueous potassium carbonate.[13]

Table 1. Antimicrobial activity of some synthesized compounds

Compd. No	Zone of inhibition				
	Sarcina Lutea	***B. Megaterium***	***B. Cerius***	***B. Subtilis***	***Pseudomonas Aeruginosa***
6a	10	6	-	-	5
6b	10	5	-	-	5
8a	13	10	10	10	15
8b	16	12	10	10	15
9	15	8	-	-	13

A recent observation by Diurno and co-workers[14,15] that spirothiazolidinone derivatives have antimicrobial and antifungal activities prompted us to synthesize 3'-aryl-spiro[2H-aceanthrene-2,2'-thiazolidine]-1,4'-diones (**8a,b)** via the Schiff-bases of aceanthrenequinone with arylamines, followed by cyclization with mercaptoacetic acid in refluxing benzene with removal of water from the reaction mixture. The chemical structure of compound **8b** was confirmed by ^{1}H-COSY spectroscopy (Scheme 2). The structure of all newly synthesized compounds was confirmed by their elemental and spectroscopic data.

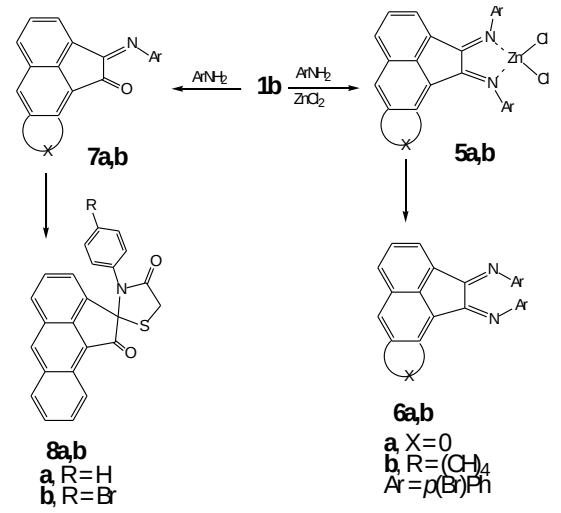

Scheme 2

Treatment of **1b** with 1-amino-3-(*N*,*N*-dimethylamino)propane under reflux afforded *2*-(imino-N,N-dimethylpropylamine)aceanthrene **(9)**.

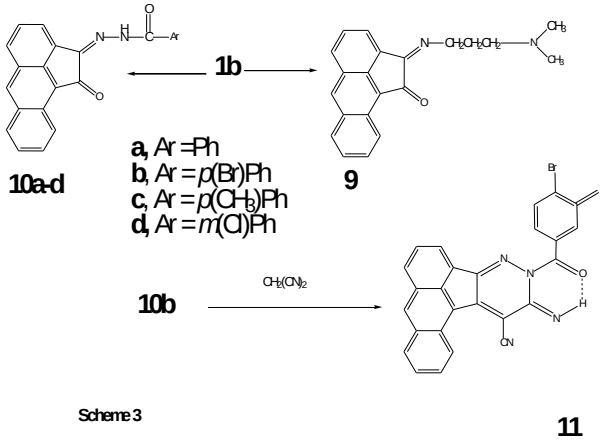

Scheme 3

Furthermore, condensation reaction of aceanthrene-quinone **1b** with aroyl hydrazine derivatives namely, benzoyl hydrazine, *p*-toluoyl hydrazine, *p*-bromobenzyoyl hydrazine and m-chlorobenzoyl hydrazine afforded the corresponding hydrazone derivatives **10a-d** respectively. Finally, our study was extended to prepare the aceanthryleno[1,2-c]-pyridazine derivative **11** by reaction of hydrazone **10b** with malononitrile to give the corresponding product (Scheme 3).

Screening for antimicrobial activities

The antimicrobial activity of some of the prepared compounds was determined by cup-plate technique (BPC, 1963) using Cork borer for making wells in agar plates. The sample of the compounds **7-10** were dissolved in DMF (20 % conc.). 0.1 cm^3 of each sample was used for some Gram-positive (*Sarina lutea*, *Bacillus Megaterium*, *Bacillus cerius* and *Bacillus subtilis*) and Gram-negative (*Pseudomonas Aeruginosa*) bacteria under aseptic conditions. The medium for cultivation of the test organisms was nutrient agar (APHA, 1985). Bacteria were incubated at 30 ˚C for 24 h and the diameters of the inhibition zones were measured in mm. Compounds **7-10** showed antimicrobial activity against both Gram-Positive and Gram-negative bacteria as shown in Table 1**.**

References

[1]Zhang, Z., Yang, H., Wu, G., Li, Z., Song, T., Li, X. Q., *Eu. J. Med. Chem*., **2011**, *46*, 3909–3916.

[2]Elinson, M. N., Ilovaisky, A. I., Merkulova, V. M., Barba, Batanero, F., B., *Tetrahedron*, **2013**, *69*, 7125–7130.

[3]Pearson, A. E. G. and Powell, A. K., *Br. J. Cancer*, **1955**, *9*, 204; *Chem. Abstr*., **1955**, *49***,** 11898.

[4]Kunz, R. M., *Helv. Chim. Acta*., **1939**, *22***,** 939.

[5]Romistrov, M. N., Kulik, G. V., Gorbonos, T. V., Bredikhina, A. N., Skrynik, E. M., *Visn. Kiiv. Univ. Ser. Biol.* **1972**, *14***,** 90; *Chem. Abstr*.**1973**, *79***,** 38890.

[6]Cain, C. K., *Fr. Patent*., **1970**, 6196, *A.72***,** 12767.

[7]William, C. R. and William, J. S., *U.S.* **1989**, 4, 806, 671, 21 Feb.; *Appl.* **1986**, ***1989***, 860, 428, 07 May; *Chem. Abstr*., *111***,** 96879.

[8]Chang, S. J., Shankar, B. K., Schechter, H., *J. Org. Chem*., **1982**, *47***,** 4226.

[9]Alberts, D. S., Dorr R., Remers, W. A., Sami, S. M., *Pct. Int. Appl. Wo*., **1992**, 9200, 281, 9 Jan.; *Chem. Abstr*., **1992**, *116***,** 214369.

 DOI: 10.17628/ecb.2014.3.1126-1130

[10]Amer, A. M., Mostafa, M. A., Amer, M. S., *Afinidad*, **1997**, *470***,** 305.

[11]Assy, M. G., Amer, A. M., El-Bahai, S., Halima, E. A., *Polish. J. Chem.*, **1998**, *72***,** 61.

[12]Chiodini, L., Di-Ciommo, M., Merlini L., *J. Heterocycl. Chem.*, **1981**, *18***,** 1141.

[13]Asselt, R., Elsevier, C. J., Smeets, W. J., Spek, A. L., Benedix, R., *Recl. Trav. Chim. Pays-Bas*, **1994**, *113***,** 88.

[14]Piscopo, E., Diurno, M. V., Mazzoni, O., Ciaccio, G., Veneruso, G., *Boll. Soc. It Bio. Sper*., **1990**, *66***,** 1187.

[15]Rajopadhye, M., Popp, F. D., *J. Heterocyclic. Chem*., **1984**, *21***,** 289.

Received: 21.11.2014.
Accepted: 20.01.2015.

HIGH ENTROPY ALLOYS AND CORROSION RESISTANCE –A BIRD'S EYE VIEW

S. John Mary[a] , R. Nagalakshmi[b]* , Susai Rajendran[c] and R. Epshipha[d]

Keywords: High entropy alloys; corrosion resistance; micro structure; properties, applications

The introduction of high entropy alloys (HEA) concept broke up the traditional rule that the main elements take up more than 50% atomic content. HEA means that alloys are composed of multi elements and each takes up a relatively high but less than 35% of atomic content. The properties of this innovative alloy are decided by the combined action of multi elements. HEA tends to form simple crystallization phase. By controlling the composition, it is possible to achieve high-hardness and high-abrasion performance at high temperature, Microstructure and properties of several HEAs prepared by various methods such as powder metallurgy laser cladding etc, are discussed. The corrosion resistance of HEAs is also discussed.

* Corresponding Author
E-Mail: nagalakshmirajan@gmail.com
[a] Department of Chemistry, Loyola College, Chennai 600 034, India.
[b] Department of Chemistry, Aarupadai Veedu Institute of Technology, Chennai- 603 104
[c] Corrosion Research centre, Department of Chemistry, RVS School of Engineering and Technology, Dindigul - 624005, India
[d] Department of Chemistry, Sri Muthukumaran Institute of Technology, Chikkarayapuram, Chennai 600 069
Email:hephzibahjesuprakash@gmail.com

Introduction

The past twenty years have witnessed the fast development of bulk metallic glasses (BMGs),[1-3] a relatively new type of metallic materials with non-crystalline or amorphous structure. Their unique mechanical and physiochemical properties have stimulated extensive research in the materials community.[2-6] High entropy alloys (HEAs), or equiatomic multi-component alloys that are often in a single solid-solution form, were developed slightly later than the bulk metallic glasses and they even share many similar properties,[7-10] but HEAs were given much less attention compared to BMGs. The concept of high-entropy bulk metallic glasses (HE-BMGs) which appeared very recently[11-13] provides an opportunity to compare and study the similarity and difference between these two types of multi-component alloys, particularly, from the alloy design perspective. A critical question relevant to the alloy design for multi-component alloys is: for a given composition with known constituent elements, can we predict which type of phases (amorphous phase, solid solution phase or inter metallic phase) will form? Alternatively, are we now capable of designing the multi-component alloys with the desired phase constitution.

Unfortunately, it is still too ambitious to answer the above two important questions. However, there do have some clues obtained over years of alloy development. For the alloy design of BMGs, the three empirical rules initiated by INOUE[1] have been proven useful: multi-component systems, significant atomic size difference and negative heats of mixing among constituent elements. As traditionally the BMGs have only one or two principle elements, the uncertainty of the suitable composition for other alloying elements complicates the alloy design as there exist too many possibilities to be tried out. It is hence not surprised to see that currently many, if not most, alloy designs for BMGs are based on micro-alloying[14-17] or substitution of similar elements[18,19]for those mature BMG formers, which were also developed from try-and-error experiments. Along this line of thinking, the alloy design in the equiatomic HEAs could be relatively easier, as once the alloy elements are chosen their compositions are known. However, we now face the uncertainty of the resultant types of crystalline phases: fcc, bcc, mixed fcc and bcc phases.[20]

In some multi-component alloys with a high mixing entropy (so in principle they can also be called HEAs even they do not form a single solid solution), intermetallic phases can form.[20] As the unique properties of HEAs mostly originate from the formation of the multi-component solid solution,[7,10] we need to know the rules governing the formation of solid solution phases. Although the name of HEAs and the fact that the HEAs have large mixing entropy give the impression that the mixing entropy is the dominating factor controlling the formation of the solid solution phases, there exists no solid evidence supporting this argument. From the classical Hume-Rothery rule [21] we know that to form a solid solution, the properties of constituent alloying elements need to be similar: they shall have similar atomic size and similar electro negativity.

However, the Hume-Rothery rule is apparently not applicable to the solid solution formation in HEAs. For example, it cannot explain why the equiatomic Co (hcp) – Cr(bcc) – Cu(fcc) – Fe(bcc) – Ni(fcc) alloy forms an fcc-typed solid solution, and how the addition of fcc-Al can eventually change the fcc-type CoCrCuFeNi to a bcc structure.[22]

Microstructure and properties of high entropy alloys prepared by various methods are discussed.

Structure and properties of FeCoNiCrCu0.5Alx high-entropy alloy[25]

Effects of Al content and heat treatment on the structure, hardness and electrochemical properties of FeCoNiCrCu0.5Alx high-entropy alloys were investigated. The phase structure of as-cast alloys evolves from FCC phase to BCC phase with the increase of Al content. The stable phase of FeCoNiCrCu0.5Alx high-entropy alloys will transform from FCC phase to FCC + BCC duplex phases when x value increases from 0.5 to 1.5. The hardness of BCC phase is higher than that of FCC phase, and the corrosion resistance of BCC phase is better than FCC phase in chlorine ion and acid medium. High hardness and good corrosion resistance can be obtained in as-cast FeCoNiCrCu0.5Al1.0 alloy.

Microstructure and corrosion resistance of AlCrFeCuCo high entropy alloy[26]

The AlCrFeCuCo high-entropy alloys were prepared by the laser cladding method. The microstructure and corrosion resistance property of AlCrFeCuCo high-entropy alloy were researched by scanning electron microscopy, X-ray diffraction and electrochemical workstation. The results show that, under the rapid solidification small microstructure gained, the morphology of AlCrFeCuCo high entropy alloy is simple, the phase mainly compose of FCC and BCC; elements segregated in the alloys; the alloy shows excellent corrosion resistance, along with the increase of the scanning speed, alloy corrosion resistance performance shows a enhancement in the first and then weakened trend. The corrosion resistance performance of AlCrFeCuCo high-entropy alloys in 1 mol L^{-1} NaCl solution is better than in 0.5 mol L^{-1} H_2SO_4 solution.

Corrosion behaviour of CuCrFeNiMn high entropy alloy system in 1 M sulfuric acid solution[27]

Immersion tests and potentiodynamic polarization measurements were conducted in 1 M sulfuric acid solution (H_2SO_4) at ambient temperature (~25 °C) to investigate the corrosion behavior of CuCrFeNiMn alloy system. The results show that the alloys display a good general corrosion resistance that is mainly influenced by the Cu content and elemental segregation degree. The corrosion resistance degrades when increasing Cu content and elemental segregation degree. Among the tested alloys, the $2Mn_2$ alloy with low Cu content and elemental segregation degree displays a better general corrosion resistance. On the contrary, the Cu2CrFe2NiMn2 alloy with high Cu content and elemental segregation degree exhibits the worst general corrosion resistance.

Effect of nitrogen content and substrate bias on mechanical and corrosion properties of high-entropy films (AlCrSiTiZr) 100-xN x[28]

High-entropy alloy and nitride films of (AlCrSiTiZr)100-xNx containing large Zr atoms and small Si atoms were deposited on 6061 aluminum alloy and mild steel substrates by DC reactive magnetron sputtering at various nitrogen flow ratio (R_N). The composition, crystalline structure, and film morphology were analyzed by electron probe X-ray micro analyzer (EPMA), X-ray diffractometer (XRD), transmission electron microscope (TEM), and scanning electron microscope (SEM), respectively. Also, their hardness and elastic modulus were studied by nano indentation. The corrosion behavior was studied by anodic polarization analysis in 0.1 M H_2SO_4 aqueous solution at room temperature. The properties of films deposited under substrate bias application were also studied. The tendency of the present composition to form amorphous or low-crystallinity structure is high because of its large difference in atomic size. Films demonstrate pure amorphous structures even as the nitrogen content reaches as high as 22.4 at.%.

All coatings can provide better corrosion resistance on both 6061 aluminum alloy and mild steel substrates. Under condition of no applied substrate bias, films of (AlCrSiTiZr)100-xNx deposited at R_N = 30 % give the best corrosion resistance. Substrate bias of -100V effectively improves the corrosion resistance of the amorphous film of (AlCrSiTiZr)100-xNx (R_N = 5 %). The factors that might influence the corrosion resistance have been reported.

Study on corrosion resistance of high-entropy alloys NiCoCrFeMnCuC in medium acid liquid[29]

High-entropy alloy of NiCoCrFeMnCuC were made by vacuum non-consumable arc furnace. The crystal structure of NiCoCrFeMnCuC was analyzed by XRD. The corrosion resistance of NiCoCrFeMnCuC in 10 % HNO_3 - 3 % HF, 10 % H_2SO_4, 5 % HCl and 10 % HF was investigated, respectively with weight loss experiment. The results show that main inter metallics of the alloy are CoCx, $FeNi_3$ and Fe_3Mn_7.The NiCoCrFeMnCuC has simple crystal structures with face-centered cubic crystal structure FCC and Quartet and has excellent corrosion resistance in some medium acid liquids.

Microstructural evolution and corrosion behaviour of directionally solidified FeCoNiCrAl high entropy alloy[30]

The FeCoNiCrAl alloys have many potential applications in the fields of structural materials, but few attempts were made to characterize the directional solidification of high entropy alloys. Recently, the micro structure and corrosion behavior of FeCoNiCrAl high entropy alloys have been investigated under directional solidification. The results show that with increasing solidification rate, the interface morphology of the alloy evolves from planar to cellular and dendritic. The electrochemical experiment results demonstrate that the corrosion products of both non-directionally and directionally solidified FeCoNiCrAl alloys appear as rectangular blocks in phases which Cr and Fe are enriched, while Al and Ni are depleted, suggesting that Al and Ni are dissolved into the NaCl solution. Comparison of the potentiodynamic polarization behaviors between the two differently solidified FeCoNiCrAl high entropy alloys in a 3.5 % NaCl solution shows that the corrosion resistance of directionally solidified FeCoNiCrAlalloy is superior to that of the non-directionally solidified FeCoNiCrAl alloy.

The property research on high-entropy alloy Al xFeCoNiCuCr coating by laser cladding[31]

High-entropy alloys have been found to have novel microstructures and unique properties. The main method of manufacturing is vacuum arc remelting. As in situ cladding laser cladding has capability of achieving a controllable dilution ratio, fabricating high-entropy alloy by laser cladding is of great significance and potential for extensive use. Recently, a novel AlxFeCoNiCuCr high-entropy alloy system was manufactured as the thin layer of the substrate by laser cladding; also high temperature hardness, abrasion performance, corrosion nature of the AlxFeCoNiCuCr high-entropy alloy were tested under the different ratio of aluminum. It is observed that higher aluminum clad exhibit higher hardness, better abrasion resistance and corrosion resistance

Electro-spark deposition of multi-element high entropy alloy coating[32]

A multi-element high entropy alloy coating AlCoCrFeNi was fabricated on AISI 1045 carbon steel substrates using electro-spark deposition. The surface morphology of the as-deposited coating was examined and the phase of the coating was identified. In addition, the hardness and the corrosion properties of the coating were evaluated. An SEM examination showed that a metallurgically bonded coating of thickness up to 100 μm can be produced on carbon steel substrates. The results of an EDX analysis suggest that the coating has the same chemical composition as the high entropy alloy without apparent dilution of content. The XRD results indicate that the coating has a simple BCC structure and no inter metallic phase was detected. The micro hardness of the coating was some two times higher than that of the substrate material. With regard to corrosion properties, the corrosion current density and the corrosion potential of the as-deposited coating were three orders of magnitude lower and 140 mV higher than those of the substrate material, respectively. Moreover, the polarization curve of the coating exhibits a passive region, indicating that the corrosion resistance of the coating is superior to that of the substrate material.

Effect of aging treatment on microstructure and properties of high-entropy Cu0.5CoCrFeNi alloy[33]

The microstructure and properties of Cu0.5CoCrFeNi high-entropy alloys with as-cast structure and heat treated structures were investigated. The as-cast alloy specimens were firstly heated at 1050 °C for a holding time of 1 h. Serial aging heat treatment processes were performed at 350 °C, 500 °C, 650 °C, 800 °C, 950 °C, 1100 °C, 1250 °C and 1350 °C with a holding time of 24 h at each temperature. The microstructures, chemical composition, and precipitate phase of alloys with as-cast and various aging heat treated specimens characterized analyses were performed by scanning electron microscopy (SEM), X-ray diffraction (XRD) and transmission electron microscopy (TEM). The results show that FCC phase structures remain unchanged after aging the Cu0.5CoCrFeNi alloy of the as-cast specimens that had been heated to 1350 °C. The microstructure of the alloy specimens consisted of FCC matrix, Cu-rich phase, and Cr-rich phase. This Cr-rich phase precipitates to FCC matrix after being aged at 1100-1350 °C. The hardness of the Cu0.5CoCrFeNi alloy was unchanged for the specimens after various heat treatments. The corrosion resistance of the specimens was evaluated by potentiodynamic polarization in immersion tests. The as-cast specimen and those that had undergone aging heat treatments from 350 to 950 °C were seriously corroded in 3.5 % NaCl solution due to segregation of the Cu-rich phase precipitate formed in the FCC matrix. Cl- ions preferentially attacked the Cu-rich phase which was a sensitive zone exhibiting an appreciable potential difference with the consequent galvanic action. The specimens that were heat treated at 1100-1350 °C showed the best corrosion properties, because the Cu-rich phase was dissolved into the FCC matrix at elevated temperatures.

Microstructure and electrochemical properties of Al-FeCuCoNiCrTi x high entropy alloys[34]

Microstructure of AlFeCuCoNiCrTix (atom weight, x=0.5, 1.0, 1.5) high entropy alloys was observed, and electrochemical behavior of the high entropy alloy was examined and compared with that of commercial 304 stainless steel in 0.5 mol H_2SO_4 solution and 1 mol NaCl solution. The results reveal that the AlFeCuCoNiCrTix (atom weight, x = 0.5, 1.0, 1.5) high entropy alloys is mainly composed of fcc structure and bcc structure. Polarization curves show that compared with that of 304 stainless steel, the alloys exhibits lower corrosion rate in 0.5 mol H_2SO_4 solution, however the pitting corrosion resistance is superior to that of 304 stainless steel in 1 mol NaCl solution

Corrosion behaviour of 6061Al - 15vol. Pct. SiC composite and its base alloy in a mixture of 1:1 hydrochloric and sulphuric acid medium[35]

Silicon carbide particulate - reinforced aluminum (SiCp-Al) composites possess a unique combination of high specific strength, high elastic modulus, good wear resistance and good thermal stability than the corresponding non-reinforced matrix alloy systems. These composites are potential structural material for aerospace and automotive applications. The corrosion characteristics of 6061Al/SiCp composite and the base alloy were experimentally assessed. The corrosion test was carried out at different temperatures in 1:1 mixture of hydrochloric acid and sulphuric acid at a concentration range of 0.01 to 1 N for each of the acid, as corrosion media using Tafel extrapolation technique and Electrochemical impedance spectroscopy (EIS). The results obtained from Tafel extrapolation technique and Electro chemical impedance spectroscopy was in good agreement. The results showed an increase in the corrosion rate with increases in temperature as well as the increase in the concentration of the corrosion media. The thermodynamic parameters like energy of activation were calculated using Arrhenius theory equation and, enthalpy of activation and entropy of activation were calculated using transition state theory equation.

Enhancing pitting corrosion resistance of AlxCrFe1.5MnNi0.5 high-entropy alloys by anodic treatment in sulfuric acid[36]

High-entropy alloys are a newly developed family of multi-component alloys that comprise various major alloying elements. Each element in the alloy system is

present in between 5 and 35 at %. The crystal structures and physical properties of high-entropy alloys differ completely from those of conventional alloys. The electrochemical impedance spectra (EIS) of the AlxCrFe1.5MnNi0.5 (x = 0, 0.3, 0.5) alloys, obtained in 0.1 M HCl solution, clearly revealed that the corrosion resistance values were determined to increase from 21 to 34 Ω cm^2 as the aluminium content increased from 0 to 0.5 mol, and were markedly lower than that of 304 stainless steel (243 Ω cm^2). At passive potential, the corresponding current declined with the anodizing time accounting, causing passivity by the growth of the multi-component anodized film in H_2SO_4 solution. X-ray photoelectron spectroscopy (XPS) analyses revealed that the surface of anodized Al0.3CrFe1.5MnNi0.5 alloy formed aluminum and chromium oxide film which was the main passivating compound on the alloy. This anodic treatment increased the corrosion resistance in the EIS measurements of the CrFe1.5MnNi0.5 and Al0.3CrFe1.5MnNi0.5 alloys by two orders of magnitude. Accordingly, the anodic treatment of the AlxCrFe1.5MnNi0.5 alloys optimized their surface structures and minimized their susceptibility to pitting corrosion.

Effect of the aluminium content of AlxCrFe1.5MnNi0.5 high-entropy alloys on the corrosion behaviour in aqueous environments [37]

High-entropy alloys (HEAs) are a newly developed family of multi-component alloys. The potentiodynamic polarization and electrochemical impedance spectroscopy of the AlxCrFe1.5MnNi0.5 alloys, obtained in H_2SO_4 and NaCl solutions, clearly revealed that the corrosion resistance increases as the concentration of aluminium decreases.

TheAlxCrFe1.5MnNi0.5 alloys exhibited a wide passive region, which extended > 1000 mV in acidic environments. The Nyquist plots of the Al-containing alloys had two capacitive loops, which represented the electrical double layer and the adsorptive layer. SEM micrographs revealed that the general and pitting corrosion susceptibility of the HEAs increased as the amount of aluminium in the alloy increased.

Effect of boron on the corrosion properties of Al 0.5CoCrCuFeNiBx high entropy alloys in 1 N sulfuric acid [38]

High entropy alloys are a newly developed family of multi-component alloys composed of several major alloying elements, such as copper, nickel, aluminum, cobalt, chromium, iron, etc. Each element in the alloy system is between 5 at % and 35 at %. High entropy alloy has a lot of advantages regarding its mechanical, magnetic and electrochemical properties. Lee et al have discussed the corrosion resistance of Al0.5CoCrCuFeNiBx alloys with various amounts of boron addition. Surface morphology and EDS analysis confirmed that the addition of boron produced Cr and Fe borides. Therefore the content of Cr in the region besides borides precipitates was very scanty. The anodic polarization curves and electrochemical impedance spectra of Al0.5CoCrCuFeNiBx alloys, obtained in 1 N H_2SO_4 aqueous solution, clearly indicated that the general corrosion resistance decreases as the amounts of boron increases.

Conclusion

High entropy alloys (HEAs), (equiatomic multicomponent alloy) are in a single solid –solution form. They have unique mechanical and physicochemical properties.They have fcc or bcc structure. These structures are inter convertible on addition of some foreign substances. The microstructure, hardness, corrosion resistance and compression resistance have made these HEAs unique. They can be prepared by various methods such as powder metallurgy and laser cladding. Their microstructures have been investigated by SEM, TEM and XRD. Corrosion resistance has been evaluated by polarization study and Electrochemical Impedance spectra.

Acknowledgement

The authors are thankful to their management for their help and encouragement, especially to Dr. K. V. Kupusamy, Chairman, RVS Educational Trust group of Institution, India.

References

[1]Inoue, A., *Acta. Mater.*, **2000**, *48*, 279.

[2]Johnson, W. L., *MRS Bull*., **1999**, *24*, 42.

[3]Wang, W. H., Dong, C., Shek, C. H., *Mat. Sci. Eng., R-Reports*, **2004**, 44, 45.

[4]Schuh, C. A., Hufnagel, T. C., Ramamurty, U., *Acta Mater.*, **2007,** *55*, 4067.

[5]Ashby, M. F., Greer, A. L., *Scripta Mater.*, **2006,** *54*, 321.

[6]Loffler, J. F., *Intermetallics***, 2003,** *11*,529.

[7]Yeh, J. W., Chen, S. K., Lin, S. J., *Adv. Eng. Mater.*, **2004**, *6*, 299.

[8]Cantor, B., Chang, I .T. H., Knight, P., *Mater. Sci. Eng. A*, **2004,** *213*, 375.

[9]Wu , W. H., Yang, C. C., Yeh, J. W., *Ann. Chim.-Sci. Mat.*, **2006**, *31*, 737.

[10]Yeh, J. W., *Ann. Chim.-Sci. Mat.*, **2006,** *31*, 633.

[11]Zhao, K., Xia, X. X., Bai, H. Y., *Appl. Phys. Lett***., 2011,** *98*, 141913.

[12]Gao, X. Q., Zhao, K., Ke, H.B., *J. Non-Cryst. Solids*, **2011**, *357*, 355.

[13]Takeuchi, A., Chen, N., Wada, T., *Intermetallics***, 2011**, *19*, 1546.

[14]Wang, W. H., *Prog. Mater. Sci.***, 2007**, *52*, 540.

[15]Liu, C. T., Chisholm, M. F., Miller, M. K., *Intermetallics*, **2002**, *10*, 1105.

[16]Lu , Z. P., Liu, C. T., *J. Mater. Sci.*, **2004**, *39*, 3965.

[17]Liu, C .T., Lu, Z. P., *Intermetallics*, **2005**, *13*, 415.

[18]Zhang, T., Li. R., Pang, S, J., *J. Alloy Compd.*, **2009**, *483*, 60.

[19]Li, R., Liu, F. J., Pang, S., *Mater. Trans. JIM.*, **2007**, *48*, 1680.

[20]Guo, S., Ng, C., Lu, J., *J. Appl. Phys.*, **2011**, *109*, 103505.

[21]Cahn, R. W., Hassen, P., *Phys. Metal*, Vol. 1., Amsterdam North Holland, **1996**

[22]Tong, C. J., Chen, Y. L., Chen, S. K., *J. Metallurg. Mater. Trans. A*, **2005**, *36*, 881.

[23]Qiu, X.-W., *J. Alloy Compd.*, **2013,** *555*, 246.

[24]Qiu, X.-W., Liu, C.-G., *J. Alloy Compd*., **2013,** *553*, 216.

[25]Li, B.-Y., Peng, K., Hu, A.-P., Zhou, L.-P., Zhu, J.-J., Li, D-Y., *Trans. Nonferr. Metal. Soc.*, **2013**(3), 735.

[26]Qiu, X.-W., zhang, Y.-P., He, L., Liu, C.-G., *J. Alloy Compd*., **2013**, *549*, 194.

[27]Ren, B., Liu, Z.X., Li, D.M., Shi, L., Cai, B., Wang, M.X. *Mater. Corros*., **2012** , *63(9)* , 828.

[28]Hsueh, H.-T., Shen, W.-J., Tsai, M.-H., Veh, J.-W., *Surf. Coat. Tech*., **2012,** *206(19-20)*, 4106.

[29]Liu, Z., Zeng, J., *Appl. Mech. Mater*., **2012**, **117-119**, 1816.

[30]Hongbao, C., Ying, W., Jinyong, W., Xuefeng, G., Hengzhi, F., *China Foundry* , **2011**, *8*, 259.

[31]Ye, X., Ma, M., Cao, Y., Liu, W.,Ye, X., Gu, Y., *Phys. Procedia* , **2011**, *12*, 303.

[32]Li, Q. H., Yue, T. M., Guo, Z. N., *Materials Science and Technology Conference and Exhibition*, **2010**, MS and T'10 3, 1538.

[33]Lin, C.-M., Tsai, H.-L., Bor, H.-Y., *Intermetallics*, **2010,** *18* ,1244.

[34]Li, W., Liu, G., Guo, J., *Tezhong Zhuzao Ji Youse Hejin/Special Casting and Nonferrous Alloys*, **2009,** *29*, 941.

[35]Pinto, G. M., Nayak, J., Shetty, A. N., *Int. J. Electrochem. Sci*., **2009,** *4*, 1452.

[36]Lee, C. P., Chen, Y. Y., Hsu, C. Y., Yeh, J. W., Shih, H. C., *Thin Solid Films*, **2008,** *517*, 1301.

[37]Lee, C. P., Chang, C. C., Chen, Y. Y., Yeh, J. W., Shih, H. C., *Corros. Sci*., **2008**, *50(7)*, 2053.

[38]Lee, C. P., Chen, Y. Y., Wu, C. H., Hsu, C. Y., Yeh, J. W., Shih, H. C., *ECS Trans*., **2007,** *2*, 15.

Received: 27.11.2014.
Accepted: 20.01.2015.

SENSING ASCORBIC ACID WITH DNA/PRUSSIAN BLUE CARBON PASTE ELECTRODE

Yugandhar Parepalli,[a] T. Ravi Sankar,[b] P. T. S. R. K. Prasada Rao,[c] Manju Shree Nair,[a] Sudhakar Reddy Pamanji[d] and Murthy Chavali[a]*

Keywords: DNA, Ascorbic Acid (AA), vitamin-c tablets, electrochemical, sensor, carbon paste electrode.

A simple sensor for the detection of ascorbic acid (AA) has been developed. The electrochemical behaviours were studied after successfully constructing the electrode through DNA electro-deposition on carbon paste electrode using Prussian blue (PB). The electrodes were characterized by Raman spectroscopy that confirmed electro-deposition of PB, functioning as a redox mediator. The detection method was based on DNA damage induced by hydroxyl radical generated by Fenton reaction in which ascorbic acid effectively scavenges the hydroxyl radical. The amount of DNA damage is proportional to the amount of ascorbic acid concentration which was analyzed by cyclic voltametry (CV). Obtained results show that DNA-based biosensor can be utilized for estimating ascorbic acid in vitamin-c tablets. The detection range of this biosensor was in the range of 1.14 µM to 12.54 µM. Interference effects and stability of the biosensor were also investigated, results show that the biosensor has high sensitivity and selectivity towards ascorbic acid concentrations.

* Corresponding Author:
Tel: +91-863-234-4756
Fax: +91-863-253-4468
E-Mail: ChavaliM@gmail.com
[a] Division of Chemistry, Department of Sciences and Humanities, Vignan's Foundation for Science, Technology and Research University (VFSTRU; Vignan University), Vadlamudi, Guntur 522 213 Andhra Pradesh, India
[b] Department of Chemistry, Acharya Nagarjuna University, Nagarjuna Nagar, Guntur 522 510 Andhra Pradesh India
[c] PG Department of Chemistry, P. B. Siddhartha College of Arts & Science, Moghalrajpuram, Vijayawada 520 010 Andhra Pradesh, India
[d] Department of Zoology, Vikrama Simhapuri University Post-Graduate Centre, Kavali 524 201 Andhra Pradesh, India

Introduction

Oxidative metabolism is extremely critical for proper functioning of cells as it produces free radicals and other reactive oxygen species that can cause oxidative damage.[1] Free radicals have unpaired electrons that are neutralized by the antioxidants produced within the body. The formation of a large number of free radicals stimulates the formation of more free radicals, leading to even more damage. Excess free radicals produced cause oxidative stress. Oxidative stress induces damage to lipids, proteins or deoxyribonucleic acid (DNA), obstructing normal cell function. These damages cause tissue damage and diseases like cancer and Alzheimer's disease.[2] Hydroxyl radical (˙OH) is the main free radical that causes DNA damage. The hydroxyl radical if generated next to the DNA attacks deoxyribose sugar and the purine and pyrimidine bases, the resulting intermediates radicals are the immediate precursors for DNA base damage.[3] However the ˙OH formation can occur in several ways, the most important mechanism in vivo is likely to be the transition metal catalyzed decomposition of superoxide and hydrogen peroxide. Transition metals, iron and copper, play a key role in the production of hydroxyl radicals in vivo.[4] Hydrogen peroxide can react with iron II (or copper I) to generate the ˙OH, a reaction first described by Fenton.[5]

In order to prevent the adverse effect of free radicals, body uses antioxidants to reduce the oxidative damage, acting as hydrogen or electron donors and scavenge the free radicals.[6] In the recent past, there is an enhanced interest to analyze substances that exert some antioxidant potential. The evaluation of antioxidant property is not an easy task, many methods are based on free radical scavenging activity for the determination of antioxidant capacity.[7] Most of these methods are time consuming and expensive. Electro-chemical methods are alternative easier and cheaper methods than those are employed for the antioxidant analysis.[8a]

L-Ascorbic acid (AA, vitamin-c) is the major antioxidant found in many plants. AA is an essential nutrient that has been widely used on a large scale as an antioxidant agent in foods, beverages and pharmaceutical applications, due to its participation in several human metabolic reactions.[8b] AA, a naturally occurring organic antioxidant, has a significant role in normal neuronal physiology and acts as an important antioxidant, enzyme co-factor, and neuromodulator in the brain.[8c] Chemically it is (5R)-[(1S)-1,2-dihydroxyethyl]-3,4-dihydroxyfuran-2(5H)-one (Figure 1). The analytical determination of AA has been reported by many methods, such as enzymatic,[8d] iodometric titration using 2,6-dichlorophenol-indophenol as indicator,[8e] spectroscopic,[8f] chromatographic,[8g] fluorimetric[8h] and electrochemical.[8i]

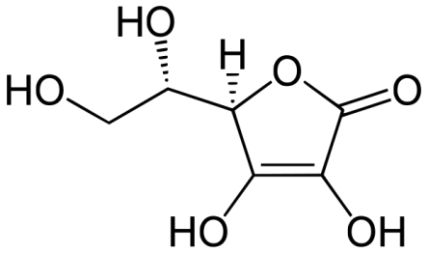

Figure 1. Structure of *L*-ascorbic acid.

 DOI: 10.17628/ecb.2014.3.1136-1141

Due to their quick response, high sensitivity, low detection limit and simple use, electrochemical methods are currently of much interest for AA determination, mostly by the electrocatalytic oxidation reaction on conventional electrodes. Though AA is an important antioxidant compound, it is difficult to determine it by direct oxidation on conventional electrodes because of interfering species such as dopamine and glucose. [8j]

In this work, we report the use of cyclic voltammetry (CV) technique to estimate the amount of ascorbic acid using a DNA based biosensor. The biosensor was developed by adsorbing DNA on a carbon paste electrode (CPE) electrodeposited with Prussian Blue (PB). Prussian blue is an efficient redox mediator which is efficiently used in many biosensors.[9-11] DNA damage is caused by the Fenton reaction and the effect of antioxidant on free radical scavenging is studied by using CV technique. The effect of DNA concentration, electrolyte, scan rate, interference and stability on the biosensor was also studied. The results were compared with pharmaceutical tablets containing ascorbic acid.

Experimental

Materials and Methods

All the chemicals were of analytical reagent grade. Disodium hydrogen phosphate was obtained from Nice Chemicals Pvt. Ltd., Kochi. Fructose, glucose, H_2O_2, H_2SO_4, $K_3[Fe(CN)_6]$ and KCl were obtained from Spectrum, Kochi. NaCl and $FeCl_3$ were obtained from Loba Chemie Pvt. Ltd., Mumbai. Ascorbic acid, paraffin liquid (heavy), NaOH and KH_2PO_4 were obtained from Merck, India. Graphite (particle size < 50 μm) was obtained from Merck, Germany. Sucrose, oxalic acid, citric acid and DNA were obtained from HIMEDIA India Ltd., Mumbai. All aqueous solutions were freshly prepared using deionized water (Resistivity, ρ≥18 MΩ cm) from Elga Purelab Option-Q system (ELGA LabWater, UK).

Vitamin-C was purchased from the market in the form of a tablet, containing 500 mg Vitamin-C ($C_6H_8O_6$). This was used as a standard sample to compare the results.

Raman Spectra were measured in air using EZRaman-N-785. Electrochemical Workstation CHI 604D (CH Inc., USA was used for CV measurements.

Measurement setup

A conventional three electrode system is used with homemade CPE as working electrode, platinum wire counter electrode and Ag/AgCl reference electrode. The CPE is prepared by mixing paraffin liquid and graphite (30:70). The unmodified carbon paste is introduced into pipette tips as shown in figure 2a with measurement setup in figure 2b and the side with maximum area is polished by using white paper. Electrical contacts were taken out from the other side using copper wire.

Electrode preparation

The CPE is prepared by the procedure mentioned above and it is subjected to pretreatment steps[12] in order to obtain reproducible results from different electrodes. The following steps were carried out for pretreatment of the electrodes.

Newly prepared electrode surface was immersed in 0.1 M H_2SO_4 solution which was held with stirring at +1.30 V for 2 min. Then the electrode surface was immersed in 0.1 M NaOH solution and held with stirring at +1.25 V for 2 min. It was then immersed in 0.1 M H_2SO_4 solution and held for 2 min while stirring, at +1.30 V. Electrode was then washed in 0.01 M phosphate buffered saline (PBS) of pH 7.4 for 1 min with stirring.

Electrodeposition of PB

The pretreated CPEs were modified by means of electro-deposition and activation of a PB film.[11] The PB layer was electro-deposited using cyclic voltammetry by applying 12 cyclic scans within the limits of –0.2 to +0.4 V at scan rate of 0.1 V s^{-1} in a solution containing 1.5 mM $K_3[Fe(CN)_6]$ and 1.5 mM $FeCl_3$ in 0.1 M KCl and 0.1 M HCl. These PB/CPEs were cleaned in water and activated by applying another 50 cycles in electrolyte solution (0.1 M KCl and 0.1 M HCl), using the same protocol. Before being used, the PB/CPE was cleaned again in water for several seconds. This CPE electro-deposited with PB is mentioned as PB/CPE.

Assay procedure

Assay experiments were carried out in three steps. DNA immobilization on the PB/CPE (DNA adsorbed electrode is mentioned as DNA/PB/CPE), damage of oligonucleotide by the immersion of DNA/PB/CPE on the Fenton mixture (DNA damaged electrode is mentioned as dDNA/PB/CPE) and analyze the dDNA/PB/CPE. For adsorbing DNA on the PB/CPE, 30 μL of 1 mg/mL DNA (unless stated otherwise) solution is placed on the polished, pretreated PB/CPE. Then it is air-dried overnight. Later, the modified electrode is soaked in ultrapure water for 4 h, in order to remove the unabsorbed DNA from the electrode surface. The electrodes are freshly prepared and for each experiment new electrode is used. Then the DNA damage of different DNA/PB/CPE was checked. This is carried out by dipping the DNA/PB/CPE in a reagent solution containing iron (freshly prepared ferrous sulphate solution, 0.416 mM $FeSO_4$) for 2 min in the presence or absence of antioxidant (1 mg/L, unless stated otherwise). The reaction was started by the addition of hydrogen peroxide (12.5 mM H_2O_2) into the non-stirred solution. After a short period of time (1-2 min) the electrode was washed with 0.01 M PBS and then it is immersed in 0.1 M PBS (pH 7.4) and CV is recorded.

The CV response with different electrolytes at different scan rates (10, 25, 50, 100, 150, 200, 250 mV/s), ascorbic acid concentration (0.2, 0.6, 1.0, 1.4, 1.8, 2.2, 2.6 mg/L), DNA concentration (0.2, 0.4, 0.6, 0.8, 1.0 mg/mL) were studied.

Results and Discussion

The studied system involved basically three important steps. It comprises of preparation of DNA-based biosensor, interaction of the biosensor with Fenton solution in absence and presence of antioxidant samples and the evaluation of the event that occurs at electrode surface.

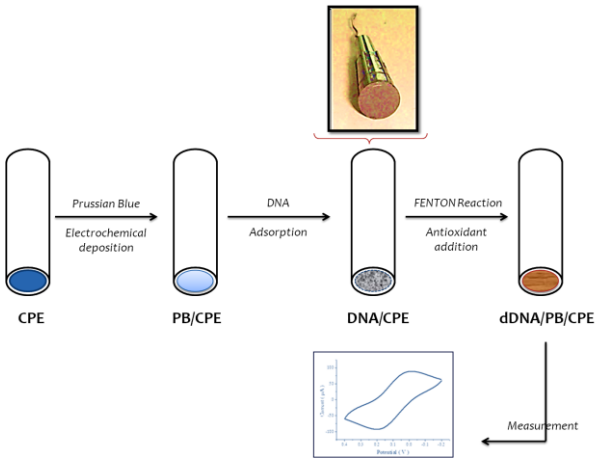

(a)

(b)

Figure 2. (a) Schematic representation of the preparation of DNA/PB/CPE and measurement of DNA damage b) Measurement setup

Characterization of electrodes

Raman Spectroscopy - Carbon materials are studied extensively with the help of Raman Spectroscopy. The study of carbon materials with Raman Spectroscopy showed that the frequencies and intensity of characteristic peaks changes with change in laser energy.[13,14] Figure 3 shows the Raman spectra of different materials and electrodes fabricated. Graphite powder showed the presence of D, G, D', G_1', G_2' bands corresponding to 1336, 1542, 1646, 2705, 2741 cm^{-1}. [14-16] The peaks at 1878, 1016, 954 cm^{-1} are characteristic for Prussian blue.[17] This indicates that PB has been electro deposited on the CPE. The bands in the region of 600-800 cm^{-1} are assigned to breathing vibration in the rings in the bases, the bands in the region 1200-1400 cm^{-1} are related to the stretching vibration of the rings of the bases.[18] After DNA adsorption, the PB/CPE electrode showed peaks at 978, 1020, 1118 cm^{-1} corresponding to DNA backbone, 1285 cm^{-1} corresponds to cytosine, 1624 and 2783 cm^{-1} correspond to tyrosine, 1459 cm^{-1} corresponds to CH_2 deformation in DNA backbone[19]

Cyclic voltametry Studies - Electrochemical behaviour of the different electrodes is shown in figure 4. Figure 4a illustrates the response of DNA/CPE and CPE. No redox peaks were observed in these electrodes. This suggested the use of Prussian blue as the redox mediator.[10] Different electrolytes were also studied (Figure 4). PBS showed better redox peaks in all the experiments. The PB modified electrodes, DNA/PB/CPE (Figure 4b) shows perfect redox peaks, which is linked to the redox process of Prussian blue

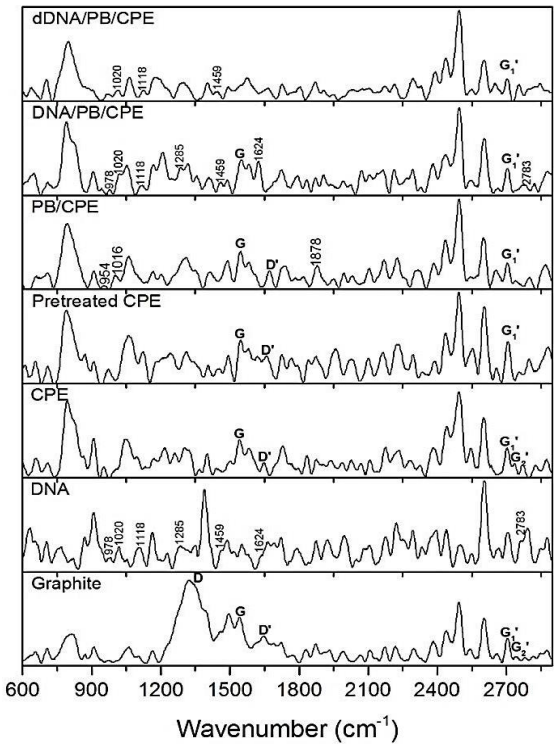

Figure 3. Raman spectra of different materials and electrodes - Graphite, DNA, CPE, Pretreated CPE, PB/CPE, DNA/PB/CPE and dDNA/PB/CPE

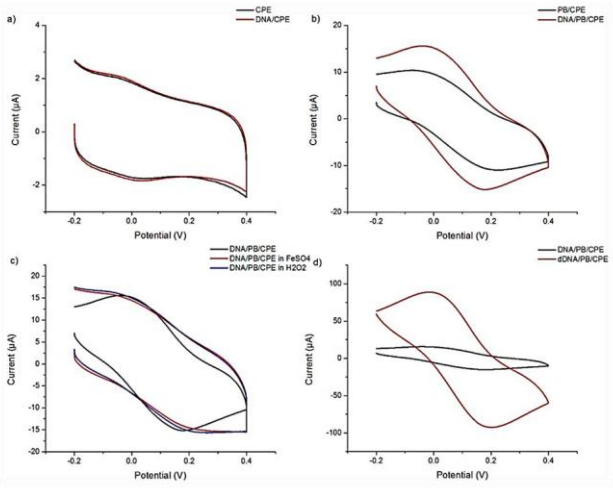

Figure 4. CV response of different electrodes a) the response of DNA/PB/CPE b) The PB modified electrodes in $FeSO_4$ and H_2O_2 c) d) CV of DNA/PB/CPE and dDNA/PB/CPE

 DOI: 10.17628/ecb.2014.3.1136-1141

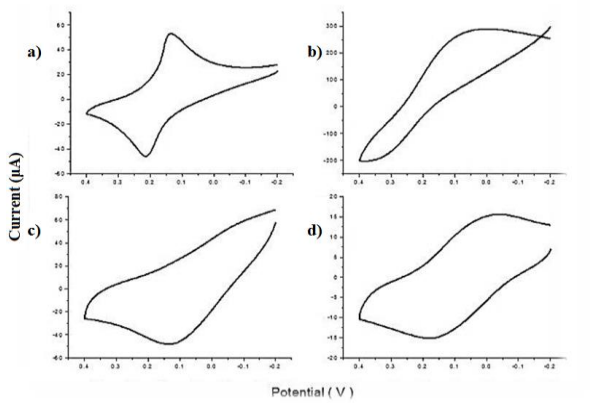

Figure 5 (i). CV at different electrolytes (before causing DNA damage) (a) 1 mM $K_3[Fe(CN)_6]$ in 0.1 M KCl (b) 6 mM $K_3[Fe(CN)_6]$ in 1 M Na_2SO_4 (c) 0.1 M H_2SO_4 (d) PBS (0.1 M, pH 7.4)

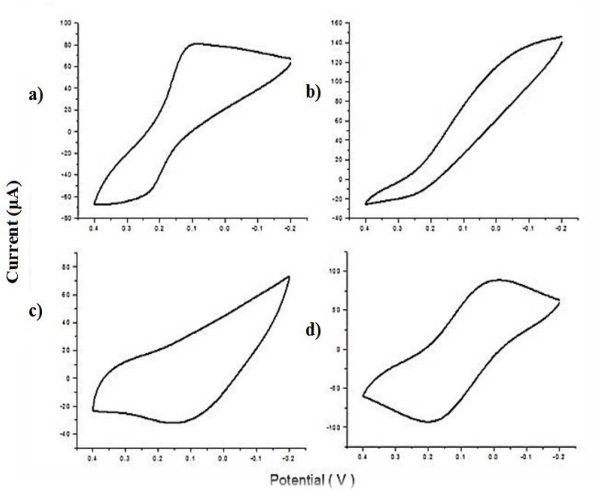

Figure 5 (ii). CV at different electrolytes (after causing DNA damage) (a) 1 mM $K_3[Fe(CN)_6]$ in 0.1 M KCl (b) 6 mM $K_3[Fe(CN)_6]$ in 1 M Na_2SO_4 (c) 0.1 M H_2SO_4 (d) PBS (0.1 M, pH 7.4)

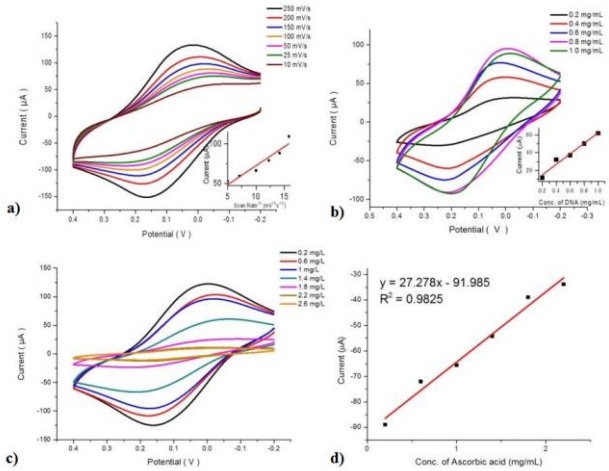

Figure 6. CV of DNA damage a) different scan rate b) different DNA concentrations c) varying ascorbic acid concentration. d) plot of ipa vs conc. of ascorbic acid.

An optimized concentration of $FeSO_4$ and H_2O_2 is used for the production of $^{\bullet}OH$.[20] Experiments were conducted to conclude the DNA damage is caused only by $^{\bullet}OH$ and not by other reagents used, the DNA damage was caused by $^{\bullet}OH$ and not by the other reagents $FeSO_4$ and H_2O_2 used to produce $^{\bullet}OH$ is given in figure 4c. The CV of DNA/PB/CPE with damaged and undamaged DNA (Figure 4d) explains that there is an increase in current at the electrode after DNA damage induced by Fenton reaction. Before DNA damage the anodic and cathodic peak current (ipa and ipc) values were calculated as -7.99 and 8.59 µA. After DNA damage the values increased to -67.7 and 67.4 µA. With increasing scan rate (Figure 6a) both redox peak currents and peak-to-peak separation increased. The peak currents are proportional to the square root of scan rate from 10 to 250 mVs^{-1} shown in figure 6a (*inset*), indicating that the redox process is diffusion limited.[21]

Influence of ascorbic acid on DNA damage

The amount of DNA adsorbed on the PB/CPE electrode also has an effect on the response of the sensor (figure 6b). As the concentration of DNA increased from 0.2 mg/mL to 1.0 mg/mL the ipa and ipc increases linearly shown in Figure. 6b (*inset*). This may be due to the fact that as the concentration of DNA increases the number of reactive species available for oxidation also increases.[22] The overcrowding of DNA on the electrode can hinder the electron transfer rate.[23] Ascorbic acid is a good antioxidant.[24] Ascorbic acid scavenges the $^{\bullet}OH$ radical and thereby prevents DNA damage. Figure 6c illustrates the effect of ascorbic acid on the DNA damage induced by $^{\bullet}OH$. As the concentration of ascorbic acid is increased, there is a decrease in the ipa and ipc. This shows there is a decrease in DNA damage, which may be due to DNA crowding. At above 2.2 mg/mL ascorbic acid concentrations, all the $^{\bullet}OH$ is scavenged indicating no DNA damage. This is the optimal concentration of ascorbic acid for $^{\bullet}OH$ scavenging under these experimental conditions. With further decrease of ascorbic acid concentration below 0.2 mg/L, the ipa and ipc value retails towards a constant value. Figure 6d shows the linear response between ascorbic acid concentration and anodic peak current.

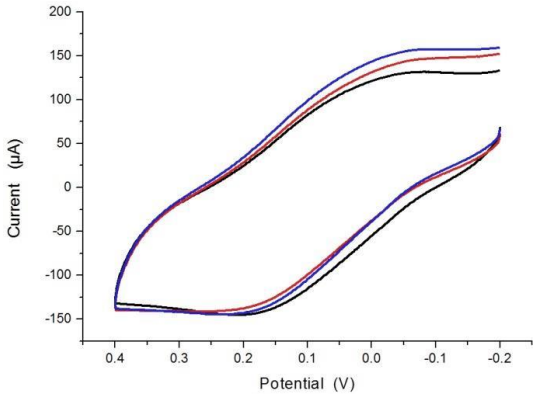

Figure 7. CV of Vitamin-C tablet

This linearity is used to calculate the amount of antioxidant in the sample. The results also indicate that ascorbic acid is a good antioxidant.

Interference Study

The influence of the possible interfering compounds commonly present in pharmaceutical formulations such as glucose, fructose, sucrose, citric acid and oxalic acid were studied. These compounds were substituted for the ascorbic acid and the measurements were carried out at a concentration of 1 mg/L. The compounds glucose, fructose, sucrose and oxalic acid did not cause any interference and the ipa and ipc values were in par with the stationary values obtained with ascorbic acid concentrations less than 0.2 mg/L. The presence of citric acid caused a decrease in ipc indicating its function as an antioxidant.[25]

Stability of the Biosensor

The stability of the fabricated DNA biosensor was investigated. The DNA/PB/CPE electrode was stored in the refrigerator at 4 °C for 4 weeks and then the experiments were carried out. The results showed that the biosensor retains about 93% of its original response. This result show that the electrode can stably operate after a long period of storage.

Real sample analysis of the biosensor

To demonstrate the practical use of this biosensor samples were measured. Ascorbic acid tablets were used for this purpose. The tablets were weighed, ground, and an accurate weight of the powder assigned to contain 0.5 mg/L ascorbic acid was dissolved in ultrapure water, this solution is used as the antioxidant in the experiments and the CV is measured in 0.1 M PBS. Figure 7 gives the CV response for the real samples (n=3). The ipa values for the measurements were calculated as −79±0.36 μA. This when converted to concentration by using the calibration curve (Figure 6d), the concentration was 0.475±0.009 mg/L, RSD=2.77%. The recovery of the biosensor is 95%. The proposed results show that the biosensor can be used to determine ascorbic acid in pharmaceutical samples. The selectivity and sensitivity of the proposed biosensor appear to be a promising candidate for measurements in real samples.

Conclusions

We have demonstrated, here, a DNA based biosensor for the determination of ascorbic acid in pharmaceutical tablets. The electrodes were prepared by electro deposition of PB on CPE, and DNA is adsorbed on to this electrode, as the DNA/PB/CPE showed higher peak current than the PB/CPE, conforming PB as a perfect redox mediator. The Fenton reagents provided a good environment for the generation of •OH and thereby inducing DNA damage. The antioxidant scavenges the •OH thereby preventing DNA damage. The amount of DNA damage is related to the concentration of antioxidant. This is measured by using CV technique. The results showed a linear response in the range of 1.14 μM (0.2 mg/L) to 12.54 μM (2.2 mg/L), R^2=0.9825. The sensor exhibited high sensitivity and selectivity in the determination of ascorbic acid. This biosensor can be used for rapid, selective and precise in the determination of ascorbic acid in pharmaceutical samples. Disposable electrode with suitable activation has extensively improved the selectivity and sensitivity of analytical systems especially towards biological targets and also clearly made it possible to detect certain analytes that are otherwise challenging. Usage of other nanomaterials via screen printing and synchronization of chemical modification with more sophisticated electrode designs can play a vital role in future applications.

Acknowledgement

Authors thank Department of Science and Technology, Govt. of India for the three R&D projects towards purchase of minor and major instruments required for material characterization, No. SR/FTP/CS-116/2007 dated 21st July 2008 (PI - Prof. Dr. techn. Murthy Chavali), No. SR/FT/CS-134/2010 dated 08th February 2012 (PI - Dr. Joseph Joly) and No. GITA/DST/TWN/P-002/2009 dated 24th March 2009 (PIs - Prof. Dr. techn. Murthy Chavali & Prof. Dr. Wu Ren-Jang). MSN also thank Mr. R. Iseac, for his assistance in performing CV experiments.

References

[1]Pihlanto, A., *Intl. Dairy J.*, **2006**, 16, 1306.

[2]Prieto-Simon. B., Cortina, M., Campas, M., Calas-Blanchard, C., *Sens. Actuat. B-Chem.*, **2008**, *129*, 459.

[3]Jaruga, P., Dizdaroglu, M., *Nucleic Acids Res.*, **1996,** *24*, 1389.

[4]Madhavi, D. L., Deshpande, S. S., Salunkhe, D. K., *Food Antioxidants: Technological: Toxicological and Health Perspectives*, **1995,** Taylor & Francis.

[5]Fenton, H., *J. Chem. Soc. Trans.*, **1894**, *65*, 899.

[6]Halliwell, B., Gutteridge, J., Cross, C., *J. Lab. Clin. Med.*, **1992**, *119*, 598.

[7]Sanchez-Moreno, C., *Food Sci. Technol. Intl.*, **2002**, *8*, 121.

[8](a) Buratti, S., Scampicchio, M., Giovanelli, G., Mannino, S., *Talanta*, **2008**, *75*, 312; (b) Zhang, L., Wang, Z., Xia, Y., Kai, G., Chen, W., Tang, K., *Crit. Rev. Biotechnol.*, **2007**, *27*, 173; (c) Rice, M. E., *Trends Neurosci.*, **2000**, *23*, 209; (d) Zhu, M., Huang, X.-M., Shen, H.-X., Li, R., *Anal. Chim. Acta*, **1996**, *334*, 303; (e) Svehla, G., Koltai, L., Erdey, L., *Anal. Chim. Acta*, **1963**, *29*, 442; (f) Chan, H. S. O., Ng, S. C., Seow, S. H., *Synth. Met.*, **1994**, *66*, 177; (g) Tai, A., Gohda, E., *J. Chromatogr. B*, **2007**, *853*, 214; (h) Wu, X., Diao, Y., Sun, C., Yang, J., Wang, Y., Sun, S., *Talanta*, **2003**, *59*, 95; (i) Ragupathy, D., Gopalan, A.I., Lee, K.-P., *Sens. Actuat. B-Chem.*, **2010**, *143*, 696; (j) Zhao, Y., Gao, Y., Zhan, D., Liu, H., Zhao, Q., Kou, Y., Shao, Y., Li, M., Zhuang, Q., Zhu, Z., *Talanta*, **2005**, *66*, 51.

[9]Wang, X., Gu, H., Yin, F., Tu, Y., *Biosens. Bioelectron.* **2009**, *24*, 1527.

[10]Zhao, H., Yuan, Y., Adeloju, S., Wallace, G., *Anal. Chim. Acta*, **2002**, *472*, 113.

[11]Salazar, P., Martín, M., O'Neill, R., Roche, R., González-Mora, *Intl. J. Electrochem. Sci.*, **2012**, *7*, 5910.

[12]Gonzalez-García, M. B., Costa-García, An., *Biosens. Bioelectron.*, **2000**, *15*, 663.

[13]Dresselhaus, M. S., Dresselhaus, G., Saito, R., Jorio, A., *Phys. Rep.*, **2005**, *409*, 47.

[14]Pimenta, M., Dresselhaus, G., Dresselhaus, M. S., Cancado, L., Jorio, A., Saito, R., *Phys. Chem. Chem. Phys.*, **2007**, *9*, 1276.

[15]Ferrari, A. C., *Solid State Commun.*, **2007**, *143*, 47.

[16]Vidano, R., Fischbach, D. B., *J. Am. Chem. Soc.*, **1978**, *61*, 13.

[17]Chaplin, T. D., Clark, R. J., and Beech, D. R., *J. Raman Spectr.*, **2002**, *33*, 424.

[18]Zhao, Y. D., Pang, D. W., Hu, S., Wang, Z. L., Cheng, J. K., Qi, Y. P., Dai, H. P., Mao, B. W., Tian, Z. Q., Luo, J., *Anal. Chim. Acta*, **1999**, *388*, 93.

[19]Prescott, B., Steinmetz, W., Thomas, G., *Biopolymers*, **1984**, *23*, 235.

[20]Wang, Y., Xiong, H., Zhang, X., and Wang, S., *Sens. Actuat. B-Chem.*, **2012**, *161*, 274.

[21]Jiang, Y., Zhang, X., Shan, C., Hua, S., Zhang, Q., Bai, X., Dan, L., Niu. L., *Talanta*, **2011**, *85*, 76.

[22]Ghanbari, K., Bathaie, S., Mousavi, M., *Biosens. Bioelectron.*, **2008**, *23*, 1825.

[23]Ricci, F., Lai, R. Y., Heeger, A. J., Plaxco, K. W., Sumner, J. J., *Langmuir*, **2007**, *23*, 6827.

[24]Carr, A., Frei, B., *FASEB J*, **1999**, *13*, 1007.

[25]Van Den Berg, A., Halkes, S., Van Ufford, H. Q., Hoekstra, M., Beukelman, C., *J. Wound Care*, **2003**, *12*, 413.

Received: 08.12.2014.
Accepted: 20.01.2015.

SYNTHESIS AND CRYSTAL STRUCTURE OF BRIDGED *peri*-AROYLNAPHTHALENE DERIVATIVES

Sayaka Yoshiwaka,[a] Shinji Ohisa,[a] Noriyuki Yonezawa[a] and Akiko Okamoto[a]

Keywords: Non-coplanarly aromatic ring accumulation, Bridged structure, Non-dilution synthesis, Syn-conformer, Crystal structure

Bridged *peri*-aroylnaphthalene compounds are satisfactorily synthesized by the reaction of bis(fluorobenzoyl)naphthalene derivatives and catechol without high dilution conditions. The preferential bond formation between the *p*-positioned carbon atoms of the terminal aromatic rings of *peri*-aroyl groups by 1,2-dioxybenzene unit shows that the starting molecules take *syn*-orientation of the aroyl groups along with *anti*-form. By comparison of the spatial organization of the bridged compound with the corresponding non-bridged homologues, the factors leading to *syn*-oriented conformation for *peri*-aroylnaphthalene derivatives in crystal packing are elucidated.

* Corresponding Authors
Fax: +81–42–388–7601
E-Mail: aokamoto@cc.tuat.ac.jp
[a] Department of Organic and Polymer Materials Chemistry, Tokyo University of Agriculture and Technology, 2–24–16 Naka-machi, Koganei, Tokyo 184–8588, Japan

Introduction

Coplanarly π-conjugated aromatic aggregate compounds have engaged material chemists' and organic ones' heart and mind because of their excellent conductivity.[1,2] Naturally, aromatic aggregate compounds having unique π-conjugated structure have been in the limelight as promising framework in nanoelectronics, e.g., fullerene analogues including bucky bowl,[3] coannulene[4] and sumanene,[5] and carbon nanotube analogues including cyclacene[6] and cycloparaphenylene.[7] The synthetic strategies and the minute structure analyses have been challenging task.[8,9] Figure 1 exhibits crystal structure of *peri*-aroylnaphthalene bearing phenoxy groups in the aroyl groups.[10,11] The authors have been studying on the synthetic procedures[12,13] and the X-ray crystal structure analysis of the *peri*-aroylnaphthalene compounds in which aromatic rings accumulate non-coplanarly giving highly congested intramolecular circumstance. As one of the categories of the π-conjugated aromatic ring accumulated compounds, *peri*-aroylnaphthalene compounds have some distinguishable structure characteristics: *peri*-Aroylnaphthalene compounds are poly(aromatic ring) compounds where aromatic rings are linked by ketonic carbonyl groups. The aroyl groups are connected with naphthalene ring at the most inner position, and they are situated in the neighbourhood. Accordingly, *peri*-aroylnaphthalene compounds have too congested molecular circumstance to make the coplanar form of aromatic rings in a molecule. Besides, diaryl ketone structure is supposed to make somewhat congested spatial organization around ketonic carbonyl groups. However, the restriction is certainly estimated less than π-conjugated aromatic molecules. So expected small flexibility of aromatic ketone compound probably shows the variety of molecular and packing structure in crystal. It means opportunity to reveal the interactions determining the structure hitherto unknown.

In crystal of *peri*-aroylnaphthalene compound, the naphthalene ring core and the benzene rings of the aroyl groups of are situated in an almost perpendicular fashion. The non-coplanar features of *peri*-aroylnaphthalene compounds are plausibly caused from avoidance of internal steric repulsion. In addition, there are possible two types of metastable conformation of molecules satisfying perpendicular molecular organization, i.e., *syn* type and *anti* type. The *syn*-oriented *peri*-aroylnaphthalene molecule has two aroyl groups aligned in a same direction; meanwhile the two aroyl groups of the *anti*-oriented molecule are situated in an opposite orientation. According to the authors' study of X-ray crystal analysis, the *anti*-oriented fashion is the majority as single molecular crystal structures of *peri*-aroylnaphthalene compounds.[11,14-16] Recently, several examples of *syn*-oriented molecular organization in crystal have been found, i. e., 1,8-bis(4-phenoxybenzoyl)-2,7-dimethoxynaphthalene (**1a**),[10] {2,7-dimethoxy-8-[4-(propan-2-yloxy)benzoyl]naphthalen-1-yl}[4-(propan-2-yloxy)phenyl]methanone,[17] and 1,8-bis(4-chlorobenzoyl)-7-methoxynaphthalen-2-ol ethanol monosolvate.[18] The authors have regarded 4-phenoxybenzoyl group as the most effective inducing moieties for *syn*-oriented conformation.

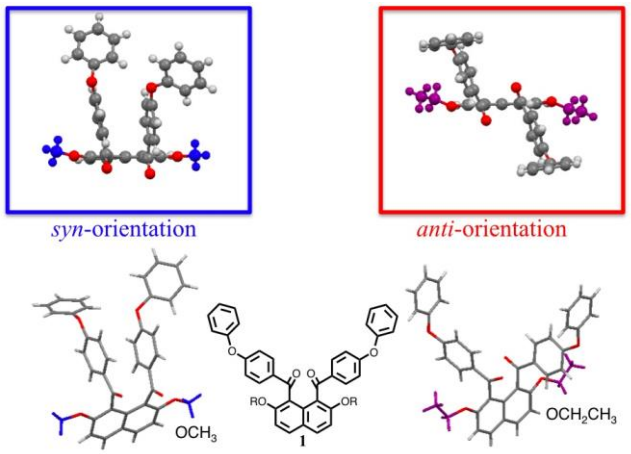

Figure 1. Crystal structures of *peri*-aroylnaphthalenes bearing phenoxy group **1a** (R = OCH_3; left) and **1b** (R = OCH_2CH_3; right)

 DOI: 10.17628/ecb.2014.3.1142-1147

Consequently, a series of 2,7-dialkoxy-1,8-bis(4-phenoxybenzoyl)naphthalene homologues, i.e., 2,7-diethoxy-1,8-bis(4-phenoxybenzoyl)naphthalene (**1b**)[11] and 2,7-diisopropoxy-1,8-bis(4-phenoxybenzoyl)naphthalene (**1c**) are designed.[19] However, these homologues (**1b** and **1c**) showed *anti*-orientation in their crystals (Figure 1).

Under these circumstances, the authors aimed to realize compelled *syn*-oriented molecules and designed the intramolecularly bridged homologous molecule, which shares terminal benzene ring connected to the benzoyl groups at 1- and 8-positions of the naphthalene ring [Figure 2, compound **2**].

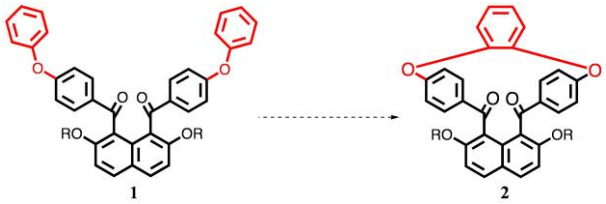

Figure 2. Design of compelled *syn*-oriented molecule **2**

The structure analysis of such compelled *syn*-oriented molecules was expected to indicate the factors for stabilization of the molecular organization in crystal. This article reports the synthesis and crystal structure of bridged *peri*-aroylnaphthalene compounds **2**, and discusses comparatively the crystal structure with the non-bridged homologues **1a** and **1b** to elucidate the determining factors for molecular spatial organization.

Results and discussion

Nucleophilic aromatic substitution reaction of compound **3a** (R=Me) and catechol gave bridged compound **2a** (R=Me) with the benzoyl groups being connected by catechol hinge unit intramolecularly (Table 1). The formation of intramolecular connection proceeded satisfactorily in rather concentrated reaction solution than conventional conditions (entry 1).

Table 1. Synthesis of bridged compound **2**

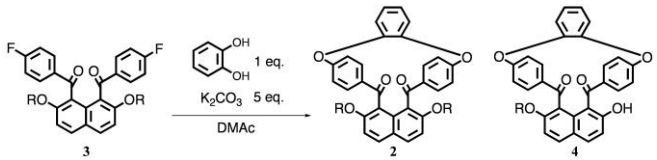

	R	*c*, 10^{-2} M	Time, h	*T*,˚C	Product distribution, %[a]			
					3	2	4	by-prod.[c]
a	Me	4	24	150	9	87 (62)[b]	4	0
a	Me	4	48	150	0	19	48	33
a	Me	6	24	150	1	18	29	52
a	Me	12	24	150	2	29	13	56
a	Me	4	24	120	51	49	0	0
a	Me	1	24	150	50	12	0	38[d]
b	Et	4	24	150	25	75	0	0
b	Et	4	48	150	3	77	20	0

a) Calculated on the basis of ^{1}H NMR spectra (3.6–3.9 ppm). b) Isolated yield. c) Distribution of by-product was determined on the basis of ^{1}H NMR spectra on condition that the by-product has two methyl groups. d) 1-Aroyl-2,7-dimethoxynaphthalene was included.

The concentration was almost one-tenth value for those of typical polycondensation synthesis of polyketones.[20] Furthermore, the amount of the by-product **4** increased at the prolonged reaction interval, i.e., 33 % for 48 h (entry 2). Further concentrated conditions also yielded significant amounts of by-products (52 % and 56 %, entry 3 and entry 4, respectively).

At 120 ˚C, the conversion was far lower than that obtained under the optimized conditions (entry 5 vs. entry 1). Ordinary high-dilution cyclization reaction is undertaken at about one-hundredth concentration compared to those for the polycondensation reaction. When compound **2** were allowed to react with catechol at fortieth concentration against typical polycondensation conditions, the reaction moderately proceeded with a 50 % conversion (entry 6 vs. entry 1).

Reaction under the non-high dilution conditions gave the bridged compound (**2a**) quantitatively, is meaning that there were enough opportunities for the precursor molecules took *syn* orientation against more stable *anti*-orientation in crystal, i.e., orientations of aroyl groups were converted easily between same and opposite directed conformations in solution.

As preparation of crystal of compound **2a** suitable for X-ray crystal structural analysis was unsuccessful unfortunately, the authors intended to analyze a homologous compound having intimately related molecular structure for bridged compound **2a**.

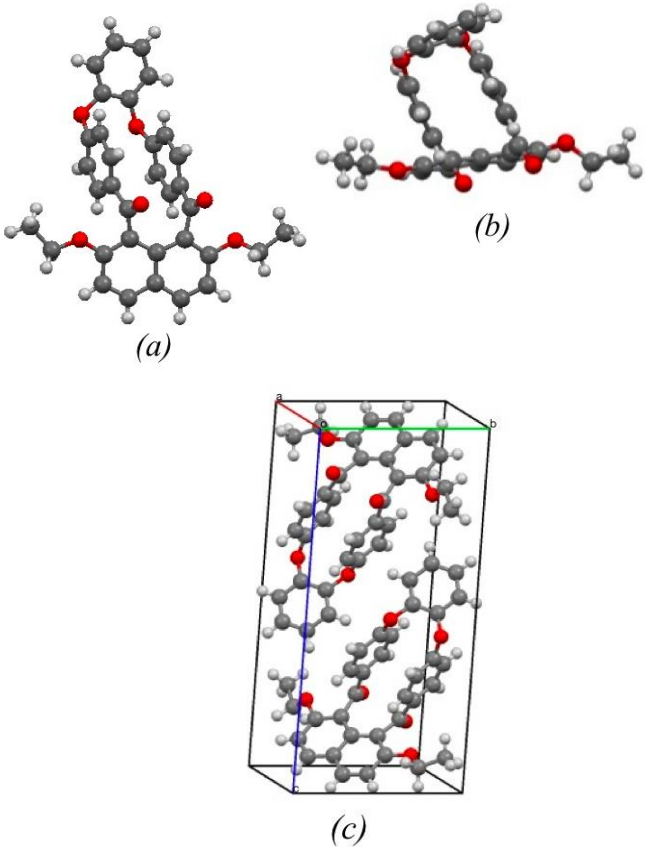

Figure 3. Crystal structure of 2,7-diethoxy homologue **2b**; displaying single structure [front view (a) and top view (b)] and unit cell (c).

 DOI: 10.17628/ecb.2014.3.1142-1147

Consequently, 2,7-di*ethoxy* homologue **2b** bearing two terminal benzoyl moieties connected intramolecularly by catechol residue at 4,4'-positions was designed and synthesized successfully according to essentially same synthetic method for bridged compound **2a**. For this compound **2b**, preparation of satisfactorily qualified crystal was achieved and the X-ray crystal structure analysis was performed (Figure 3).[21]

In crystal, the molecule of compound **2b** shows *syn*-oriented single molecular structure. Two planes of the internal benzene rings are parallel [dihedral angle between internal benzene rings and naphthalene ring; 3.83(8)˚] and are inclined in conrotatory directions [dihedral angles between internal benzene ring and naphthalene ring; 71.63(6)˚ and 72.58(6)˚]. The plane of the catechol hinge moiety situates almost in *exo* site and parallel to the naphthalene ring [dihedral angle between naphthalene (C1–10) and catechol (C25–C30); 17.03(7)˚].

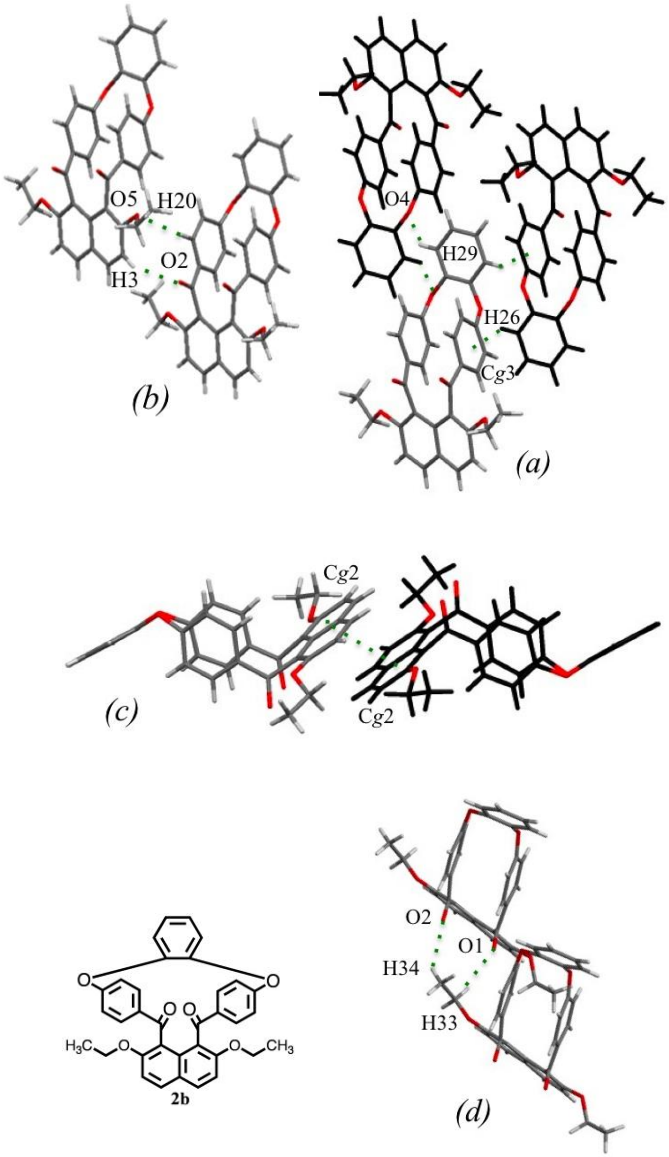

Figure 4. Intermolecular interactions of compound **2b**. Dashed lines indicate the intermolecular C–H…π and C–H…O–catechol moiety interactions in part (a), benzoyl C–H…O–ethoxy interaction in part (b), π…π stacking between naphthalene rings in part (c), and ethylene C–H…O=C interactions in part (d).

Table 2 Intermolecular interactions and molecular packing density of compounds **1a**, **1b**, and **2b** (Å, g cm^{-3})

Interactions	2b	1a	1b
D–H…A			
$_{hinge}$C26–H26…$_{inter}$C*g*3	3.00^{i}		
$_{term}$C35–H35…$_{inter}$C*g*3		2.78^{vii}	
$_{term}$C18–H18…$_{inter}$C*g*3			3.17^{x}
$_{Naph}$C3–H3…O2=C	2.49^{ii}		
$_{Naph}$C3–H3…O1=C		2.44^{viii}	
$_{Naph}$C6–H6…O6–Ph		2.56^{ix}	
O6–C33–H33…O1=C	2.67^{iii}		
O6–CH$_2$–C34–H34…O2=C	2.69^{iii}		
$_{inter}$C20–H20…O5–CH$_2$CH$_3$	2.60^{iv}		
$_{term}$C29–H29…O4–catechol	2.68^{v}		
$_{Naph}$C*g*2…$_{Naph}$C*g*2	3.59^{vi} (3.27^{a})		
$_{inter}$C12–H12…O1=C			2.64^{xi}
$_{term}$C19–H19…O1=C			2.68^{x}
$_{term}$C18–H18…O1=C			2.66^{x}
Density	1.369	1.292	1.275

Symmetry codes: i) –x+1, –y+1, –z+1; ii) x, y+1, z; iii) x–1, y, z; iv) x, y–1, z; v) –x, –y+2, –z+1; vi) –x+1, –y+1, –z; vii) –x+2, –y+1, –z+2; viii) –x+3/2, y+1/2, –z+3/2; ix) x–1/2, –y+1/2, z–1/2; x) –x+1/2, –y+1/2, z+1/2; xi) x, –y+1, z+1/2.

a) Interplanar distance between naphthalane ring and naphthalane ring of neighboring molecule.

The molecules are aligned as dimeric units in crystal packing. One molecule of compound **2b** interacts with the neighbouring five molecules at seven points including three kinds of strong intermolecular interactions (Figure 4): 1) C–H…π interaction (non-covalent bonding) between a H atom at the 3-position of the catechol hinge moiety and the benzene ring of the internal benzoyl moiety of the adjacent counterpart molecule of dimeric aggregate [C26–H26…C*g*3; 3.00 Å, Table 2, C*g*3; internal benzene ring (C12–C17)], 2) intermolecular C–H…O=C interaction between a H atom at the 3-position of the naphthalene ring and the carbonyl group of the adjacent molecule (C3–H3…O2=C18; 2.49 Å, Table 2; entry 4), and 3) intermolecular C–H…O–C_2H_5 interaction between a H atom of the internal benzene ring and the O atom of the alkoxy moiety at 2-position of the naphthalene ring of the adjacent molecule(C20–H20…O5(ethoxy); 2.60 Å, Table 2; entry 9).

The intermolecular C–H…O interactions concerning ethoxy group at 7-position of naphthalene ring can be regarded to contribute to increase of density of crystal packing cooperatively with above three kinds of interactions against the steric repulsion by tightening of contact of molecules [O6–C33–H33…O1=C11; 2.67 Å, Table 2; entry 7: O6–CH3–C34–H34…O2=C18; 2.69 Å, Table 2; entry 8]. The other interactions are likely to function rather subsidiary for stabilization of crystal packing [π…π stacking; 3.27 Å (interplaner distance between the naphthalene ring and the naphthalene ring of the neighboring molecule), Table 2; entry 11: C29–H29…O4; 2.68 Å, Table 2; entry 10].

To elucidate the governing interactions in determining the crystal packing and the single molecular structure, the authors planned comparison of crystal data of compound **2b** with those of other related compounds. For this purpose, the authors chose the analogous compound **1b** in addition to compound **1a**, of which crystal structure has been already determined. Compound **1b**, 2,7-diethoxy-1,8-bis(4-phenoxybenzoyl)naphthalene (**1b**),[11] has phenoxybenzoyl groups at the 1- and 8-positions of the naphthalene ring without bridged moiety. The structural difference between the homologue **1b** and compound **1a** is only whether the 2,7-dialkoxy groups of the molecule are ethoxy or methoxy.

According to the crystal structure analysis, spatial organization of homologue **1b** essentially differs from the bridged compound **2b** in orientation of phenoxybenzoyl groups. The two 4-phenoxybenzoyl groups of homologue **1b** are oriented in an anti-orientation despite of the 2,7-diethoxy groups version of compound **1a**. For crystal packing structure, homologue **1b** apparently has no effective intermolecular interactions. C–H…π interaction between a H atom at the 3-position of the terminal benzene ring and the benzene ring of the internal benzoyl moiety of the adjacent molecule for compound **1b** [Figure 5, C18–H18…Cg3; 3.17 Å, Cg3; internal benzene ring (C10–C15)] seems to be resemble fashion to that of bridged compound **2b**. From the viewpoint of effective interactions in crystal, the intermolecular C–H…π interaction has a distance longer than 3 Å. Therefore, the contribution of the intermolecular C–H…π interaction to the molecular packing in compound **1b** is smaller than that observed in crystal structure of bridged compound **2b**.

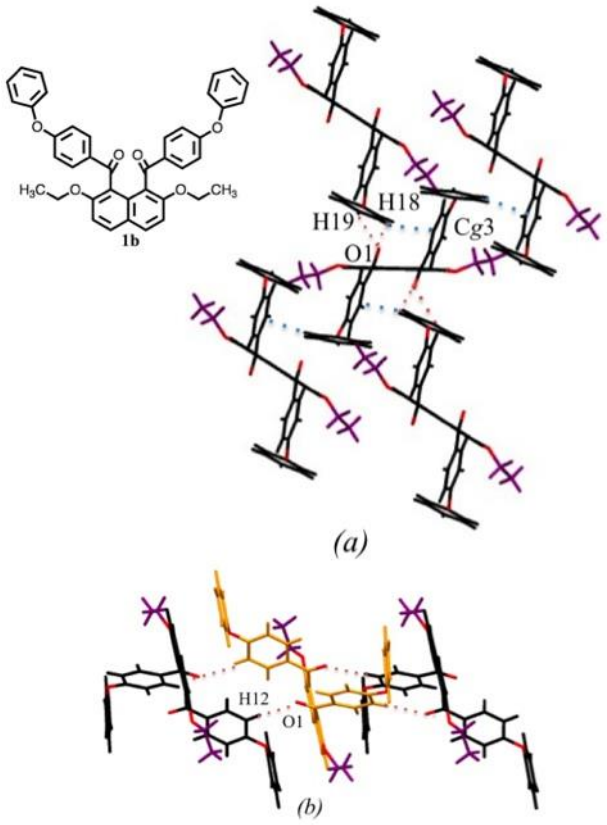

Figure 5. Intermolecular interactions of non-bridged compound **1b**. Dashed lines indicate the intermolecular C–H…π and terminal C–H…O=C interactions in part (a), internal benzene C–H…O=C interactions in part (b). As described in the text, all contact distances are longer than the sum of van der Waals radii.

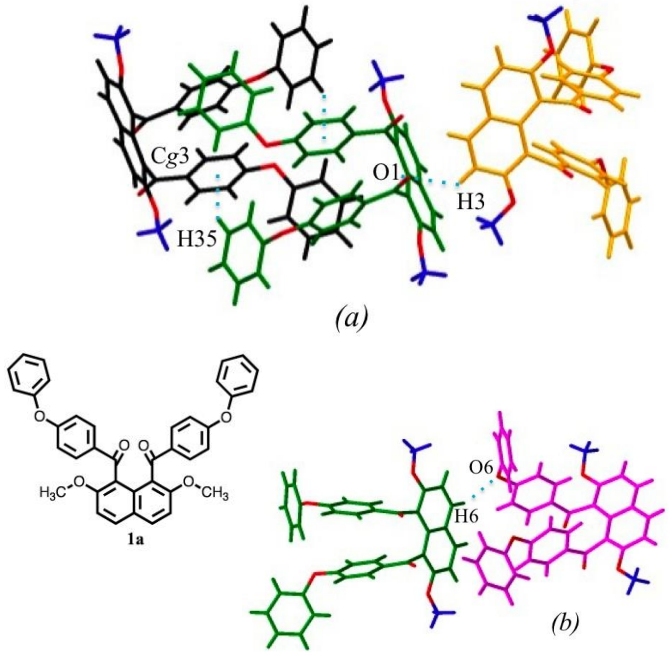

Figure 6. Intermolecular interactions of homologue **1a**. Dashed lines indicate the intermolecular C–H…π and C–H…O=C in part (a), and C–H…O–phenyl interactions in part (b).

Besides, three types of C–H···O=C hydrogen bonds are observed in the crystal of compound **1b** (C19–H19···O1; 2.68 Å**,** C18–H18···O1; 2.66 Å**,** and C12–H12···O1; 2.64 Å). However, they have almost same distances. So, their significance as structure-directing interactions is doubtful. On the other hand, the spatial organization of the *syn*-oriented molecular structure shown in the crystal of bridged compound **2b** is essentially in the same style with that of homologue **1a** (Figure 6). In crystal of compound **1a**,[10] the H atom at 3-position of terminal benzene ring of 4-phenoxybenzoyl moiety interacts with the π-system of internal benzene ring of 4-phenoxybenzoyl moiety of the adjacent molecule [C35–H35…C*g*3; 2.78 Å, Table 2, C*g*3; internal benzene ring (C12–C17)]. Two sets of strong C–H···π interactions force the two molecules of the homologue (**1a**) to form a dimeric aggregate with centrosymmetry. Furthermore, intermolecular C–H…O=C interaction between a H atom of naphthalene ring and the O atom of the carbonyl group is observed (C3–H3…O1=C11; 2.44 Å). Another intermolecular C–H…O interaction is observed between the H atom of the naphthalene ring and the O atom of the terminal benzeneoxy moiety (C6–H6…O6–Ph; 2.56 Å). The distance of intermolecular C–H···π interaction becomes shorter in the order of homologue **1b**, bridged compound **2b** and homologue **1a** [3.17 Å for homologue **1b**; 3.00 Å for bridged homologue **2b**; 2.44 Å for homologue **1a**]. Dimeric fashion means that the C–H…π interaction is one of the important factors for appearance of *syn*-orientation of 4-phenoxybenzoyl moieties. The C–H…O=C interactions seem to be formed effectively between the dimeric aggregates as shown in the crystal packing of compounds **2b** and **1a**. Another weak van der Waals interactions between the dimeric pairs might contribute cooperatively to stabilize the molecular packing.

The *syn*-orientation of the aroyl groups exemplified in non-bridged homologue **1a** is the minor conformation compared to the major packing figure without dimer unit

formation of other non-bridged *peri*-aroylnaphthalene derivatives. Based on this crystal structure similarity in compounds **1a** and **2b**, the intermolecular C–H…π interaction is supposed as the most effective directing factor for the crystal packing of these *syn*-oriented compounds. The intermolecular interactions involving the H atoms of naphthalene ring are considered to contribute to arrange the molecules as dimeric formulae in the crystal structures of the *syn*-oriented molecules. Furthermore, the intermolecular C–H…O=C interaction, together with the C–H···π interaction, observed in crystal packing of both bridged compound **2b** and 2,7-dimethoxy non-bridged homologue **1a** is interpreted to assist formation of the molecular pairs.

Conclusion

Bridged *peri*-aroylnaphthtalene compounds **2** having intramolecular connection between the benzene rings of the 1,8-diaroyl groups have successfully synthesized by base-mediated reaction of 1,8-bis(4-fluorobenzoyl)naphthalene derivatives **3** with catechol in a rather non-dilution solution compared to ordinary high-dilution solution synthesis. In crystal of one of the bridged homologues, 2,7-diethoxy derivative **2b**, the intramolecularly connected aroyl groups are situated as *syn*-orientation. Furthermore, two molecules of the bridged compound (**2b**) form a dimeric aggregate with centrosymmetry having a set of strong C–H···π interactions between a H atom of the catechol hinge moiety and the phenylene ring of the oxybenzoyl group of the other molecule, essentially the same with the 2,7-dimethoxy non-bridged homologue (**1a**). The ready formation of bridged derivatives from non-bridged homologues in non-dilution conditions manifests the smooth interconversion between *anti* and *syn* forms of the substrate molecule in solution.

This susceptibility is surely caused from lack of conjugation of aromatic rings, which makes the molecule to take *anti* conformer and *syn* one. Both semi-stable structures have satisfactorily high energy making the conversion easy. Then, in solution there is enough opportunity the molecule stays in syn structure to convert bridged-derivatives. By the same governing factors, the selection of *anti* or *syn* conformer in crystal is interpreted. These semi-stable conformers are still in rather high energy conditions, so the small perturbation of substituent sums up to exchange the level of conformers resulting in drastic alteration of single molecular conformation in crystal.

Experimental

All reagents were of commercial quality and were used as received. Solvents were dried and purified using standard techniques.[22] 2,7-dimethoxynaphthalene[23] and 2,7-diethoxynaphthalene,[24] non-bridged 1,8-bis(4-phenoxybenzoyl)-2,7-dialkoxynaphthalene (**1a** and **1b**) were prepared according to literatures.[10,11]

Measurements

^{1}H NMR spectra were recorded on a JEOL JNM-AL300 spectrometer (300 MHz) and a JEOL ECX400 spectrometer (400 MHz). Chemical shifts are expressed in ppm relative to internal standard of Me_4Si (δ 0.00). ^{13}C NMR spectra were recorded on a JEOL JNM-AL300 spectrometer (75 MHz). Chemical shifts are expressed in ppm relative to internal standard of $CDCl_3$ (δ 77.0). IR spectra were recorded on a JASCO FT/IR-4100 spectrometer. Elemental analyses were performed on a Yanaco CHN CORDER MT-5 analyzer. High-resolution FAB mass spectra were recorded on a JEOL MStation (MS700) ion trap mass spectrometer in positive ion mode.

X-ray Crystallography

For the crystal structure determination, the single-crystal of the compound **2b** was used for data collection on a fourcircle Rigaku RAXIS RAPID diffractometer (equipped with a two-dimensional area IP detector). The graphite-monochromated CuKα radiation (λ = 1.54187 Å) was used for data collection. The lattice parameters were determined by the least-squares methods on the basis of all reflections with $F^2 > 2\sigma(F^2)$. The data collection and cell refinement were performed using *PROCESS-AUTO* software. The data reduction was performed using *CrystalStructure*. The structures were solved by direct methods using *SIR2004* and refined by a full-matrix least-squares procedure using the program *SHELXL97*. All H atoms were found in a difference map and were subsequently refined as riding atoms, with the aromatic C–H = 0.95 Å, methyl C–H = 0.98 Å and methylene C–H = 0.99 Å, and with U_{iso}(H) = 1.2U_{eq}(C).

Synthesis of bridged *peri*-aroylnaphthalene 2 without high dilution conditions

To a solution of 1,8-bis(4-fluorobenzoyl)-2,7-dimethoxy-naphthalene (**3a**, 0.3 mmol, 130.7 mg) in dimethylacetamide (7.5 mL), K_2CO_3 (1.5 mmol, 208.3 mg) and catechol (0.3 mmol, 34 mg) were added and the resulting solution was stirred at 423 K for 24 h. The reaction mixture was poured into aqueous 2 M HCl (75 mL) at r.t. resulting in formation of pale yellow precipitates. The precipitates were collected by filtration and dried in vacuo. giving crude product (141 mg). The crude material was purified by column chromatography (silica gel, toluene : acetone = 5 : 1) and recrystallization from AcOEt to give the target compound (2a) (m.p. 440.3–441.5 K).

Compound **2b** was prepared according to essentially the same way to synthesize compound **2a**. The crude material was purified by column chromatography (silica gel, $CHCl_3$: acetone = 20 : 1) and recrystallization from AcOEt. Single crystal of compound **2b** suitable for X-ray diffraction was obtained by crystallization from AcOEt (m.p. 402.5–404.4 K).

Bridged compound **2a**: ^{1}H NMR δ (300 MHz, CDCl3): 7.91 (2H, d, *J* = 9.0 Hz), 7.80 (2H, dd, *J* = 8.7 Hz), 7.22–7.38 (4H, m), 7.20 (2H, d, *J* = 9.0 Hz), 6.84 (2H, dd, *J* = 8.7 Hz), 6.54–6.74 (2H, br), 6.20–6.40 (2H, br), 3.74 (6H, s) ppm; ^{13}C NMR δ (125 MHz, $CDCl_3$): 56.80, 111.19, 121.63, 125.46, 126.08, 126.83, 128.86, 131.05, 132.23, 132.80, 134.60, 147.77, 156.37, 161.54, 193.85 ppm; IR ν (KBr): 1670 (C=O), 1597, 1512, 1485 (Ar, naphthalene), 1501 (Ar, benzene), 1259 (C–O–C) cm^{-1}; HRMS (m/z): $[M+Na]^+$ calcd. for $C_{32}H_{22}O_6Na$, 525.1309. Found 525.1328.

Bridged compound **2b**: ^{1}H NMR δ (300 MHz, $CDCl_3$): 7.87 (2H, d, *J* = 9.0 Hz), 7.80 (2H, dd, *J* = 8.7 Hz), 7.25–7.40 (4H, m), 7.18 (2H, d, *J* = 9.0 Hz), 6.85 (2H, dd, *J* = 8.7 Hz), 6.60–6.75 (2H, br), 6.25–6.40 (2H, br), 3.95–4.16 (4H, m), 1.12 (6H, t, *J* = 6.6 Hz) ppm; ^{13}C NMR δ (75 MHz, $CDCl_3$): 14.64, 65.37, 112.42, 122.20, 125.37, 125.92, 126.66, 128.89, 130.86, 131.88, 132.84, 134.35, 147.68, 155.57, 161.27, 193.68 ppm; IR ν (KBr): 1676 (C=O), 1597, 1510, 1484 (Ar, naphthalene), 1500 (Ar, benzene), 1258 (C–O–C) cm^{-1}; HRMS (m/z): $[M+H]^+$ Calcd. for $C_{34}H_{27}O_6$, 637.2590. Found, 531.1842.

References

[1]Lu, B., Yan, J., Xu, J., Zhou, S., Hu, X., *Macromolecules*, **2010**, *43*(10), 4599–4608.

[2]Fraind, A. M., Tavor, J. D., *J. Phys. Chem. B*, **2010**, *114*(9), 3104–3116.

[3]Schmidt, B. M., Topolinski, B., Higashibayashi, S., Kojima, T., Kawano, M., Lentz, D., Sakurai, H., *Chem. Eur. J.*, **2013**, *19*(10), 3282-3286.

[4]Yoshimoto, S., Kobayashi, N., *Structure and Bonding* (Berlin, Germany), **2010**, *135*, 137-168.

[5]Shrestha, B. B., Higashibayashi, S., Sakurai, H., *Beil. J. Org. Chem.*, **2014**, *10*, 841-847.

[6]Choi, H. S., Kim, K. S., *Angew. Chem. Int. Ed.*, **1999**, *38*(15), 2256–2258.

[7]Bunz, U. H. F., Menning, S., Martin, N., *Angew. Chem., Int. Ed.*, **2012**, *51*, 7094–7101.

[8]Kayahara, E.; Patel, V. K.; Yamago, S., *J. Am. Chem.* **2014**, *136*, 2284–2287.

[9]Segawa, Y., Fukazawa, A., Matsuura, S., Omachi, H., Yamaguchi, S., Irle, S., Itami, K., *Org. Biomol. Chem.*, **2012**, *10*, 5979–5984.

[10]Hijikata, D., Takada, T., Nagasawa, A., Okamoto, A., Yonezawa, N., *Acta Cryst.*, **2010,** *E66*, o2902–o2903.

[11]Yoshiwaka, S., Sasagawa, K., Noguchi, K., Okamoto, A., Yonezawa, N. *Acta Cryst.*, **2014**, *C70*, 1096–1100.

[12]Okamoto, A.; Yonezawa, N.; *Chem. Lett.*, **2009**, *38*, 914.

[13]Okamoto, A; Mitsui, R.; Yonezawa, N.; *Chem. Lett.*, **2011**, *40*, 1283.

[14]Nakaema, K.; Noguchi, K.; Okamoto, A.; Yonezawa, N.; *Acta Cryst.*, **2008**, *E64*, o2497.

[15]Mohri, S.; Ohisa, S.; Noguchi, K.; Yonezawa, N.; Okamoto, A.; *Acta Cryst.*, **2014**, *E70*, 138-141.

[16]Nishijima, T.; Kataoka, K.; Nagasawa, A.; Okamoto, A.; Yonezawa, N.; *Acta Cryst.*, **2010**, *E66*, o2904–o2905.

[17]Sasagawa, K., Takeuchi, R., Kusakabe, T., Yonezawa, N., Okamoto, A., *Acta Cryst.*, **2013**, *E69*, o444–o445.

[18]Mitsui, R., Nagasawa, A., Noguchi, K., Okamoto, A., Yonezawa, N., *Acta Cryst.*, **2010**, *E66*, o1790.

[19]Yoshiwaka, S., Hijikata, D., Sasagawa, K., Okamoto, A., Yonezawa, N., *Acta Cryst.*, **2013**, *E69*, o242.

[20]Okamoto, A., Hijikata, D., Sakai, N., Yonezawa, N., *Polymer J.*, **2013**, *45*, 277–280.

[21]CCDC-1039291 contains the supplementary crystallographic data for this paper. These data can be obtained free of charge from The Cambridge Crystallographic Data Centre via www.ccdc.cam.ac.uk/data_request/cif.

[22]Armarego, W.L. F.; Perrin, D. D.; "*Purification of Laboratory Chemicals",* Fourth edition, Reed Educational and Professional Publishing Ltd, Oxford, **1996**.

[23]Domasevitch, K. V.; Solnsev, P. V.; Krautscheid, H.; Zhylenko, I. S.; Rusanov, E. B.; Chernega, A. N. *Chem. Commun.*, **2012**, *48*, 5847.

[24]Kuwano, R.; Morioka, R.; Kashiwabara, M.; Kameyama, N. *Angew. Chem., Int. Ed*., **2012**, *51*, 4136.

Received: 17.12.2014.
Accepted: 26.01.2015.